forests

Carbon and Nitrogen in Forest Ecosystems

Series I

Edited by

Yowhan Son

Printed Edition of the Special Issue Published in *Forests*

www.mdpi.com/journal/forests

MDPI

Carbon and Nitrogen in Forest Ecosystems—Series I

Carbon and Nitrogen in Forest Ecosystems—Series I

Editor

Yowhan Son

MDPI • Basel • Beijing • Wuhan • Barcelona • Belgrade • Manchester • Tokyo • Cluj • Tianjin

Editor
Yowhan Son
Korea University
Korea

Editorial Office
MDPI
St. Alban-Anlage 66
4052 Basel, Switzerland

This is a reprint of articles from the Special Issue published online in the open access journal *Forests* (ISSN 1999-4907) (available at: https://www.mdpi.com/journal/forests/special_issues/Carbon_Nitr_system).

For citation purposes, cite each article independently as indicated on the article page online and as indicated below:

LastName, A.A.; LastName, B.B.; LastName, C.C. Article Title. *Journal Name* **Year**, *Article Number*, Page Range.

ISBN 978-3-03936-744-3 (Hbk)
ISBN 978-3-03936-745-0 (PDF)

Cover image courtesy of Yowhan Son.

Contents

About the Editor

Yowhan Son is mainly interested in carbon and nutrient distribution and cycling in forest ecosystems in addition to in the context of natural and human influences on ecosystem structure and function, organic matter production and decomposition in soils, nitrogen cycling in trees and forest soils, and soil and water pollution under different natural and human disturbances in forests. Prof. Son is an Editorial Advisory Board Member of *Forest Ecology and Management*.

Preface to "Carbon and Nitrogen in Forest Ecosystems—Series I"

When studying forest ecosystems, it is essential to understand the differences between carbon and nitrogen spatial and temporary distribution and cycling when using various approaches. In addition, biotic/abiotic factors and natural/artificial disturbances on carbon and nitrogen cycling need to be better understood to draw implication on forest management practices.

Relevant matters investigated within this Special Issue are as follows:

- different approaches to measure carbon and nitrogen distribution and cycling in forest ecosystems including field measurement, remote sensing, and modeling;
- differences in carbon and nitrogen cycling within an ecosystem and among ecosystems;
- changes in carbon and nitrogen cycling in forest ecosystems along successional gradients;
- roles of microbes, insects, and animals in carbon and nitrogen cycling in forest ecosystems;
- influences of climate change on carbon and nitrogen cycling in forest ecosystems;
- artificial manipulation of trees to simulate carbon and nitrogen cycling to climate change;
- influences of forest management practices on carbon and nitrogen cycling in forest ecosystems;
- ecosystem based forest management.

This Special Issue aims to understand carbon and nitrogen distribution and cycling in forest ecosystem for ecosystem-based forest management under different natural and artificial disturbances.

Yowhan Son
Editor

forests

MDPI

Article

Biometric and Eddy Covariance Methods for Examining the Carbon Balance of a *Larix principis-rupprechtii* Forest in the Qinling Mountains, China

Jie Yuan [1], Shibu Jose [2], Zhaoyong Hu [1], Junzhu Pang [1,3], Lin Hou [1,3] and Shuoxin Zhang [1,3,*]

1 College of Forestry, Northwest A&F University, Xianyang 712100, China; yuanjie@nwsuaf.edu.cn (J.Y.); huzy418@gmail.com (Z.H.); pangjunzhu@nwsuaf.edu.cn (J.P.); houlin1969@163.com (L.H.)
2 School of Natural Resources, University of Missouri, Columbia, MO 65211, USA; joses@missouri.edu
3 Qinling National Forest Ecosystem Research Station, Huoditang, Ningshan 711600, China
* Correspondence: sxzhang@nwsuaf.edu.cn; Tel./Fax: +86-29-8708-2993

Received: 20 December 2017; Accepted: 25 January 2018; Published: 29 January 2018

Abstract: The carbon balance of forests is controlled by many component processes of carbon acquisition and carbon loss and depends on the age of vegetation, soils, species composition, and the local climate. Thus, examining the carbon balance of different forests around the world is necessary to understand the global carbon balance. Nevertheless, the available information on the carbon balance of *Larix principis-rupprechtii* forests in the Qinling Mountains remains considerably limited. We provide the first set of results (2010–2013) from a long-term project measuring forest-atmosphere exchanges of CO_2 at the Qinling National Forest Ecosystem Research Station (QNFERS), and compare the net ecosystem exchange (NEE) based on biometric measurements with those observed via the eddy covariance method. We also compare the total ecosystem respiration via scaled-up chamber and eddy covariance measurements. The net primary productivity (NPP) was 817.16 ± 81.48 $g{\cdot}C{\cdot}m^{-2}{\cdot}y^{-1}$, of which ΔB_{living} and D_{total} accounted for 77.7%, and 22.3%, respectively. Total ecosystem respiration was 814.47 ± 64.22 $g{\cdot}C{\cdot}m^{-2}{\cdot}y^{-1}$, and cumulative annual soil respiration, coarse woody debris respiration, stem respiration, and leaf respiration were 715.47 ± 28.48, 15.41 ± 1.72, 35.28 ± 4.78, and 48.31 ± 5.24 $g{\cdot}C{\cdot}m^{-2}{\cdot}y^{-1}$, respectively, accounting for 87.85%, 1.89%, 4.33%, and 5.93% of the total ecosystem respiration. A comparison between ecosystem respiration from chamber measurements and that from eddy covariance measurements showed a strong linear correlation between the two methods (R^2 = 0.93). The NEE of CO_2 between forests and the atmosphere measured by eddy covariance was −288.33 ± 25.26 $g{\cdot}C{\cdot}m^{-2}{\cdot}y^{-1}$, which revealed a carbon sink in the *L. principis-rupprechtii* forest. This number was 14% higher than the result from the biometric measurements (−336.71 ± 25.15 $g{\cdot}C{\cdot}m^{-2}{\cdot}y^{-1}$). The study findings provided a cross-validation of the CO_2 exchange measured via biometric and eddy covariance, which are beneficial for obtaining the true ecosystem fluxes, and more accurately evaluating carbon budgets.

Keywords: carbon balance; Qinling Mountains; biomass regression model; eddy covariance; net primary productivity; net ecosystem exchange

1. Introduction

Forests play a critical role in the global carbon cycle [1,2], and since the 1990s, substantial data have been acquired to clarify the contributions of forest ecosystems to the global carbon cycle [3–5]. The Qinling Mountains in central China provide an important climate boundary between the southern subtropics and the northern temperate zone, where the typical vegetation of both climate zones is present together with astonishingly high biodiversity [6]. Nevertheless, information relevant to the

carbon balance from forests in the Qinling Mountains remains considerably limited. Studies have demonstrated that mountain forests are 'hot spots' for carbon cycling and are expected to be more strongly affected by climate change than lowland forests due to their sensitivity to warming [7,8]. Therefore, there is an urgent need for increased knowledge about the carbon fluxes in various mountain forests, especially those in the Qinling Mountains.

Larix principis-rupprechtii is adapted to high light levels and can tolerate freezing temperatures. This species grows in deep, well-drained acidic or neutral soils and is a valuable reforestation species in China that is distributed over ten provinces. Due to its rapid growth, high-quality wood, resistance to adverse climate and soil conditions, and high wind resistance, the tree is used for forest regeneration and afforestation of barren hills. *L. principis-rupprechtii* forests in the Qinling Mountains serve as major research sites for forest ecosystem studies because they represent the regional vegetation in the temperate coniferous forest domain of China and are also a major component of temperate forests globally. In addition, the *L. principis-rupprechtii* forest is sensitive to global change [9]. In the Qinling Mountains, from 1958 to 1986, the area afforested with *Larix* reached 0.3×10^4 ha [10]. Although Zhou et al. estimated the carbon budget of a *Larix* forest in China [11], there is still considerable uncertainty about the strength of the carbon source/sink in this forest due to discrepancies in estimation methods and variations in age, management, and climate [12,13]. Thus, to accurately determine the carbon balance of *Larix* forests, an adequate understanding of the processes that control net CO_2 exchange in a young *L. principis-rupprechtii* planted forest in the temperate regions is required.

The carbon balance at the ecosystem level (net ecosystem exchange, NEE) is controlled by many component processes of carbon acquisition (photosynthesis, tree growth, forest ageing, and carbon accumulation in soils) and carbon loss (respiration of living biomass, tree mortality, microbial decomposition of litter, oxidation of soil carbon, degradation, and disturbance) [14]. However, previous studies have suggested respiration as the main determinant in controlling the carbon balance of ecosystems [13]. Ecosystem respiration is composed of autotrophic and heterotrophic components, whose contributions to total respiration vary in space and time. Components of respiration include soil (roots and microorganisms), coarse woody debris (CWD), and stem and leaf respiration, which are controlled by the complex interaction of many factors, including temperature, moisture, canopy cover, stand age, and nutrient contents [4,15]. Few studies have investigated the seasonal and annual variability of these respiratory components in detail [4,16]. Hence, it is absolutely necessary to quantify the ecosystem's respiratory components, which can allow researchers to determine the contribution of each component flux to the overall ecosystem respiration and improve our understanding of ecosystem respiration dynamics [17].

Currently, the foremost techniques for measuring NEE are the eddy covariance technique and the biometric technique. Each technique has advantages and disadvantages. The eddy covariance method is a micrometeorological technique and has been widely used in different ecosystems [18,19]. The eddy covariance technique has numerous advantages: (1) it is nondestructive and has a low workload, (2) it provides observations at the ecosystem scale, and (3) it yields continuous records that address time scales every half hour to the length of the data record [16,20]. Since the early 1990s, more than 500 eddy covariance flux towers have been built in numerous ecosystems around the world [21]. However, there are still deficiencies in the eddy covariance method. Firstly, the measurements become unreliable or unavailable when the atmospheric conditions (wind, temperature, humidity, CO_2) are unsteady, the terrain is uneven, or there is very weak turbulence, as sometimes occurs at night [22,23]. Secondly, this method is valid for usage on large-scale field plots and cannot provide information on the component carbon fluxes [16]. The biometric method offers the advantages of lower cost and simplicity, in principle. Moreover, the chambers are portable and well suited for small-scale studies, which is appropriate for replicated measurements in multiple small plots of field trials and is also necessary for estimating the contributions of component carbon fluxes (for example, net primary production (NPP), heterotrophic respiration, and autotrophic respiration) to the total fluxes. However, some drawbacks have limited the application of the biometric method for NEE measurements. For example, (1) a variety

of potential errors, such as modifications in the enclosed microclimate, pressure artefacts, and spatial heterogeneity, may occur [24]; (2) it cannot effectively sample the full spatial variation of patch-specific fluxes; (3) it cannot observe the full short-term (intra-daily) and intermediate (inter-daily) temporal variations that occur within a site; and (4) large uncertainties in scaled-up estimates may result in over- or underestimates of the actual fluxes [25].

In short, both the eddy covariance and the biometric methods must be inaccurate in measuring NEE due to the weaknesses associated with using either method alone. Few studies have conducted comparisons of eddy covariance and biometric-based measurements of NEE, especially relative to measurements taken simultaneously at the same site using the two different methods [26]. Thus, comparing the NEE measured using the eddy covariance and the biometric methods is necessary to highlight the potential sources of errors. Such a comparison is straightforward but requires a strict methodology for testing the accuracy and consistency of the eddy covariance and the biometric fluxes.

This paper presents the first set of results (2010–2013) from a long-term project measuring forest-atmosphere exchanges of CO_2 using the eddy covariance and biometric methods in a *L. principis-rupprechtii* forest in the Qinling Mountains. The objectives of our study were as follows: (1) to describe measurements of soil, coarse woody debris (CWD), stem, and leaf respiration based on chamber methods and to combine these measured fluxes with continuous measurements of temperature to model the respiration of each ecosystem component; (2) to estimate the spatial and temporal variability of ecosystem respiration and the percentage of the total ecosystem respiration of each component based on chamber measurements; and (3) to compare the total ecosystem respiration based on scaled-up chamber measurements and NEE based on biometric measurements with those observed via the eddy covariance method and to evaluate the carbon balance of the *L. principis-rupprechtii* forest at this site.

2. Materials and Methods

2.1. Study Area

The study area for the ecosystem component measurements covered 1 ha centered on a tower equipped for eddy covariance measurements of carbon dioxide exchange located at the Huoditang Experimental Forest Farm of Northwest A&F University in the Qinling Mountains, Shaanxi Province, China (Figure S1). The altitude is 2150 m, and the geographic coordinates are 33°27′42″ N latitude and 108°28′54″ E longitude. The annual average temperature is 10.80 °C, the annual precipitation 1200 mm, and the climate belongs to the temperate zone. The period of snow cover is from December to March, with a maximum depth of approximately 20 cm. The soil is classified as mountain brown earth.

The study area was selectively logged in the 1960s and 1970s, and since then, there have been no major anthropogenic disturbances except for small amounts of illegal logging. Since the natural forest protection project was initiated in 1998, human activities have almost vanished in the region. To reduce disturbance, the permanent plot was protected by an enclosure. The site is level (a mean slope of 5°), which is ideal for this study, and the overstory and understory of the forest are homogeneous. Moreover, the results of the data quality estimate (footprint analysis, energy balance estimate, eddy statistic estimate, and power spectrum estimate) implied that not only the location selected but also the configuration of this observational system are comparable for observations of the fluxes in the long run [27].

The forest used for the current research was 50 years old and was dominated by *L. principis-rupprechtii*. The mean stand height, diameter at breast height (DBH), and stand density were 16 m, 18 cm, and 1585 trees·ha^{-1}, respectively. In the shrub layer, the height varied from 80 cm to 520 cm and the percent cover was 28%. The major shrubs species present were *Euonymus phellomanus*, *Lonicera hispida*, *Lindera glauca*, and *Rubus pungens*, together with herbs such as *Carex leucochlora*, *Deyeuxia arundinacea*, *Lysimachia christinae*, *Thalictrum minus*, *Anaphalis aureopunctata*, *Dioscorea nipponica*,

Rubia cordifolia, and *Sinacalia tangutica*, and the fern *Dryopteris goeringiana*. The average height of the herbs was 60 cm, and the percent cover was 40%.

2.2. Biometric Measurements

2.2.1. Plot Measurements

In summer 2009, we established a permanent plot in the *L. principis-rupprechtii* forest. The 1 ha plot was divided into 25 quadrats 20 m × 20 m in size. The quadrats were each subdivided into 16 sub-quadrats 5 m × 5 m in size. A total of 1585 trees and 2728 shrubs in these sub-quadrats were permanently marked with aluminum labels and numbered consecutively. Based on the plot investigation, 10 standard trees outside the plot were felled. The leaves and branches at different canopy positions and orientations and the stems of different diameters were all collected, and the roots were dug up from the 10 standard trees to measure the carbon content ratio and evaluate the biomass. The DBH of all trees (including dead and new trees) were documented in August of each year during 2009–2013 to estimate (the annual change in) the biomass, which was calculated via the regression model developed in a previous study in this region (Table S2) [28].

We also documented the species, height, crown width, and basal stem diameter of all shrubs (including dead and new shrubs) in August of each year during 2009–2013 for biomass calculations. Based on the species present within the plots, *E. phellomanus, L. hispida, L. glauca*, and *R. pungens* outside the plot were dug up, with totals of 55, 48, 78, and 62 individual plants, respectively. The species, height, crown width, and basal stem diameter of these harvested shrubs were recorded, and they were then taken back to the laboratory to measure the carbon content ratio and develop a biomass regression model (Table S3).

To reduce disturbance, based on the plot investigation, we selected twenty 1 m × 1 m groundcover quadrats outside the plot in August of 2009–2013. All of the herbs were dug out in the twenty quadrats each year in order to measure the carbon content ratio and biomass. The twenty quadrats were not repeated each year, and new quadrats were selected each year.

In order to accurately estimate the root biomass and correct the fine root loss caused by digging, we used soil coring to supplement the fine root biomass [29]. A representative root sample was extracted from soil cores of 30 cm in length and 1.8 cm in diameter (76 cm^3). We selected twenty soil cores outside the plot in August of 2009–2013. All soil cores were extracted each year to supplement the fine root biomass. The twenty soil cores were not repeated each year, and new soil cores were selected each year. Litterfall was collected from the beginning of August 2009 to August 2013 at monthly intervals. Twenty 1 m × 1 m litter traps were randomly erected in the plot. Each trap consisted of 2 mm mesh nylon netting (on a wooden frame) suspended from a wire hoop and held 30 cm above the ground by four metal poles.

2.2.2. Carbon Content Ratio

The samples of trees, shrubs, and herbs were classified into species and organs (stem, bark, branch, leaf, and root), and the stems, branches, and roots were cut into 10 cm lengths. In each species, the same organs of the samples were pooled into one composite sample, while the twenty litterfall traps were also pooled into one composite sample. These composite samples were dried at 85 °C to constant weight (approximately 72 h) and then crushed to pass through a No. 200 mesh (0.074 mm) in order to measure the carbon content ratio. Each composite sample was repeatedly measured three times with a TOC analyzer (TOC-VTH-2000A, Shimadzu, Japan), and the average value was obtained for the carbon content ratio of litterfall and the different organs of the trees, shrubs, and herbs.

2.2.3. Net Primary Productivity (NPP)

Forest NPP estimates have been based primarily upon measurements of stems, bark, branches, and roots (including coarse and fine roots) biomass gain using regression models for trees and shrubs

and harvest methods for other ecosystem components (herbs and litterfall). NPP was estimated using the following equations:

$$NPP = \Delta B_{living} + D_{total} \quad (1)$$

$$\Delta B_{living} = \sum T_i O_i + \sum S_j O_j + \sum H_r O_r \quad (2)$$

$$D_{total} = \sum D_{ti} O_i + \sum D_{sj} O_j + L \times P \quad (3)$$

where ΔB_{living} is the increment in live plant biomass, T_i is the live tree biomass increment of the ith organ (except for leaf), O_i is the tree carbon content ratio of the ith organ, S_j is the live shrub biomass increment of the jth organ (except for leaf), O_j is the shrub carbon content ratio of the jth organ, H_r is the herbaceous biomass increment of the root, O_r is the herbaceous carbon content ratio of the root, D_{total} is the sum of dead plant mass, D_{ti} is the dead tree mass of the ith organ (except for leaf), O_i is the tree carbon content ratio of the ith organ, D_{sj} is the dead shrub mass of the jth organ (except for leaf), O_j is the shrub carbon content ratio of the jth organ, L is the mass of litterfall, and P is the carbon content ratio of litterfall. Herbivore loss is often assumed to be negligible in healthy stands [30] and was not estimated in this study.

2.2.4. Leaf Area Index

The LAI-2000 plant canopy analyzer (LI-COR, Inc., Lincoln, NE, USA) is designed to estimate the leaf area index (LAI) of plant canopies indirectly from measurements of radiation above and below the canopy based on a theoretical relationship between leaf area and canopy transmittance [31]. The below-canopy measurements were made at 40 points, which were marked with red stakes and located along permanent transects; the sampling distance was 15 m in this forest. Above-canopy measurements were taken automatically every 15 s by a second instrument in the center of an open field situated nearby. The fish-eye lens of the instrument was covered by a view cap with a 90° opening to ensure that the reference measurements were not influenced by the trees surrounding the clearings or by the operator [32]. In taking canopy measurements, the sensor was held so that the same portion of the sky and the same level (between 1 and 1.5 m above ground) was occluded for both sensors (above- and below-canopy measurements). The LAI measurements were made every 2 weeks from April to November in 2010–2013.

2.2.5. Micrometeorological Measurements

A full suite of micrometeorological measurements was taken from the weather station located 20 m away from the plot, including air temperature and humidity (HMP45C, Vaisala, Helsinki, Finland), photosynthetically active radiation, soil temperature (10 cm), and precipitation. Data from all the sensors were recorded on data loggers (CR-1000, Campbell Scientific, Logan, UT, USA), and the data were downloaded every 2 weeks to a laptop personal computer (PC).

2.2.6. Soil Respiration

Soil respiration was measured using an LI-6400-09 soil chamber connected to an LI-6400 portable photosynthesis system (LI-COR, Inc., Lincoln, NE, USA). Thirty soil collars, each with a height of 10 cm and a diameter of 10 cm, were randomly placed in the 1 ha plot. To avoid influence on the measurement of soil respiration, the soil collars were inserted into the soil at the depth of 2 cm one week before the measurement of soil respiration. The surface vegetation inside the soil collars was cleared 1 day before the measurement, and the topsoil was kept intact to avoid its influence on the measured results. Surface efflux was measured three times in succession for each collar during each measurement period. Soil temperature at 10 cm was measured adjacent to each respiration collar with a portable temperature probe provided with the LI-6400. The measurements were made every 2 weeks from April to November in 2010–2013.

We used an exponential equation to analyze the relationship between respiration and temperature:

$$R = R_0 e^{\beta T} \quad (4)$$

where R is the component respiration (soil ($\mu mol \cdot m^{-2} \cdot s^{-1}$), root ($\mu mol \cdot m^{-2} \cdot s^{-1}$), coarse woody debris ($\mu mol \cdot m^{-3} \cdot s^{-1}$), stem ($\mu mol \cdot m^{-3} \cdot s^{-1}$), or leaf ($\mu mol \cdot g^{-1} \cdot d^{-1}$)); T is the temperature of each component (°C); and R_0 and β are fitted parameters. The temperature dependence of respiration is often described by the Q_{10} value, which is called the temperature sensitivity of respiration. The respiration parameter, Q_{10}, can be derived from $Q_{10} = \exp(10\beta)$. Estimated parameters were used to predict the soil respiration for every 0.5 h over 4 years based on continuous temperature measurements from the weather station.

2.2.7. Root Respiration

The trenching method was used to estimate the root respiration [33]. The trenched plot (20 m × 20 m) was established adjacent to the permanent plot at this site. We also randomly established twenty 50 cm × 50 cm subplots in the trenched plot in August 2009. Each subplot was prepared by making vertical cuts along the boundaries to 50 cm below the ground surface (approximately the bottom of the root zone) with a steel knife, severing all roots. The roots were removed, and fiberglass sheets were installed to prevent roots from entering. The trenches were backfilled with the same soil. The aboveground parts of all plants growing in the subplots were cut off, and new seedlings and re-growth from the roots were periodically clipped when necessary.

Twenty soil collars, each with a height of 10 cm and a diameter of 10 cm, were inserted into the soil in the subplots. The soil respiration in the trenched plot was measured using the same method for soil respiration.

We used the following equation to calculate the root respiration (R_R, $\mu mol \cdot m^{-2} \cdot s^{-1}$):

$$R_R = R_S - R_C \quad (5)$$

where R_S is the soil respiration in the permanent plot ($\mu mol \cdot m^{-2} \cdot s^{-1}$) and R_C is the soil respiration in the trenched plot ($\mu mol \cdot m^{-2} \cdot s^{-1}$).

2.2.8. Coarse Woody Debris Respiration

We used the standard method developed by the United States Department of Agriculture (USDA) Forest Service and the Long Term Ecological Research (LTER) programme to define woody debris as CWD, which was further categorized into logs, snags, and stumps [34]. The downed or leaning deadwood with a diameter at the widest point ≥10 cm and length ≥1 m were included in the group. The dead trees with a gradient (departure from vertical direction) ≤45° were considered as snags, while those with a gradient >45° were classified as logs. The vertical deadwood with a height ≤1 m was considered as stumps. Each piece of CWD was assigned to one of five decay classes on the basis of differences in internal and external tissue characteristics (Table S4) [35]. The numbers 1, 2, 3, 4, and 5 represent different decomposition stages, i.e., 1 represents the initial stage and 5 represents the final stage.

CWD respiration was measured for the five decay classes in the plot. Three pieces of CWD were sampled for CWD respiration in each decay class, and three fixed plates were mounted on each low decay class of CWD (sufficient sound wood was present) with silicon sealant at a random azimuth. A custom Plexiglas cuvette, 800 cm^3 in volume with an 80 cm^2 opening, was closely attached to the mounting plate just before each measurement. CWD respiration was measured three times in succession for each cuvette during each measurement and three times during the day at each cuvette. CWD temperature at 10 cm deep was measured adjacent to each cuvette with a portable temperature probe provided with the LI-6400. For the more advanced decay classes, these CWD samples were

placed into the containers to measure. The measurements were made every 2 weeks from April to November in 2010–2013.

The measured CWD respiration rates per unit area were converted to rates per unit volume. We used the exponential function (Q_{10} function) to analyze the response of CWD respiration per unit of volume to CWD temperature (Equation (4)). Continuous CWD temperatures were calculated by the model, which simulated the relationship between CWD temperatures and 10 cm soil temperatures (Figure S5).

To upscale the chamber measurements of CWD respiration to the stand level, we calculated the volume of the five decay classes of CWD in the plot. Forest censuses were conducted in August of each year during 2009–2013 to determine the CWD volume. Each log or stump was considered as a cylinder; consequently, we used Smalian's formula to produce a volume estimate through the length and cross-sectional areas at the basal and distal ends of the cylinder [36]. For snags, we used the height and diameter in a species-specific wood volume equation, thus calculating the volume of each piece of the snag.

2.2.9. Stem Respiration

Fifty fixed plates were mounted on the trunks of 50 standard trees with silicon sealant at approximately 130 cm in height and a random azimuth. We used the same cuvette that was used to measure CWD respiration for measuring stem respiration; the cuvette was closely attached to the mounting plate just before each measurement. For the CWD respiration measurements, stem respiration rates were measured three times in succession for each cuvette during each measurement and three times during the day at each cuvette. The measurements were made every 2 weeks with an LI-6400 portable photosynthesis system (LI-COR, Inc., Lincoln, NE, USA) from April to November in 2010–2013. Stem temperature was measured with a portable temperature probe provided with the LI-6400 inserted into the sapwood near the cuvette of each sample tree. The sapwood thickness and wood mass density of each standard tree were measured from tree cores.

Measured stem respiration rates per unit area were converted to rates per unit of sapwood volume based on sapwood area and tree DBH, assuming a wedge-shape volume had contributed to the respiration rates. We used the exponential function (Q_{10} function) to analyze the response of stem respiration per unit of sapwood volume to stem temperature (Equation (4)). Continuous stem temperatures were calculated by the model, which simulated the relationship between stem temperatures and air temperatures (Figure S6).

To upscale the chamber measurements of stem respiration to the stand level, we estimated the total sapwood volume per unit of ground area in the plot. We assumed that branch respiration per volume had the same rate as stem (bole) respiration, similar to the assumptions made by Law et al. [37], Xu et al. [38], and Bolstad et al. [4].

After measuring the DBH and sapwood thickness, we estimated the sapwood volume of 30 sample trees to develop the regression model for sapwood volume:

$$\ln V_p = 0.90589 \ln (D^2H) - 10.31542 \quad (6)$$

where V_p is the sapwood volume including that from stems and branches (m^3), D is the DBH (m), H is the tree height (m), and the correlation coefficient is 0.9452. Equation (6) was used to estimate the sapwood volume of the whole stand and the average sapwood volume per ground area.

2.2.10. Leaf Respiration

Leaf respiration was measured from 30 leaves collected from 10 *L. principis-rupprechtii* trees, 30 leaves from shrubs, and 30 leaves from herbs from April to November in 2010–2013. Following the method of Bolstad et al. [4], branches from species from random heights and directions in the canopy were detached at night and immediately placed in a plastic bag with a moistened paper towel and

transported in the dark to a nearby laboratory. Fully expanded leaves were detached just before measurement. All measurements were made within 3 h of branch harvest. Leaf respiration rates were measured from 5 to 25 °C with a controlled temperature LI-6400 portable photosynthesis system (LI-COR, Inc., Lincoln, NE, USA). Leaf area was measured with an AM-300 portable leaf area meter (ADC Bioscientific Limited, SG12, 9TA, Cambridge, UK). Leaves were oven dried at 65 °C and weighed. The measured leaf respiration rates per unit area were converted to rates per unit of dry biomass.

We used the exponential equation (Equation (4)) to fit the leaf respiration per unit of dry biomass as a function of leaf temperature for each species. We assumed in this study that the leaf temperature was the air temperature.

To upscale chamber measurements of leaf respiration to the stand level, we estimated the total leaf dry biomass per unit of ground area in the plot. The dry leaf biomass of shrubs and herbs was estimated by our study, while the dry leaf biomass of *L. principis-rupprechtii* was estimated by the regression model based on a previous study in this region [28].

2.2.11. Net Ecosystem Exchange

The annual net ecosystem exchange of CO_2 (NEE, $g{\cdot}C{\cdot}m^{-2}{\cdot}y^{-1}$) can be estimated using the following equation according to the measured annual rates of component respirations and net primary production (NPP):

$$NEE = R_S + R_{CWD} - R_R - NPP \quad (7)$$

where R_S is the soil respiration ($g{\cdot}C{\cdot}m^{-2}{\cdot}y^{-1}$), R_{CWD} is the CWD respiration ($g{\cdot}C{\cdot}m^{-2}{\cdot}y^{-1}$), Equation (5) was used to calculate the R_R ($g{\cdot}C{\cdot}m^{-2}{\cdot}y^{-1}$), and Equation (1) was used to calculate the NPP ($g{\cdot}C{\cdot}m^{-2}{\cdot}y^{-1}$).

2.3. Eddy Covariance Measurements

To compare with biometric measurements, fluxes of CO_2 were measured from a tower at 30 m above ground in the *center* of the stand. A three-dimensional sonic anemometer (CSAT-3, Campbell Scientific, Inc., Logan, UT) and an open-path infrared gas analyzer (LI-7500, LI-COR, Lincoln, NE, USA) mounted at a height of 25 m measured the three components of the wind velocity vector, sonic temperature, and the densities of water vapor and CO_2. These components were sampled at 10 Hz by a data logger (CR-5000, Campbell Scientific, Logan, UT, USA), which also calculated the 30 min covariance using Reynolds block averaging. Surface fluxes were later calculated off-line after performing a two-dimensional coordinate rotation and accounting for density fluctuations [39]. NEE data were screened for weak turbulence friction velocity at night. Although we found only a negligible trend of increasing NEE with u^*, we calculated an annual NEE using a u^* threshold of $0.15\ m{\cdot}s^{-1}$. To fill the gaps, a double-directional interpolation model of artificial neural networks (ANNs) was used [27]. Nighttime NEE was assumed to be a measurement of ecosystem respiration and was extrapolated to all times by using a temperature response function as described by Cook et al. [40] and Desai et al. [41].

2.4. Statistical Analyses

One-way ANOVAs were used to determine the effect of the 10 cm soil temperature on the soil respiration, of CWD temperature on the respiration of different CWD decay classes, of sapwood temperature on the stem respiration, and of air temperature on the leaf respiration. An exponential equation was used to simulate the relationship between respiration and temperature. The relationship between the CWD temperature and the 10 cm soil temperature was simulated using a regression model. A regression model was also used to simulate the relationship between sapwood temperature and air temperature. The sapwood volume was estimated by a regression model. Moreover, the eddy covariance technique and chamber-based estimates were simulated based on a linear model. All statistical analyses were conducted using the SAS 8.0 Statistical Package, with a p-value of 0.05 set

as the limit for statistical significance. Origin 8.0 (OriginLab Corporation, Northampton, MA, USA) was used to draw the graphs.

3. Results

3.1. Environmental Factors

There was a clear seasonal pattern in air temperature and 10 cm soil temperature during 2010–2013 (Figure S7). The air temperature changed more dramatically, but the variation of the 10 cm soil temperature was consistent with the air temperature. The annual mean air temperature was 10.82 ± 9.66, 10.94 ± 9.78, 10.59 ± 9.60, and 10.89 ± 9.84 °C for 2010 to 2013, respectively. The annual mean 10 cm soil temperature was 11.12 ± 8.09, 11.22 ± 8.19, 10.93 ± 8.04, and 11.18 ± 8.24 °C for 2010 to 2013, respectively. Due to rain, the photosynthetic active radiation was relatively low from June to August for all years (Figure S8). The annual mean photosynthetically active radiation was 147.81 ± 92.09, 149.05 ± 103.63, 146.19 ± 94.49, and 144.54 ± 81.05 $\mu mol \cdot m^{-2} \cdot s^{-1}$ for 2010 to 2013, respectively.

3.2. Soil Respiration

There was a significant exponential relationship between soil respiration and the 10 cm soil temperature. The parameters in Equation (4) for soil respiration are summarized in Table 1. Equation (4) allows us to estimate the year-round soil respiration using the 10 cm soil temperature as an independent variable. There was an obvious seasonal pattern of soil respiration in 2010–2013 (Figure 1). Soil respiration includes soil heterotrophic respiration, root respiration, and litter respiration; root respiration accounted for 35% ± 7% of the soil respiration on average in 2010–2013 (Figure 1). The total soil respiration was 710.37 ± 20.14, 721.45 ± 22.45, 692.77 ± 19.64, and 737.27 ± 24.27 $g \cdot C \cdot m^{-2} \cdot y^{-1}$ for 2010 to 2013, respectively. The lower soil respiration in 2012 was consistent with the soil temperature in 2012, which was lower than in other years.

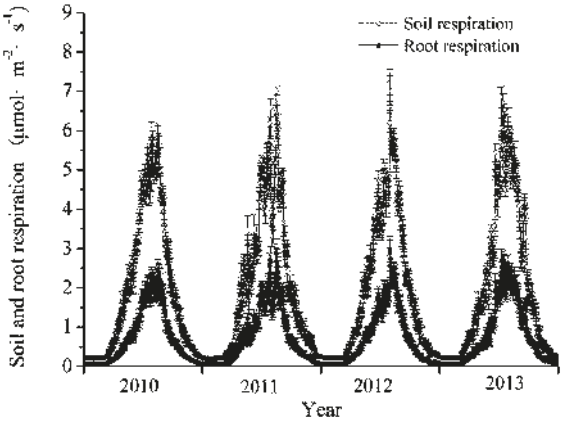

Figure 1. Daily mean soil and root respiration in the *L. principis-rupprechtii* forest during 2010–2013. Error bars are based on 0.5 h soil temperatures as experimental unit (n = 48).

Table 1. Parameters in the temperature response function (Equation (4)) for soil respiration (R_S, μmol·m^{-2}·s^{-1}), root respiration (R_R, μmol·m^{-2}·s^{-1}), coarse woody debris (CWD) respiration (R_{CWD}, μmol·m^{-3}·s^{-1}), stem respiration (R_T, μmol·m^{-3}·s^{-1}), and leaf respiration (R_L, μmol·g^{-1}·d^{-1}).

Respiration (R)		R_0	β	Q_{10}	Coefficient of Determination (R^2)	Samples (*n*)
R_S		0.22	0.14	4.19	0.76	5760
R_R		0.12	0.11	3.00	0.66	3840
R_{CWD}	1	1.03	0.12	3.44	0.72	576
	2	1.30	0.10	2.62	0.81	576
	3	3.25	0.07	2.06	0.73	576
	4	3.43	0.10	2.81	0.76	576
	5	3.03	0.10	2.59	0.82	576
R_T		1.42	0.09	2.51	0.72	9600
R_L	Tree	3.52	0.07	1.98	0.65	1920
	Shrub	4.81	0.06	1.85	0.68	1920
	Herb	2.75	0.07	1.92	0.65	1920

3.3. Coarse Woody Debris (CWD) Respiration

There was a strong exponential correlation between the respiration of different CWD decay classes and temperature (Table 1). To estimate continuous CWD respiration in the *L. principis-rupprechtii* forest during 2010–2013, we calculated continuous CWD temperature using the model that simulated the relationship between the CWD temperature and the 10 cm soil temperature. The seasonal variation of the CWD respiration per volume indicated that the CWD respiration peaked in July and then followed a decreasing trend with time (Figure 2). We found significant differences in the CWD respiration among the different decay classes in 2010–2013. The maximum respiration across the four years, with a mean of 15.33 ± 1.32 μmol·m^{-3}·s^{-1}, appeared in decay class 4, which was more than 3 times higher than the minimum in decay class 1 (4.65 ± 0.37 μmol·m^{-3}·s^{-1}). Over time, the volume of different CWD decay classes increased (Table 2). The respiration of different CWD decay classes per unit ground area also increased over time, except for a slight decrease in 2012 (Table 2), which was consistent with the temperature of different CWD decay classes.

Table 2. Volume (m^3·ha^{-1}) and the respiration of different coarse woody debris (CWD) decay classes per ground area (g·C·m^{-2}·y^{-1}) during 2010–2013.

CWD Decay Classes		Year			
		2010	2011	2012	2013
1	Volume	16.83 (1.23)	17.90 (1.51)	18.17 (1.31)	19.21 (1.62)
	Respiration	2.85 (0.23)	3.06 (0.18)	3.02 (0.26)	3.31 (0.28)
2	Volume	14.64 (1.18)	14.90 (1.22)	15.89 (1.08)	16.41 (1.33)
	Respiration	3.03 (0.17)	3.12 (0.25)	3.21 (0.23)	3.49 (0.27)
3	Volume	8.95 (0.82)	9.28 (0.78)	9.40 (0.68)	9.82 (0.72)
	Respiration	2.84 (0.23)	2.97 (0.18)	2.94 (0.23)	3.16 (0.22)
4	Volume	6.39 (0.51)	6.63 (0.48)	6.71 (0.53)	7.03 (0.38)
	Respiration	3.69 (0.19)	3.88 (0.26)	3.80 (0.31)	4.16 (0.34)
5	Volume	5.11 (0.31)	5.30 (0.28)	5.38 (0.38)	5.65 (0.27)
	Respiration	2.16 (0.16)	2.27 (0.21)	2.23 (0.27)	2.44 (0.26)
Total	Volume	51.92 (3.86)	54.01 (4.51)	55.55 (4.39)	58.12 (4.88)
	Respiration	14.57 (1.58)	15.30 (1.35)	15.20 (1.61)	16.56 (1.48)

Note: standard error is provided in brackets.

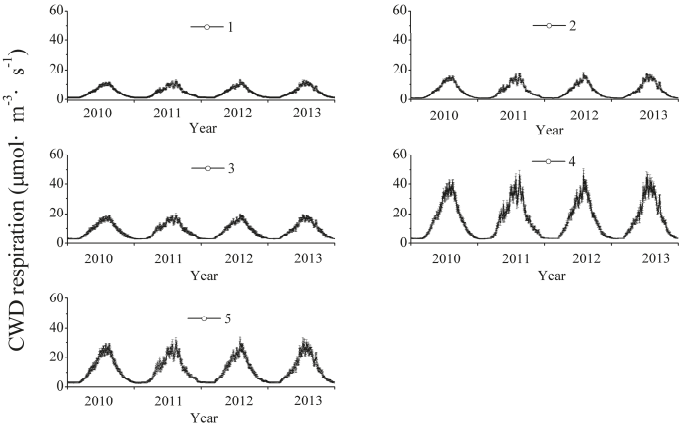

Figure 2. The daily mean respiration of different coarse woody debris (CWD) decay classes in the *L. principis-rupprechtii* forest during 2010–2013. Error bars are based on 0.5 h soil temperatures as experimental unit (n = 48).

3.4. Stem Respiration

We found an exponential relationship between stem respiration and sapwood temperature, and the parameters are summarized in Table 1. Because sapwood temperature was not recorded for the whole year, we developed a correlation between sapwood temperature (y) and air temperature (x) ($y = 0.62385 + 0.88813x$, $R^2 = 0.98674$, $n = 108$, $p < 0.0001$). Stem respiration varied seasonally, with the lowest rate in February and the highest in July (Figure 3). Sapwood volume was 189.21 ± 12.31, 193.52 ± 11.08, 196.28 ± 15.57, and 215.21 ± 18.11 $m^3 \cdot ha^{-1}$ during 2010 to 2013, respectively. We estimated the stem respiration per unit of ground area as 33.52 ± 2.86, 34.68 ± 3.18, 34.12 ± 2.17, and 38.82 ± 3.22 $g \cdot C \cdot m^{-2} \cdot y^{-1}$ from 2010 to 2013, respectively.

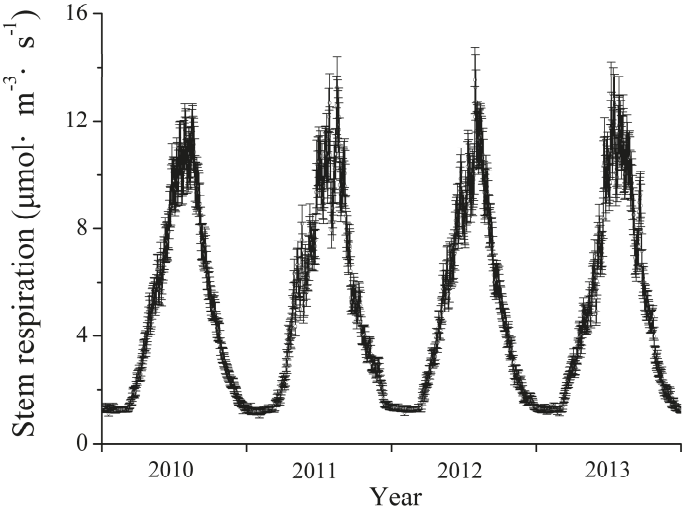

Figure 3. Daily mean stem respiration in the *L. principis-rupprechtii* forest during 2010–2013. Error bars are based on 0.5 h air temperatures as experimental unit (n = 48).

3.5. Leaf Respiration

The diurnal and seasonal variations in the leaf respiration rate related well with the corresponding variation in air temperature (Table 1). The minimum leaf respiration for trees, shrubs, and herbs all appeared in March, rose sharply until July, and then decreased until November (Figure 4). Shrub leaves per unit of biomass had slightly higher respiration than tree and herb leaves. Leaf biomass increased with time (Table 3), which was consistent with the LAI measured by LAI-2000. Cumulative leaf respiration per unit of ground area for trees, shrubs, and herbs indicated that tree leaves had higher respiration than shrub and herbaceous leaves (Table 3), corresponding mainly with the highest leaf biomass for trees. Over time, the leaf respiration per unit of ground area increased.

Table 3. Leaf dry biomass ($t \cdot ha^{-1}$) and leaf respiration per ground area ($g \cdot C \cdot m^{-2} \cdot y^{-1}$) for trees, shrubs, and herbs, and leaf area index (LAI) during 2010–2013.

Items		Year			
		2010	**2011**	**2012**	**2013**
Tree	Biomass	10.35 (0.86)	11.23 (0.78)	12.11 (1.14)	13.42 (1.21)
	Respiration	41.53 (3.89)	45.28 (4.15)	45.21 (3.71)	53.39 (4.82)
Shrub	Biomass	0.10 (0.04)	0.11 (0.03)	0.13 (0.02)	0.15 (0.01)
	Respiration	0.46 (0.03)	0.50 (0.04)	0.54 (0.06)	0.71 (0.08)
Herb	Biomass	0.42 (0.04)	0.45 (0.05)	0.48 (0.04)	0.51 (0.04)
	Respiration	1.28 (0.15)	1.37 (0.18)	1.40 (0.11)	1.56 (0.17)
All	Biomass	10.87 (1.04)	11.79 (0.82)	12.72 (1.14)	14.08 (1.31)
	Respiration	43.27 (3.92)	47.15 (4.27)	47.15 (4.11)	55.66 (4.52)
LAI		2.15 (0.56)	2.47 (0.62)	2.74 (0.46)	3.15 (0.48)

Note: standard error is provided in brackets.

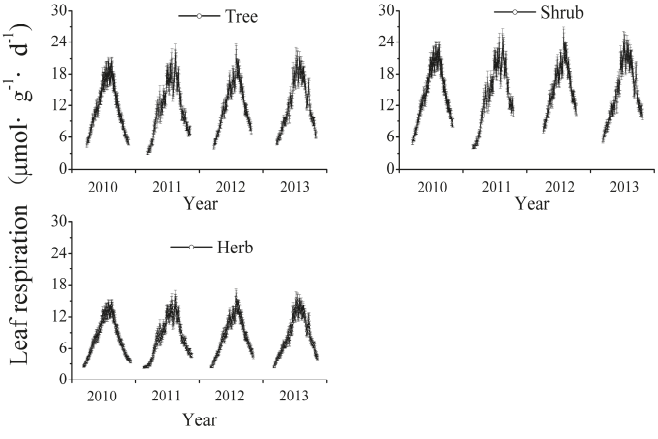

Figure 4. Daily mean leaf respiration for trees, shrubs, and herbs in the *L. principis-rupprechtii* forest during 2010–2013. Error bars are based on 0.5 h air temperatures as experimental unit (n = 48).

3.6. Ecosystem Respiration

The minimum ecosystem respiration appeared in January–March, rose sharply until July, and then decreased until winter (Figure 5). Ecosystem respiration ranged from 0.22 ± 0.02 to 7.86 ± 0.38 $\mu mol \cdot m^{-2} \cdot s^{-1}$ in 2010–2013. The component respiration demonstrated a similar seasonal variation with ecosystem respiration. Soil was the strongest source of annual respiration for the

ecosystem, which was approximately 50 times higher than the minimum respiration for CWD (Table 4). Soil, CWD, stem, leaf, and ecosystem respiration in 2013 was the highest among 2010–2013. Aboveground autotrophic respiration (stem + leaf respiration) comprised 10.26% of the total respiration, with leaf respiration slightly higher than stem respiration.

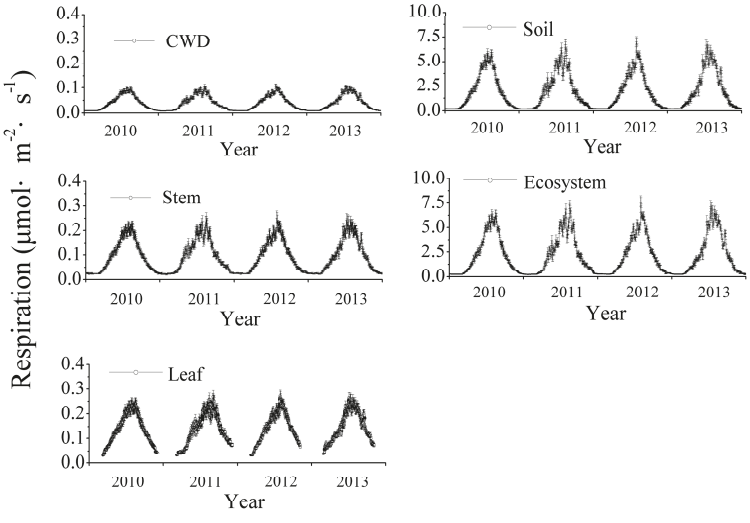

Figure 5. Daily mean soil, CWD, stem, leaf, and total ecosystem respiration in the *L. principis-rupprechtii* forest during 2010–2013. Error bars are based on 0.5 h soil temperatures and air temperatures as experimental unit, respectively (n = 48).

Table 4. Ecosystem respiration, component respiration ($g \cdot C \cdot m^{-2} \cdot y^{-1}$), and percentage (%) during 2010–2013 and the average over four years.

Year	Soil	CWD	Stem	Leaf	Ecosystem
2010	710.37 (20.14)	14.57 (1.58)	33.52 (2.86)	43.27 (3.92)	801.73 (58.67)
Percentage	88.60%	1.82%	4.18%	5.40%	100%
2011	721.45 (22.45)	15.30 (1.35)	34.68 (3.18)	47.15 (4.27)	818.58 (68.14)
Percentage	88.13%	1.87%	4.24%	5.76%	100%
2012	692.77 (19.64)	15.20 (1.61)	34.12 (2.17)	47.15 (4.11)	789.24 (51.55)
Percentage	87.78%	1.93%	4.32%	5.97%	100%
2013	737.27 (24.27)	16.56 (1.48)	38.82 (3.22)	55.66 (4.52)	848.31 (74.12)
Percentage	86.91%	1.95%	4.58%	6.56%	100%
Average	715.47 (28.48)	15.41 (1.72)	35.28 (4.78)	48.31 (5.24)	814.47 (64.22)
Percentage	87.85%	1.89%	4.33%	5.93%	100%

Note: standard error is provided in brackets.

3.7. Net Primary Productivity

The carbon content ratio was measured to calculate the carbon density, and the carbon content ratio was different in various components of vegetation in the *L. principis-rupprechtii* forest (Table S9). NPP was highest in 2013 (833.33 ± 80.14 $g \cdot C \cdot m^{-2} \cdot y^{-1}$), with an average of 817.16 ± 81.48 $g \cdot C \cdot m^{-2} \cdot y^{-1}$ in the *L. principis-rupprechtii* forest, of which ΔB_{living} and D_{total} accounted for 77.7%, and 22.3%, respectively (Table 5). NEE was the lowest in 2012 (-344.14 ± 22.32 $g \cdot C \cdot m^{-2} \cdot y^{-1}$), and the average in all years was -336.71 ± 25.15 $g \cdot C \cdot m^{-2} \cdot y^{-1}$, which revealed a carbon sink in the *L. principis-rupprechtii* forest.

Table 5. Annual net primary productivity (NPP) and net ecosystem exchange (NEE) during 2010–2013 ($g \cdot C \cdot m^{-2} \cdot y^{-1}$).

Items	2010	2011	2012	2013	Average
ΔB_{living}	656.48 (51.22)	623.35 (52.25)	605.88 (51.14)	654.15 (53.33)	634.97 (52.52)
D_{total}	155.04 (12.85)	190.82 (18.17)	203.76 (18.82)	179.18 (15.69)	182.19 (16.85)
NPP	811.52 (72.28)	814.17 (67.58)	809.64 (72.66)	833.33 (80.14)	817.16 (81.48)
NEE	−335.21 (20.52)	−329.93 (19.64)	−344.14 (22.32)	−337.55 (17.34)	−336.71 (25.15)

Note: standard error is provided in brackets.

3.8. Comparison between Biometric and Eddy Covariance Measurements

Eddy covariance measurements of NEE showed seasonal variation, with a maximum in November (2.71 ± 0.22 $g \cdot C \cdot m^{-2} \cdot d^{-1}$) and a minimum in August (-6.84 ± 0.56 $g \cdot C \cdot m^{-2} \cdot d^{-1}$) (Figure 6). Eddy covariance measurements of NEE from May to September were negative, which suggested a carbon sink during the growing season. Overall, eddy covariance measurements of NEE showed an average of -288.33 ± 25.26 $g \cdot C \cdot m^{-2} \cdot y^{-1}$ (-292.28 ± 18.17 $g \cdot C \cdot m^{-2} \cdot y^{-1}$, -281.02 ± 17.22 $g \cdot C \cdot m^{-2} \cdot y^{-1}$, -270.56 ± 20.21 $g \cdot C \cdot m^{-2} \cdot y^{-1}$, and -309.47 ± 24.37 $g \cdot C \cdot m^{-2} \cdot y^{-1}$ for 2010 to 2013, respectively), which indicated a sink at this site. These numbers are close to the results from the biometric measurements but average 14% higher. Based on eddy covariance measurements, annual ecosystem respiration was estimated as 780.37 ± 82.18 $g \cdot C \cdot m^{-2} \cdot y^{-1}$ (759.12 ± 62.51 $g \cdot C \cdot m^{-2} \cdot y^{-1}$, 766.38 ± 71.17 $g \cdot C \cdot m^{-2} \cdot y^{-1}$, 781.49 ± 64.82 $g \cdot C \cdot m^{-2} \cdot y^{-1}$, and 814.48 ± 75.18 $g \cdot C \cdot m^{-2} \cdot y^{-1}$ for 2010 to 2013, respectively). Daily mean ecosystem respiration based on chamber measurements and eddy covariance measurements are plotted in Figure 7. The curve shows a good correlation between these two measurement methods, with $R^2 = 0.93$.

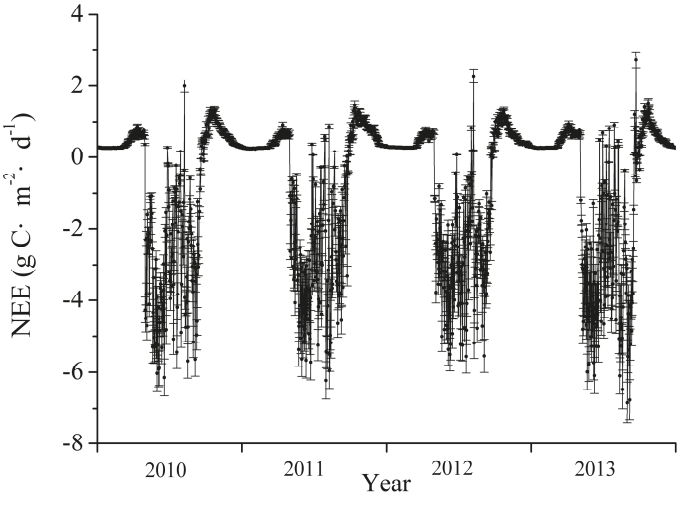

Figure 6. Eddy covariance measurements of NEE in the *L. principis-rupprechtii* forest. Data are daily mean NEE during 2010–2013. Error bars are based on 0.5 h eddy covariance measurements of NEE as experimental unit ($n = 48$).

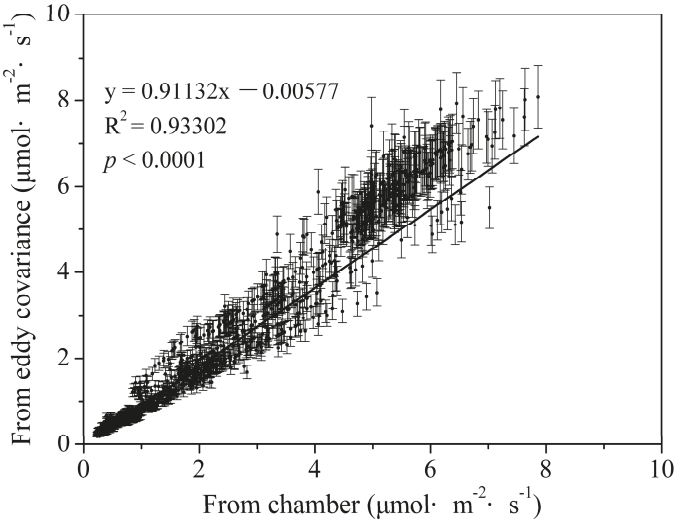

Figure 7. Comparison between chamber-based and eddy covariance measurements of ecosystem respiration. Data are daily mean respiration during 2010–2013. The solid line indicates a linear fit.

4. Discussion

The seasonal variation of component respiration was driven by temperature, and temperature was strongly exponentially correlated with component respiration. This conclusion has been reported in several studies [16,26]. According to our analysis, the ecosystem respiration based on eddy covariance measurements was also exponentially related to the air temperature, explaining 94% of the variability in the ecosystem respiration (Figure S10).

Biometric-based flux measurements combined with spatial and temporal upscaling allowed us to estimate the respiration of each component of the ecosystem. The CO_2 flux of soil from our site was higher than that from a mature temperate mixed forest in the Changbai Mountains (0.49–4.12 μmol·m^{-2}·s^{-1}), which may be due to the higher temperature at our site (Annual average temperature is 3.6 °C in the Changbai Mountains) [26]. Soil respiration is influenced by many factors, including abiotic factors, such as the soil temperature, soil moisture, rainfall, and soil C/N, and biotic factors, such as vegetation cover, litter thickness on the ground, fine root mass, soil organic matter, soil characteristics, leaf area index, and human activities. A number of studies concluded that soil moisture is an important factor influencing soil respiration [42–44]. However, a comparison of recent findings in this region showed that soil moisture had little impact on soil respiration relative to in situ temperature. An adequate soil moisture level may explain the non-significant influence of soil moisture on soil respiration [26]. The Q_{10} value was the highest in soil respiration, with a value of 4.19, which revealed that there was a stronger sensitivity of soil respiration to temperature in different component respirations, which was different from other ecosystems. For example, Raich and Schlesinger reviewed global soil respiration values and found a median Q_{10} value of 2.4 [45]. In a temperate mixed-hardwood forest, the Q_{10} value ranged from 3.4 to 5.6 [46]. The Q_{10} value ranged from 1.93 to 4.80 in different vegetation communities in the Belgian Campine region [47]. Moreover, Cao et al. reported Q_{10} values of 2.75 and 3.22 in an alpine meadow on the Tibetan Plateau of China [48]. Wu et al. reported a value of 4.07 in the Changbai Mountains of China [49]. On the eastern part of the Loess Plateau of China, the Q_{10} value ranged from 2.37 to 5.53 [50]. The various Q_{10} values reported in different ecosystems may be due to both methodology and differences in biotic and abiotic factors that affect soil respiration differently [50].

Whole-ecosystem respiration is dominated by soil respiration in forests [4]. Soil respiration has been found to account for 30–90% of total ecosystem respiration in temperate forests [13], and our result was close to the upper limit, at 87.85%. The percentage of soil respiration was higher, possibly due to the lower precipitation (600 mm) at our site, but there were lower nutrients in the soil (sandy loam) at a Michigan site and in a ponderosa pine forest in Oregon (76%) [37]. Total soil respiration is always regarded as a critical component of the carbon balance of an ecosystem. The estimated annual soil respiration was 715.47 ± 28.48 $g{\cdot}C{\cdot}m^{-2}{\cdot}y^{-1}$, which was similar to that reported by Raich and Schlesinger for temperate coniferous forests, at 681 ± 95 $g{\cdot}C{\cdot}m^{-2}{\cdot}y^{-1}$ [45]. Other ecosystems reported various values for soil respiration, including 600–700 $g{\cdot}C{\cdot}m^{-2}{\cdot}y^{-1}$ in beech forests in France [51], 485 $g{\cdot}C{\cdot}m^{-2}{\cdot}y^{-1}$ in hardwood forests in the USA [52], 581 $g{\cdot}C{\cdot}m^{-2}{\cdot}y^{-1}$ in a warm-temperate mixed forest in Japan [53], 963.98 $g{\cdot}C{\cdot}m^{-2}{\cdot}y^{-1}$ in a Korean pine and broadleaf mixed forest in China [54], and 454 $g{\cdot}C{\cdot}m^{-2}{\cdot}y^{-1}$ in a tropical seasonal rainforest in China [55]. These different results demonstrate that soil respiration is closely related to vegetation and climate.

In our study, leaf respiration was second in magnitude among the respiration fractions. This result is consistent with that of previous studies [5,26]. However, the leaf respiration at our site was lower than that in an old-growth hardwood forest (114.85 $g{\cdot}C{\cdot}m^{-2}{\cdot}y^{-1}$) and a hemlock forest (72.20 $g{\cdot}C{\cdot}m^{-2}{\cdot}y^{-1}$) in the USA [16]. Moreover, Law et al. compared leaf respiration in young (124 $g{\cdot}C{\cdot}m^{-2}{\cdot}y^{-1}$) and old (136 $g{\cdot}C{\cdot}m^{-2}{\cdot}y^{-1}$) ponderosa pine forests of the USA [56], which were all higher than ours. In the present study, this lower leaf respiration may have been caused by (1) the lower annual mean LAI (4.1 in the hardwood forest and 3.8 in the hemlock forest), (2) reduced air temperature and photosynthetic active radiation [57], or (3) decreased foliage N and chlorophyll concentrations [37]. In addition, both the canopy position and foliage age had significant effects on leaf respiration [12].

Because of difficulties in measurement, little attention was paid to stem respiration in the past. However, with increasing atmospheric CO_2 concentrations and as an important part of the annual carbon balance of forest ecosystems, studies of stem respiration have generated active debate. Stem respiration was strongly correlated with temperature, and the Q_{10} value at our site was similar to that of other ecosystems. For example, in a *Pinus koraiensis* forest in China, the Q_{10} value ranged from 2.56 to 3.32 [58]. In a temperate mixed forest in China, the Q_{10} value ranged from 1.86 to 2.41 [26]. Ryan et al. reported that the Q_{10} value ranged from 1.3 to 1.9 in four conifer forests in the USA [59]. According to our study, stem respiration was slightly lower than leaf respiration, which was consistent with others [5,26,37,38]. However, the stem respiration at our site was much lower than those in an old-growth hardwood forest (130.5 $g{\cdot}C{\cdot}m^{-2}{\cdot}y^{-1}$) and a hemlock forest (206.5 $g{\cdot}C{\cdot}m^{-2}{\cdot}y^{-1}$) in the USA [16], which may be due to lower sapwood volume (296.3 $m^3{\cdot}ha^{-1}$ in the hardwood forest and 448.5 $m^3{\cdot}ha^{-1}$ in the hemlock forest). In addition, stem respiration is influenced by numerous factors, including meteorological factors (e.g., stem temperature, CO_2 concentration, and humidity) and biological factors (tree species, tree age, diameter at breast height, sapwood size, and nitrogen content in the stem). Latitude, altitude, and topographic factors indirectly influence respiration rates through meteorological or biological factors [60]. Moreover, scaling up based on measurements of the stem respiration rate and sapwood volume may underestimate total stem respiration rates because younger woody tissues have higher respiration rates [38]. Future studies are required to develop a more accurate scaling-up scheme.

In general, CWD has high ecological relevance, contributes significantly to crucial ecological processes in forest ecosystems, and plays an essential role in carbon pools [61]. Furthermore, CWD respiration as a component of ecosystem respiration is essential to determining a forest's carbon budget [62]. However, few studies of CWD respiration have been conducted in most forest types [63]. In particular, quantification of the contribution of CWD respiration to total ecosystem respiration in the Qinling Mountains has not been previously conducted. Our study showed that the seasonality of CWD respiration was mainly driven by the CWD temperature and showed an overall bell-shaped curve for all five decay classes. This conclusion is corroborated by previous studies [64,65]. The Q_{10} ranged from 1.7 to 4.1 for different decay classes in various ecosystems [62,65], and our result fell within this range.

Moreover, Wu et al. reported that the Q_{10} value ranged from 2.41 to 2.95 in the Changbai Mountains of China [66]. In a montane moist evergreen broadleaf forest of China, the Q_{10} value ranged from 1.73 to 2.08 [67]. Furthermore, the Q_{10} value was significantly affected by the temperature ranges. For example, the Q_{10} value was 4.1 for 5–20 °C and 1.7 for 20–42 °C in a boreal black spruce forest in Canada [65].

CWD respiration is a complex process that depends on many factors, including tree species, temperature, moisture, substrate quality, diameter class, and decomposer type [68,69]. According to our study, the annual CWD respiration was much lower than that in an old-growth Amazonian forest (171.8 $g{\cdot}C{\cdot}m^{-2}{\cdot}y^{-1}$) [70], which may be mainly caused by the reduced CWD biomass at our site. Meanwhile, the annual CWD respiration was slightly lower than that in an old-growth hardwood forest (43 $g{\cdot}C{\cdot}m^{-2}{\cdot}y^{-1}$) and a hemlock forest (29 $g{\cdot}C{\cdot}m^{-2}{\cdot}y^{-1}$) in the USA [16]. The reason for higher annual CWD respiration in hardwood and hemlock forests may be the surface area of CWD for upscaling [16]. In our study, we quantified the CWD into five decay classes. The CWD respiration rates measured per unit volume might underestimate the CWD respiration rates, whereas CWD respiration rates measured per unit surface area might overestimate the CWD respiration rates. A large log may have large volume but smaller surface area than many small logs. As such, the conversion of CWD respiration rates measured per unit area to rates per unit volume might be more appropriate to CWD respiration in this forest. Moreover, to upscale chamber measurements of CWD respiration to the stand level, the volume was more convenient and accurate than the surface area. Measuring the CWD respiration accurately is important for estimating forest ecosystem respiration. Thus, further research should be done by using the surface area or volume of CWD for upscaling. In addition, future studies are necessary to measure CWD respiration in different diameter classes.

Daily mean ecosystem respiration measured from eddy covariance and chamber methods was shown in Figure 7. The eddy covariance (y) and chamber (x) methods were in better agreement after adjusting the CO_2 flux in this forest using the equation $y = 0.91132x - 0.00577$ (Figure 7). The comparisons between chamber and eddy covariance ecosystem respiration measurements were more consistent than in other studies [71,72]. Our result showed that the daily mean ecosystem respiration upscaled from chamber measurements agreed well with eddy covariance measurements, with $R^2 = 0.93$, which was similar to that of an old-growth forest in the Great Lakes region of the USA [16], with $R^2 = 0.96$, although some studies suggested that the result from chamber measurements was higher than that from eddy covariance measurements [37,73].

An annual average ecosystem respiration of 780.37 ± 82.18 $g{\cdot}C{\cdot}m^{-2}{\cdot}y^{-1}$ was calculated from eddy covariance measurements. Based on chamber measurements, the corresponding value was 814.47 ± 64.22 $g{\cdot}C{\cdot}m^{-2}{\cdot}y^{-1}$. Our result is very close to that in a boreal black spruce forest in Canada, which had a range of 790–890 $g{\cdot}C{\cdot}m^{-2}{\cdot}y^{-1}$ [74]. However, ecosystem respiration from our site was much lower than that from old-growth Amazon tropical forests, with an estimate of 2337.6 $g{\cdot}C{\cdot}m^{-2}{\cdot}y^{-1}$ [75]. Higher temperatures, longer growing seasons, and higher photosynthesis and growth rates in tropical forests may explain the higher respiration than that from our temperate coniferous forests.

Our study found that the annual average ecosystem respiration measured by the chamber method was 5% higher than that measured by the eddy covariance. The error sources for explaining this discrepancy are complicated. Firstly, chambers may disturb the environment and alter CO_2 concentrations, as well as pressure gradients, turbulent fluctuations, and air flow. Thus, they may interfere with the production and transport of CO_2 [26]. Closed chambers completely cover the ecosystem during the measurement process and thereby alter the natural long-wave radiation balance to almost zero. This causes reduced surface cooling, weak development of stable stratification, and, finally, higher respiration than those obtained via eddy covariance measurements [76]. Secondly, our annual average ecosystem respiration estimates based on chamber measurements may have uncertainties. One possible source of uncertainty is in the method of extrapolating a temperature-respiration relationship to the winter. Under a 95% confidence interval, the uncertainties

in predicting daily mean soil respiration, CWD respiration, stem respiration, and leaf respiration averaged 10%, 8%, 12%, and 14%, respectively, of the predicted values. The uncertainties may also derive from the estimation of CWD and stem volumes, the dry leaf biomass, and the chamber upscaling processes. Thirdly, nocturnal eddy covariance measurements with low friction velocity, extrapolation of nighttime respiration to daytime respiration may underestimate the ecosystem respiration by the eddy covariance method. Annual NEE estimates were as high as -336.71 ± 25.15 g·C·m^{-2}·y^{-1} from biometric measurements but -288.33 ± 25.26 g·C·m^{-2}·y^{-1} from eddy covariance measurements. Our results revealed that this site was a carbon sink, which was consistent with the findings of Zhou et al. [11]; they found that a carbon sink in a *L. principis-rupprechtii* forest in China was -271 g·C·m^{-2}·y^{-1}. Meanwhile, our estimations of NEE fall well within the range reported between -70 and -740 g·C·m^{-2}·y^{-1} for temperate forests [15,77].

Our study found that the NEE measured by the eddy covariance method was 14% higher than that measured by the biometric, which is consistent with Wang et al. [26]. However, our study showed that the discrepancy was lower than that of Wang et al. (22.5%), and the mean difference (48.38 ± 9.67 g·C·m^{-2}·y^{-1}) was also lower than that of temperate forests (100 g·C·m^{-2}·y^{-1}) [78], which indicated that these two methods had good agreement in measuring the NEE in this forest. However, there was still a discrepancy between the biometric and eddy covariance measurements, which may be due to the complicated error sources.

The error in the result from both biometric and eddy covariance was associated with sampling methods of flux measurement [30]. Ehman et al. concluded that the largest error source in the biometric method may be attributable to sampling (that is, inter-plot variability) [79]. All natural ecosystems are heterogeneous at some scale, and so the question arises whether estimation of fluxes based on a limited number of samples represents the average of the total ecosystem. In our study, the sampling error included estimating the NPP for sampling the trees, shrubs, herbs, fine roots, and litterfall. Additionally, we used soil collars to measure R_S and R_R and sampled the CWD to measure R_{CWD}, which all may produce the sampling error. In addition, Ohtsuka et al. considered that the topography may introduce sampling errors when estimating the NEE based on the eddy covariance method [30].

Another error was more likely to be related to estimation of NPP. Although Ohtsuka et al. deemed annual forest census within a large permanent plot and adequate number of litter traps for detritus production to be the most suitable method for measuring NPP [30], there were still some uncertainties. One possible uncertainty was derived from the biomass regression model. Under a 95% confidence interval, the uncertainties in predicting tree and shrub biomass averaged 8% and 14%, respectively, of the predicted values. Clark et al. considered that using off-site allometric equations could alter NPP by as much as 20% [80]. Also, these allometric relationships do not take into account seasonal changes in wood C concentration that may occur. Our study showed that the carbon content ratio values were diverse among varying plant species and different organs in the same plant (Table S9). However, many researchers used 50% as the carbon content ratio [81,82], which would overestimate the NPP by 7.4% in this forest. D_{total} is an important component of NPP; a study by Curtis et al. revealed that the detritus made up nearly two-thirds of the annual C production [77]. However, in our study, we found the D_{total} accounted for less than a quarter of NPP. CWD as a part of D_{total} can be difficult to measure precisely due to the heterogeneous distribution of forest floor detritus [79,80,83], which was the largest source of uncertainty in the estimation of NPP. However, we have adequately quantified annual variability in CWD production according to the annual forest census. Moreover, underestimation could have been caused by minor NPP components typically neglected (for example, root exudation, net accumulation of non-structural carbohydrates, herbivory consumption, production of volatile organic compounds [78,80]), which in general contribute between 1% and 4% of NPP [84]. In addition, Ohtsuka et al. considered that the estimation of R_{CWD} represented a critical source of potential error [30]; few studies have measured the R_{CWD}. Ehman et al. reported the R_{CWD} was 7% of R_S [79], but this proportion was only 2% in our study. We quantified the CWD into five decay classes to obtain more accurate measurements of R_{CWD}. However, the respirations of CWD at different diameter

classes and fine woody debris (1 cm $\leq$ diameter < 10 cm) were not measured, which may result in a lower observed R_{CWD} at this site.

The permanent plot was protected by an enclosure, and this site was level (a mean slope of 5°), and the overstory and understory of the forest were homogeneous, which are ideal conditions for measuring the NEE using the eddy covariance method in this forest. However, there were still error sources for measuring the NEE based on eddy covariance measurements. In our study, these eddy covariance error sources mainly include a double-directional interpolation model of artificial neural networks (ANNs) to fill the gaps, nocturnal low friction velocity, and the extrapolation of nighttime respiration from the eddy covariance measurements to daytime respiration.

5. Conclusions

This paper presents the first set of results (2010–2013) from a long-term project measuring forest-atmosphere CO_2 exchanges using eddy covariance and biometric methods simultaneously in a *L. principis-rupprechtii* forest. In our study, temperature was the primary controlling factor for respiration in this forest. Exponential functions explained most of the observed temporal variations in respiration in response to temperature. Based on the chamber upscale processes, we obtained the cumulative annual ecosystem respiration (814.47 $\pm$ 64.22 g·C·m^{-2}·y^{-1}), but this number was 5% higher than that from the eddy covariance measurements. We considered this small discrepancy to have arisen mainly because the respiration of CWD at different diameter classes and fine woody debris (1 cm $\leq$ diameter < 10 cm) was not measured due to the possible uncertainty in the method of extrapolating a temperature-respiration relationship to the winter and due to the uncertainties in the estimation of CWD and stem volumes, dry leaf biomass, and the chamber upscale processes.

Using measurements of the NPP (817.17 $\pm$ 81.48 g·C·m^{-2}·y^{-1}) combined with the heterotrophic respiration based on the chamber method (480.45 $\pm$ 52.24 g·C·m^{-2}·y^{-1}), we obtained the NEE ($-$336.71 $\pm$ 25.15 g·C·m^{-2}·y^{-1}) in this forest. This result was close to that from eddy covariance measurements ($-$288.33 $\pm$ 25.26 g·C·m^{-2}·y^{-1}), which indicated that these two methods had good agreement in measuring the NEE in this forest. In our study, we calibrated the instruments periodically, repeatedly measured a variety of respiration components for 4 years, reduced the disturbance of chamber measurements, quantified the CWD into five decay classes, and measured the carbon content ratio of various components, all of which can enhance the consistency of the eddy covariance and the biometric fluxes. However, there was still a 14% discrepancy between the biometric and eddy covariance measurements, which may be due to the complicated error sources. Thus, more detailed experiments and related theoretical studies are needed in the future.

Supplementary Materials: The following are available online at http://www.mdpi.com/1999-4907/9/2/67/s1, Figure S1: Some photos of *L. principis-rupprechtii* forest and flux tower in this region, Table S1: The regression model of biomass, volume, and height of *L. principis-rupprechtii*, Table S2: The regression model of shrub biomass in the *L. principis-rupprechtii* forest, Table S3: CWD characteristics of different decay classes in forest system, Figure S2: The relationship between temperature of different CWD decay classes and 10 cm soil temperature, Figure S3: The relationship between air temperature and stem temperature, Figure S4: Daily mean air temperature and 10 cm soil temperature in the *L. principis-rupprechtii* forest during 2010–2013, Figure S5: Daily mean photosynthetically active radiation in the *L. principis-rupprechtii* forest during 2010–2013, Table S4: Average carbon content ratio of litterfall and various organs of trees, shrubs, and herbs in the *L. principis-rupprechtii* forest (%), Figure S6: The relationship between ecosystem respiration based on eddy covariance measurement and air temperature. Data shown are daily means during 2010–2013.

Acknowledgments: We are grateful to the Qinling National Forest Ecosystem Research Station for providing some data and the experimental equipment. This research was funded by the project "Technical management system for increasing the capacity of carbon sink and water regulation of mountain forests in the Qinling Mountains" (201004036) of the State Forestry Administration of China.

Author Contributions: J.Y. and S.Z. conceived and designed the experiments; J.Y., Z.H., and J.P. performed the experiments; J.Y. analyzed the data; L.H. contributed reagents/materials/analysis tools; J.Y. and S.J. wrote the paper.

Conflicts of Interest: The authors declare no conflict of interest.

References

1. Post, W.M.; Peng, T.H.; Emanuel, W.R.; King, A.W.; Dale, V.H.; Angelis, D.L. The global carbon cycle. *Am. Sci.* **1990**, *78*, 310–326.
2. Conway, T.J.; Tans, P.P.; Waterman, L.S.; Thoning, K.W.; Kitzis, D.R.; Masarie, K.A.; Ni, Z. Evidence for interannual variability of the carbon cycle from the National Oceanic and Atmospheric Administration/Climate Monitoring and Diagnostics Laboratory Global Air Sampling Network. *J. Geophys. Res.* **1994**, *99*, 22831–22855. [CrossRef]
3. Houghton, R.; Hackler, J.; Lawrence, K. The US carbon budget: Contributions from land-use change. *Science* **1999**, *285*, 574–578. [CrossRef] [PubMed]
4. Bolstad, P.; Davis, K.; Martin, J.; Cook, B.; Wang, W. Component and whole-system respiration fluxes in northern deciduous forests. *Tree Physiol.* **2004**, *24*, 493–504. [CrossRef] [PubMed]
5. Guan, D.X.; Wu, J.B.; Zhao, X.S.; Han, S.J.; Yu, G.R.; Sun, X.M.; Jin, C.J. CO_2 fluxes over an old, temperate mixed forest in northeastern China. *Agric. For. Meteorol.* **2006**, *137*, 138–149. [CrossRef]
6. Kang, Y.X.; Chen, Y.P. Woody plant flora of Huoditang forest region. *J. Northwest For. Coll.* **1996**, *11*, 1–10. (In Chinese)
7. Schröter, D.; Cramer, W.; Leemans, R.; Prentice, I.C.; Araújo, M.B.; Arnell, N.W.; Bondeau, A.; Bugmann, H.; Carter, T.R.; Gracia, C.A.; et al. Ecosystem service supply and vulnerability to global change in Europe. *Science* **2005**, *310*, 1333–1337. [CrossRef] [PubMed]
8. Etzold, S.; Ruehr, N.K.; Zweifel, R.; Dobbertin, M.; Zingg, A.; Pluess, P.; Häsler, R.; Eugster, W.; Buchmann, N. The carbon balance of two contrasting mountain forest ecosystems in Switzerland: Similar annual trends, but seasonal differences. *Ecosystems* **2011**, *14*, 1289–1309. [CrossRef]
9. Leng, W.; He, H.S.; Bu, R.; Dai, L.; Hu, Y.; Wang, X. Predicting the distributions of suitable habitat for three larch species under climate warming in Northeastern China. *For. Ecol. Manag.* **2008**, *254*, 420–428. [CrossRef]
10. Lei, R.D.; Dang, K.L.; Zhang, S.X.; Tan, F.L. Effect of a *Larix principis-rupprechtii* forest plantation on soil in middle zone of south-facing slope of the Qinling mountains. *Sci. Silvae Sin.* **1997**, *33*, 463–470. (In Chinese)
11. Zhou, Y.R.; Yu, Z.L.; Zhao, S.D. Carbon storage and budget of major Chinese forest types. *Chin. J. Plant Ecol.* **2000**, *24*, 518–522. (In Chinese)
12. Brooks, J.R.; Hinckley, T.M.; Ford, E.D.; Sprugel, D.G. Foliage dark respiration in Abies amabilis (Dougl.) Forbes: Variation within the canopy. *Tree Physiol.* **1991**, *9*, 325–338. [CrossRef] [PubMed]
13. Valentini, R.; Matteucci, G.; Dolman, A.J.; Schulze, E.D.; Rebmann, C.; Moors, E.J.; Granier, A.; Gross, P.; Jensen, N.O.; Pilegaard, K.; et al. Respiration as the main determinant of carbon balance in European forests. *Nature* **2000**, *404*, 861–865. [CrossRef] [PubMed]
14. Malhi, Y.; Baldocchi, D.D.; Jarvis, P.G. The carbon balance of tropical, temperate and boreal forests. *Plant Cell Environ.* **1999**, *22*, 715–740. [CrossRef]
15. Baldocchi, D.D.; Wilson, K.B. Modeling CO_2 and water vapor exchange of a temperate broadleaved forest across hourly to decadal time scales. *Ecol. Model.* **2001**, *142*, 155–184. [CrossRef]
16. Tang, J.; Bolstad, P.V.; Desai, A.R.; Martin, J.G.; Cook, B.D.; Davis, K.J.; Carey, E.V. Ecosystem respiration and its components in an old-growth forest in the Great Lakes region of the United States. *Agric. For. Meteorol.* **2008**, *148*, 171–185. [CrossRef]
17. Khomik, M.; Arain, M.A.; Brodeur, J.J.; Peichl, M.; Restrepo Coupé, N.; Mclaren, J.D. Relative contributions of soil, foliar, and woody tissue respiration to total ecosystem respiration in four pine forests of different ages. *J. Geophys. Res. Biogeosci.* **2015**, *115*, 4209–4224. [CrossRef]
18. Grace, J.; Lloyd, J.; Mcintyre, J.; Miranda, A.C.; Meir, P.; Miranda, H.S.; Nobre, C.; Moncrieff, J.; Massheder, J.; Malhi, Y. Carbon dioxide uptake by an undisturbed tropical rain forest in southwest Amazonia, 1992 to 1993. *Science* **1995**, *270*, 778–780. [CrossRef]
19. Black, T.A.; Den Hartog, G.; Neumann, H.H.; Blanken, P.D.; Yang, P.C.; Russell, C.; Nesic, Z.; Lee, X.; Chen, S.G.; Staebler, R.; et al. Annual cycles of water vapour and carbon dioxide fluxes in and above a boreal aspen forest. *Glob. Chang. Biol.* **1996**, *2*, 219–229. [CrossRef]
20. Luyssaert, S.; Reichstein, M.; Schulze, E.D.; Janssens, I.A.; Law, B.E.; Papale, D.; Dragoni, D.; Goulden, M.L.; Granier, A.; Kutsch, W.L. Toward a consistency cross-check of eddy covariance flux-based and biometric estimates of ecosystem carbon balance. *Glob. Biogeochem. Cycles* **2009**, *23*, 1159–1171. [CrossRef]

21. Speckman, H.N.; Frank, J.M.; Bradford, J.B.; Miles, B.L.; Massman, W.J.; Parton, W.J.; Ryan, M.G. Forest ecosystem respiration estimated from eddy covariance and chamber measurements under high turbulence and substantial tree mortality from bark beetles. *Glob. Chang. Biol.* **2015**, *21*, 708–721. [CrossRef] [PubMed]
22. Goulden, M.L.; Munger, J.W.; Fan, S.M.; Daube, B.C.; Wofsy, S.C. Exchange of carbon dioxide by a deciduous forest: Response to interannual climate variability. *Science* **1996**, *271*, 1576–1578. [CrossRef]
23. Billesbach, D. Estimating uncertainties in individual eddy covariance flux measurements: A comparison of methods and a proposed new method. *Agric. For. Meteorol.* **2011**, *151*, 394–405. [CrossRef]
24. Davidson, E.; Savage, K.; Verchot, L.; Navarro, R. Minimizing artifacts and biases in chamber-based measurements of soil respiration. *Agric. For. Meteorol.* **2002**, *113*, 21–37. [CrossRef]
25. Myklebust, M.C.; Hipps, L.E.; Ryel, R.J. Comparison of eddy covariance, chamber, and gradient methods of measuring soil CO_2 efflux in an annual semi-arid grass, Bromus tectorum. *Agric. For. Meteorol.* **2008**, *148*, 1894–1907. [CrossRef]
26. Wang, M.; Guan, D.X.; Han, S.J.; Wu, J.L. Comparison of eddy covariance and chamber-based methods for measuring CO_2 flux in a temperate mixed forest. *Tree Physiol.* **2010**, *30*, 149–163. [CrossRef] [PubMed]
27. Dou, Z.Y.; Liu, J.J. Application of artificial neural networks to interpolation and extrapolation of flux data. *J. Northwest For. Univ.* **2009**, *24*, 58–62. (In Chinese)
28. Chen, C.G.; Peng, H. Standing crops and productivity of the major forest-types at the Huoditang forest region of the Qinling Mountains. *J. Northwest For. Coll.* **1996**, *11*, 92–102. (In Chinese, with English Abstract)
29. Rieger, I.; Lang, F.; Kleinschmit, B.; Kowarik, I.; Cierjacks, A. Fine root and aboveground carbon stocks in riparian forests: The roles of diking and environmental gradients. *Plant Soil* **2013**, *370*, 497–509. [CrossRef]
30. Ohtsuka, T.; Mo, W.; Satomura, T.; Inatomi, M.; Koizumi, H. Biometric based carbon flux measurements and net ecosystem production (NEP) in a temperate deciduous broad-leaved forest beneath a flux tower. *Ecosystems* **2007**, *10*, 324–334. [CrossRef]
31. Stenberg, P.; Linder, S.; Smolander, H.; Flower-Ellis, J. Performance of the LAI-2000 plant canopy analyzer in estimating leaf area index of some Scots pine stands. *Tree Physiol.* **1994**, *14*, 981–995. [CrossRef] [PubMed]
32. Cutini, A.; Matteucci, G.; Mugnozza, G.S. Estimation of leaf area index with the Li-Cor LAI 2000 in deciduous forests. *For. Ecol. Manag.* **1998**, *105*, 55–65. [CrossRef]
33. Munir, T.; Khadka, B.; Xu, B.; Strack, M. Partitioning forest-floor respiration into source based emissions in a boreal forested bog: Responses to experimental drought. *Forests* **2017**, *8*. [CrossRef]
34. Ringvall, A.; Ståhl, G. Field aspects of line intersect sampling for assessing coarse woody debris. *For. Ecol. Manag.* **1999**, *119*, 163–170. [CrossRef]
35. Yan, E.R.; Wang, X.H.; Huang, J.J.; Zeng, F.R.; Gong, L. Long-lasting legacy of forest succession and forest management, characteristics of coarse woody debris in an evergreen broad-leaved forest of eastern China. *For. Ecol. Manag.* **2007**, *252*, 98–107. [CrossRef]
36. Wenger, K.F. *Forestry Handbook*; John Wiley & Sons: New York, NY, USA, 1984.
37. Law, B.E.; Ryan, M.G.; Anthoni, P.M. Seasonal and annual respiration of a ponderosa pine ecosystem. *Glob. Chang. Biol.* **1999**, *5*, 169–182. [CrossRef]
38. Xu, M.; Debiase, T.A.; Qi, Y.; Goldstein, A.; Liu, Z. Ecosystem respiration in a young ponderosa pine plantation in the Sierra Nevada Mountains, California. *Tree Physiol.* **2001**, *21*, 309–318. [CrossRef] [PubMed]
39. Webb, E.K.; Pearman, G.I.; Leuning, R. Correction of flux measurements for density effects due to heat and water vapour transfer. *Q. J. R. Meteorol. Soc.* **1980**, *106*, 85–100. [CrossRef]
40. Cook, B.D.; Davis, K.J.; Wang, W.G.; Desai, A.; Berger, B.W.; Teclaw, R.M.; Martin, J.G.; Bolstad, P.V.; Bakwin, P.S.; Yi, C.X.; et al. Carbon exchange and venting anomalies in an upland deciduous forest in northern Wisconsin, USA. *Agric. For. Meteorol.* **2004**, *126*, 271–295. [CrossRef]
41. Desai, A.R.; Bolstad, P.V.; Cook, B.D.; Davis, K.J.; Carey, E.V. Comparing net ecosystem exchange of carbon dioxide between an old-growth and mature forest in the upper Midwest, USA. *Agric. For. Meteorol.* **2005**, *128*, 33–55. [CrossRef]
42. Rey, A.; Pegoraro, E.; Tedeschi, V.; De Parri, L.; Jarvis, P.G.; Valentini, R. Annual variation in soil respiration and its components in a coppice oak forest in central Italy. *Glob. Chang. Biol.* **2002**, *8*, 851–866. [CrossRef]
43. Curiel, Y.J.; Janssens, I.A.; Carrara, A.; Meiresonne, L.; Ceulemans, R. Interactive effects of temperature and precipitation on soil respiration in a temperate maritime pine forest. *Tree Physiol.* **2003**, *23*, 1263–1270.

44. Flanagan, L.B.; Johnson, B.G. Interacting effects of temperature, soil moisture and plant biomass production on ecosystem respiration in a northern temperate grassland. *Agric. For. Meteorol.* **2005**, *130*, 237–253. [CrossRef]
45. Raich, J.W.; Schlesinger, W.H. The global carbon dioxide flux in soil respiration and its relationship to vegetation and climate. *Tellus B* **1992**, *44*, 81–99. [CrossRef]
46. Davidson, E.A.; Belt, E.; Boone, R.D. Soil water content and temperature as independent or confounded factors controlling soil respiration in a temperate mixed hardwood forest. *Glob. Chang. Biol.* **1998**, *4*, 217–227. [CrossRef]
47. Curiel, Y.J.; Janssens, I.A.; Carrara, A.; Ceulemans, R. Annual Q_{10} of soil respiration reflects plant phonological patterns as well as temperature sensitivity. *Glob. Chang. Biol.* **2004**, *10*, 161–169. [CrossRef]
48. Cao, G.M.; Tang, Y.H.; Mo, W.H.; Wang, Y.S.; Li, Y.N.; Zhao, X.Q. Grazing intensity alters soil respiration in an alpine meadow on the Tibetan plateau. *Soil Biol. Biochem.* **2004**, *36*, 237–243. [CrossRef]
49. Wu, J.B.; Guan, D.X.; Wang, M.; Pei, T.F.; Han, S.J.; Jin, C.J. Year-round soil and ecosystem respiration in a temperate broad-leaved Korean Pine forest. *For. Ecol. Manag.* **2006**, *223*, 35–44. [CrossRef]
50. Li, H.J.; Yan, J.X.; Yue, X.F.; Wang, M.B. Significance of soil temperature and moisture for soil respiration in a Chinese mountain area. *Agric. For. Meteorol.* **2008**, *148*, 490–503. [CrossRef]
51. Granier, A.; Ceschia, E.; Damesin, C.; Dufrêne, E.; Epron, D.; Gross, P.; Lebaube, S.; Le Dantec, V.; Le Goff, N.; Lemoine, D.; et al. The carbon balance of a young Beech forest. *Funct. Ecol.* **2000**, *14*, 312–325. [CrossRef]
52. Simmons, J.A.; Fernandez, I.J.; Briggs, R.D.; Delaney, M.T. Forest floor carbon pools and fluxes along a regional climate gradient in Maine, USA. *For. Ecol. Manag.* **1996**, *84*, 81–95. [CrossRef]
53. Yuji, K.; Mayuko, J.; Masako, D.; Yoshiaki, G.; Koji, T.; Takafumi, M.; Yoichi, K.; Shinji, K.; Motonori, O.; Noriko, M.; et al. Biometric and eddy-covariance-based estimates of carbon balance for a warm-temperate mixed forest in Japan. *Agric. For. Meteorol.* **2008**, *148*, 723–737.
54. Wang, M.; Liu, Y.Q.; Hao, Z.Q.; Wang, Y.S. Respiration rate of broad-leaved Korean pine forest ecosystem in Changbai Mountain. *Chin. J. Appl. Ecol.* **2006**, *17*, 1789–1795. (In Chinese, with English Abstract)
55. Tan, Z.H.; Zhang, Y.P.; Yu, G.R.; Sha, L.Q.; Tang, J.W.; Deng, X.B.; Song, Q.H. Carbon balance of a primary tropical seasonal rain forest. *J. Geophys. Res.* **2010**, *115*, 411–454. [CrossRef]
56. Law, B.E.; Thornton, P.E.; Irvine, J.; Anthoni, P.M.; Van Tuyl, S. Carbon storage and fluxes in ponderosa pine forests at different developmental stages. *Glob. Chang. Biol.* **2001**, *7*, 755–777. [CrossRef]
57. Amthor, J.S. Higher plant respiration and its relationships to photosynthesis. *Ecophysiol. Photosynth.* **1993**, *100*, 71–102.
58. Wang, M.; Ji, L.Z.; Li, Q.R.; Xiao, D.M.; Liu, H.L. Stem respiration of Pinus koraiensis in Changbai Mountain. *Chin. J. Appl. Ecol.* **2005**, *16*, 7–13. (In Chinese, with English Abstract)
59. Ryan, M.G.; Gower, S.T.; Hubbard, R.M.; Waring, R.H.; Gholz, H.L.; Cropper, W.P., Jr.; Running, S.W. Woody tissue maintenance respiration of four conifers in contrasting climates. *Oecologia* **1995**, *101*, 133–140. [CrossRef] [PubMed]
60. Ma, Y.E.; Xiang, W.H.; Lei, P.F. Stem respiration and its controlling factors in forest ecosystems. *Chin. J. Plant Ecol.* **2007**, *31*, 403–412. (In Chinese, with English Abstract)
61. Gough, C.M.; Vogel, C.S.; Kazanski, C.; Nagel, L.; Flower, C.E.; Curtis, P.S. Coarse woody debris and the carbon balance of a north temperate forest. *For. Ecol. Manag.* **2007**, *244*, 60–67. [CrossRef]
62. Bond-Lamberty, B.; Wang, C.; Gower, S.T. Annual carbon flux from woody debris for a boreal black spruce fire chronosequence. *J. Geophys. Res.* **2002**, *108*, 8220–8230. [CrossRef]
63. Manies, K.L.; Harden, J.W.; Bond-Lamberty, B.; O'Neill, K.P. Woody debris along an upland chronosequence in boreal Manitoba and its impact on long-term carbon storage. *Can. J. For. Res.* **2005**, *35*, 472–482. [CrossRef]
64. Progar, R.A.; Schowalter, T.D.; Freitag, C.M.; Morrell, J.J. Respiration from coarse woody debris as affected by moisture and saprotroph functional diversity in Western Oregon. *Oecologia* **2000**, *124*, 426–431. [CrossRef] [PubMed]
65. Wang, C.K.; Bond-Lamberty, B.; Gower, S.T. Environmental controls on carbon dioxide flux from black spruce coarse woody debris. *Oecologia* **2002**, *132*, 374–381. [CrossRef] [PubMed]
66. Wu, J.B.; Guan, D.X.; Han, S.J.; Pei, T.F.; Shi, T.T.; Zhang, M. Respiration of fallen trees of Pinus koraiensis and Tilia amurensis in Changbai Mountain, northeastern China. *J. Beijing For. Univ.* **2008**, *30*, 14–19. (In Chinese, with English Abstract)

67. Zhang, S.B.; Zheng, Z.A. Preliminary research on respiration of woody debris of hollow-bearing tree in the montane moist evergreen broad-leaved forest of Ailao Mountain, Yunnan, China. *J. Mt. Sci. Engl.* **2008**, *26*, 300–307.
68. Weedon, J.T.; Cornwell, W.; Cornelissen, J.H.C.; Zanne, A.E.; Wirth, C.; Coomes, D.A. Global meta-analysis of wood decomposition rates, a role for trait variation among tree species? *Ecol. Lett.* **2009**, *12*, 45–56. [CrossRef] [PubMed]
69. Shorohova, E.; Ekaterina, K. Influence of the substrate and ecosystem attributes on the decomposition rates of coarse woody debris in European boreal forests. *For. Ecol. Manag.* **2014**, *315*, 173–184. [CrossRef]
70. Rice, A.H.; Pyle, E.H.; Saleska, S.; Hutyra, L.; Palace, M.; Keller, M.; De Camargo, P.B.; Portilho, K.; Marques, D.F.; Wofsy, S.C. Carbon balance and vegetation dynamics in an old growth Amazonian forest. *Ecol. Appl.* **2004**, *14*, 55–71. [CrossRef]
71. Cook, B.D.; Bolstad, P.V.; Martin, J.G.; Heinsch, F.A.; Davis, K.J.; Wang, W.G.; Desai, A.R.; Teclaw, R.M. Using light-use and production efficiency models to predict photosynthesis and net carbon exchange during forest canopy disturbance. *Ecosystems* **2008**, *11*, 26–44. [CrossRef]
72. Nagy, Z.; Pintér, K.; Pavelka, M.; Darenová, E.; Balogh, J. Carbon fluxes of surfaces vs. ecosystems: Advantages of measuring eddy covariance and soil respiration simultaneously in dry grassland ecosystems. *Biogeosciences* **2011**, *8*, 2523–2534. [CrossRef]
73. Goulden, M.L.; Munger, J.W.; Fan, S.M.; Daube, B.C.; Wofsy, S.C. Measurements of carbon sequestration by long-term Eddy covariance: Methods and a critical evaluation of accuracy. *Glob. Chang. Biol.* **1996**, *2*, 169–182. [CrossRef]
74. Goulden, M.L.; Wofsy, S.C.; Harden, J.W.; Trumbore, S.E.; Crill, P.; Gower, S.T.; Fries, T.; Daube, B.C.; Fan, S.M.; Sutton, D.J.; et al. Sensitivity of boreal forest carbon balance to soil thaw. *Science* **1998**, *279*, 214–217. [CrossRef] [PubMed]
75. Grace, J.; Malhi, Y.; Lloyd, J.; Mcintyre, J.; Miranda, A.C.; Meir, P.; Miranda, H.S. The use of eddy covariance to infer the net carbon dioxide uptake of Brazilian rain forest. *Glob. Chang. Biol.* **1996**, *2*, 209–217. [CrossRef]
76. Riederer, M.; Serafimovich, A.; Foken, T. Net ecosystem CO_2 exchange measurements by the closed chamber method and the eddy covariance technique and their dependence on atmospheric conditions. *Atmos. Meas. Tech.* **2014**, *7*, 1057–1064. [CrossRef]
77. Curtis, P.S.; Hanson, P.J.; Bolstad, P.; Barford, C.; Randolph, J.C.; Schmid, H.P.; Wilson, K.B. Biometric and eddy-covariance based estimates of annual carbon storage in five eastern north american deciduous forests. *Agric. For. Meteorol.* **2002**, *113*, 3–19. [CrossRef]
78. Campioli, M.; Malhi, Y.; Vicca, S.; Luyssaert, S.; Papale, D.; Peñuelas, J.; Reichstein, M.; Migliavacca, M.; Arain, M.A.; Janssens, I.A. Evaluating the convergence between eddy-covariance and biometric methods for assessing carbon budgets of forests. *Nat. Commun.* **2016**, *7*, 13717. [CrossRef] [PubMed]
79. Ehman, J.L.; Schmid, H.P.; Grimmond, C.S.B.; Randolph, J.C.; Hanson, P.J.; Wayson, C.A.; Cropley, F.D. An initial intercomparison of micrometeorological and ecological inventory estimates of carbon exchange in a mid-latitude deciduous forest. *Glob. Chang. Biol.* **2002**, *8*, 575–589. [CrossRef]
80. Clark, D.A.; Brown, S.; Kicklighter, D.W.; Chambers, J.Q.; Thomlinson, J.R.; Ni, J. Measuring net primary production in forests: Concepts and field methods. *Ecol. Appl.* **2001**, *11*, 356–370. [CrossRef]
81. Houghton, R.A.; Skole, D.L.; Nobre, C.A.; Hackler, J.L.; Lawrence, K.T.; Chomentowski, W.H. Annual fluxes of carbon from deforestation and regrowth in the Brazilian Amazon. *Nature* **2000**, *403*, 301–304. [CrossRef] [PubMed]
82. Fang, J.Y.; Chen, A.P.; Peng, C.H.; Zhao, S.Q.; Ci, L.J. Changes in forest biomass carbon storage in China between 1949 and 1998. *Science* **2001**, *292*, 2320–2322. [CrossRef] [PubMed]
83. Gough, C.M.; Vogel, C.S.; Schmid, H.P.; Su, H.B.; Curtis, P.S. Multi-year convergence of biometric and meteorological estimates of forest carbon storage. *Agric. For. Meteorol.* **2008**, *148*, 158–170. [CrossRef]
84. Vicca, S.; Luyssaert, S.; Peñuelas, J.; Campioli, M.; Chapin, F.S.; Ciais, P.; Heinemeyer, A.; Högberg, P.; Kutsch, W.L.; Law, B.E.; et al. Fertile forests produce biomass more efficiently. *Ecol. Lett.* **2012**, *15*, 520–526. [CrossRef] [PubMed]

forests

MDPI

Article

Carbon Mass Change and Its Drivers in a Boreal Coniferous Forest in the Qilian Mountains, China from 1964 to 2013

Shu Fang [1,2], Zhibin He [1,*], Jun Du [1], Longfei Chen [1], Pengfei Lin [1,2] and Minmin Zhao [1,2]

[1] Linze Inland River Basin Research Station, Chinese Ecosystem Research Network, Key Laboratory of Eco-hydrology of Inland River Basin, Northwest Institute of Eco-Environment and Resources, Chinese Academy of Sciences, Lanzhou 730000, China; fangs@lzb.ac.cn (S.F.); dujun159@126.com (J.D.); chenlongfei_mail@163.com (L.C.); linpengfei@lab.ac.cn (P.L.); zhaomm@lab.ac.cn (M.Z.)

[2] University of Chinese Academy of Sciences, Beijing 100049, China

* Correspondence: hzbmail@lzb.ac.cn; Tel.: +86-136-6930-4220

Received: 16 November 2017; Accepted: 22 January 2018; Published: 25 January 2018

Abstract: Carbon storage of mountain forests is vulnerable to climate change but the changes in carbon flux through time are poorly understood. Moreover, the relative contributions to carbon flux of drivers such as climate and atmospheric CO_2 still have significant uncertainties. We used the dynamic model LPJ-GUESS with climate data from twelve meteorological stations in the Qilian Mountains, China to simulate changes in carbon mass of a montane boreal forest, and the influence of temperature, precipitation, and CO_2 concentration from 1964 to 2013 on carbon flux. The results showed that the carbon mass has increased 1.202 kg/m^2 from 1964 to 2013, and net primary productivity (NPP) ranged from 0.997 to 1.122 kg/m^2/year. We concluded that the highest carbon mass proportion for this montane boreal forest was at altitudes 2700–3100 m (proportion of ecosystem carbon was between 93–97%), with maximum carbon density observed at 2700–2900 m. In the last 50 years, the increase in precipitation and in CO_2 concentration is expected to increase carbon mass and NPP of *Picea crassifolia* Kom. (Pinaceae) (Qinghai spruce). The effect of temperature on NPP was positive but that on carbon mass was not clear. The increase in CO_2 concentration over the past 50 years was a major contributor to the increase in carbon storage, and drought was the foremost limiting factor in carbon storage capacity of this montane boreal forest. *Picea crassifolia* forest was vulnerable to climate change. Further studies need to focus on the impact of extreme weather, especially drought, on carbon storage in *Picea crassifolia* forests.

Keywords: carbon mass; NPP; *Picea crassifolia*; climate change

1. Introduction

Climate change influences the carbon and water cycles in mountain areas [1]. Forests in mountain areas provide important ecological and socio-economic services; however, carbon storage is vulnerable to the effects of climate change and may decrease its ecological service function over time [2,3]. Research on the response of mountain ecosystems, especially of alpine forests and tree species, to climate change, is lacking [1,2]. Additionally, the impacts of climate change on montane forests are examined distinctively with dendroclimatic techniques [2–4]. High mountain boreal forests, which have numerous organic pools stored aboveground and in the permafrost, play an important role in regional carbon budgets and are exposed to rapid climate change; however, research on carbon pools at high elevations and controls on carbon flux through time lag behind [5,6] due primarily to insufficient data [7]. Ecosystem models are useful tools for describing and quantifying water, matter, and momentum fluxes between the biosphere and the atmosphere [8]. Using biomass models to

obtain mass data can facilitate simulation of forest carbon dynamics in areas where such data are lacking, while analyses of the montane boreal forest biome will improve the accuracy of global carbon models [3].

Climate change is primarily related to changes since the 1950s in solar radiation, temperature, and precipitation that have not been observed before [9]. Climate change and related disturbances may substantially impact the species ranges, population sizes, and extinction risks in mountain forests, and even shift the carbon sink activity of a forest to a net carbon source [10–12]. In a simulation of a species distribution in Mediterranean mountains, the cold-adapted species decreased in significance, and the species range and communities changed under global warming [13]. Extreme climates may change plant intrinsic characteristics and increase the possibility of mountain ecosystem shifts from forest to shrubland or grassland [14]. These climate change-induced species conversions will result in a long-term loss of carbon stock in mountain forest ecosystems [15]. One stark example of this was observed with mountain pine beetle in western North America; this insect outbreak, caused by climate change, compromised the ability of forests to take up and store carbon [12].

The response of mountain forests to climate change depends heavily on relative changes in temperature, precipitation, CO_2, and their interaction effect [10]; the relative contributions of individual historical drivers can be assessed by high-resolution climate data and modeling [16,17]. Sensitivity analyses of climate factors focused on tropical and temperate areas. However, analyses of the driving factors of carbon storage changes in recent years at high latitudes and in high elevation areas are still lacking [18]. The sensitivity to climate change of carbon storage in mountain forests is based on initial climatic variability; thus, increased mean annual temperature at high elevations results in sensitivity of tree growth and changes in forest productivity [3]. Examined by three ecological models (LPJ-GUESS, ForClim, LandClim), carbon storage across all elevations revealed a lower sensitivity than other ecosystem services to a 2 °C warming [19]. However, under the influence of global warming, mountain forests at high altitudes exhibited positive growth, whereas drought stress led to a negative effect on carbon mass at lower altitudes [4]. The impacts of climate change on mountain forests were also closely related to the frequency and intensity of extreme weather, especially precipitation-related events [5]. Extreme warming events may influence mountain boreal plant activity, plant litter production, soil moisture, and insect life cycles, while extreme weather events such as precipitation extremes and severe storms may lead to damage and may influence the recovery capacity of mountain boreal forest ecosystems [6]. Uncertainties exist as to the main climatic controls on carbon changes in long-term simulations of carbon mass in mountain forests [9,10]. Investigating carbon flux sensitivity to climate change will reduce the uncertainty of the past factors of climate change and help guide forest management. For a better understanding of the effects of climate change on boreal forests, it is necessary to quantify the driving parameters of carbon changes in boreal forests during the last 50 years.

The Qilian Mountains, located in the northwestern part of China at the north-eastern edge of the Tibetan Plateau, are typical arid mountains, and the source of key inland rivers; these mountains are sensitive to climate change [20]. The average temperature rise is 80% higher than the national rate (0.14 °C/10a), and extreme climate and precipitation events occurred more frequently here in the past 50 years than in other parts of China [21]. Under climate change, environmental degradation, soil erosion, and loss of biodiversity have increased, and vegetation cover and growth in the Qilian Mountains have changed significantly in recent years [22]. Montane Boreal forest is the dominant forest type, and it plays important roles in the hydrology and biogeochemistry of the area due to high altitudes (2000–5500 m) and minimal human-induced ecological deterioration [23]. Between 1957 and 2007, temperature increased by 0.29 °C/10a and precipitation by 5.5 mm/10a, resulting in a shift of the tree line of the montane boreal forest in this area to higher elevations [24]. Simple regression models of phenological dynamics in this montane boreal forest revealed that the length of the growing season can be expected to increase during the next two decades [25]. This prompted new research efforts to determine the relationships between montane boreal forest carbon dynamics and climate

change. Ecosystem stability of the montane boreal forest in the Qilian Mountains supports downstream economy and production because the forest serves as the most important water conservation entity in the area. Better understanding of the role of climate and atmospheric CO_2 in determining carbon flux in this montane boreal forest, and the relationship between the NPP and biomass is critical for guiding ecology policy to optimize carbon storage.

To address this knowledge need, we used climate and CO_2 concentration data to reconstruct carbon storage in living biomass for the montane boreal forest in the Qilian Mountains, China from 1964–2013. With this, we examined the carbon stock in this forest type at different elevations and its carbon flows during the last 50 years. Subsequently, we used the LPJ-GUESS model to explore the sensitivity of forest carbon stocks in this region to temperature, precipitation, CO_2, and extreme conditions to determine the main past factor controlling the change in carbon flux in the last 50 years.

2. Materials and Models

2.1. Area Description and Data Collection

The Qilian Mountains are one of the major arid mountain ranges in northwestern China, located in the northeastern Tibetan Plateau, between 93°33′36″–103°54′00″ E and 35°50′24″–40°01′12″ N. The distribution of vegetation is strongly controlled by altitude and can be separated into five types (from low to high altitude): desert steppe, forest steppe, sub-alpine shrubby meadow, alpine cold desert, and ice/snow zone. In the forest steppe, the montane boreal forest is located at high altitudes where the level of human impact is low [26]. The dominant boreal species, *Picea crassifolia*, grows on shady and partly-shady north slopes at altitudes ranging from 2600 to 3400 m, and accounts for as much as 76% of the total forested area in the forest steppe zone [27]. In total, twelve sampling sites were selected across an elevation gradient from 2300–3500 m at intervals of 200 m to analyze the carbon change of montane boreal forest by altitude.

We selected twelve meteorological stations located within the tree-growing areas to extract the climate parameters (Figure 1). In an earlier study of the spatial distribution of *Picea crassifolia* biomass and carbon storage in the Qilian Mountains, the average carbon content was calculated as 0.52 [28]; this was similar to the results based on a synthesis of carbon contents for temperate and boreal conifer wood (n = 36) of 50.8 ± 0.6% [29]. In this study, we used a carbon content of 0.52 for *Picea crassifolia*.

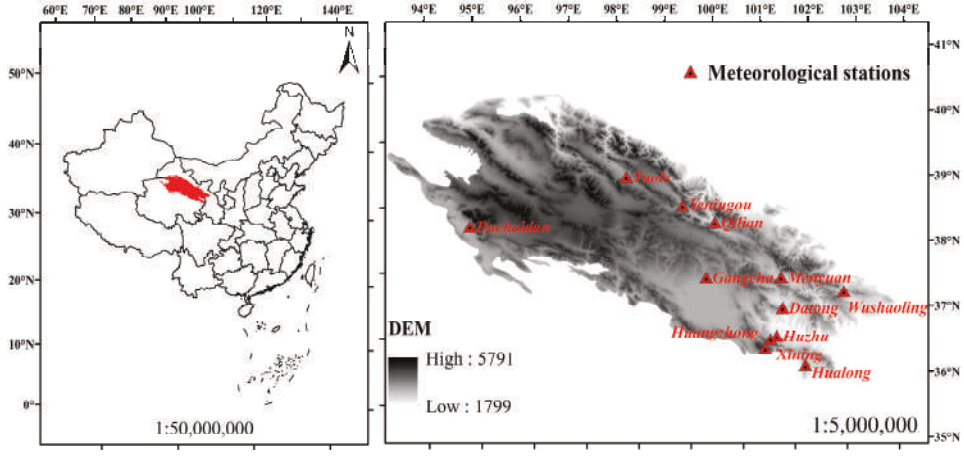

Figure 1. Study area and locations of meteorological stations used in the study in the Qilian Mountains.

The climate data, including mean monthly temperature, monthly precipitation, mean monthly daily proportion of sunshine hours, and monthly rainy days, were obtained from the climate data repository of Chinese meteorological stations (http://data.cma.cn/site/index.html), and of Qinghai Province (Table 1). Atmospheric CO_2 concentrations for 1964–2013 were derived from the atmospheric carbon dioxide mixing ratios from NOAA (National Oceanic and Atmospheric Administration) ESRL (Earth System Research Laboratory) Carbon Cycle Cooperative Global Air Sampling Network (http://www.esrl.noaa.gov/gmd/ccgg/mbl/data.php).

Table 1. Site information.

Groups	Name	Level	Longitude (°)	Latitude (°)	Altitude (m)
2300–2500 m	Xining	Provincial-Qinghai	101.45	36.44	2295
	Huzhu	Provincial-Qinghai	101.57	36.49	2480
2500–2700 m	Datong	Provincial-Qinghai	101.67	36.92	2587
	Huangzhong	Provincial-Qinghai	101.35	36.3	2668
2700–2900 m	Qilian	National-China	100.25	38.18	2787
	Hualong	Provincial-Qinghai	102.15	36.06	2835
	Menyuan	National-China	101.62	37.38	2850
2900–3100 m	Wushaoling	National-China	102.52	37.12	3045
3100–3300 m	Dachaidan	National-China	95.37	37.85	3173
	Yeniugou	National-China	99.58	38.42	3180
3300–3500 m	Gangcha	National-China	100.13	37.33	3302
	Tuole	National-China	98.42	38.8	3367

2.2. The LPJ-GUESS Model

LPJ-GUESS is a validated vegetation carbon dynamics model [30]. The basic use of the model is to simulate carbon balance of different tree species and to predict changes in carbon pools and fluxes under global climate change [31,32]. A LPJ-GUESS simulation of the spatial and temporal patterns of carbon fluxes associated with regrowth after agricultural abandonment indicated that semi-arid regions, where carbon balance was strongly associated with both precipitation and temperature, were key to the understanding and predicting of the global carbon cycle [33]. Further, changes in the spatial patterns of wildfires, estimated by LPJ-GUESS, were critical to the proposal for a more reasonable climate policy [34]. The model can simulate and predict the responses of plant water fluxes to elevated CO_2 at leaf and stand scales [35]. In addition to natural vegetation, agricultural crop production and crop responses to climate change were analyzed in an effort to increase food security [36]. In China, the model has been applied in subtropical, temperate, and mountain zones [37–39], and to the entire country [40]. Carbon simulation by LPJ-GUESS using an individual climate factor demonstrated carbon release by management, and CO_2 as the most important driver for carbon change in Lady Park Wood in the last 20 years [16].

Plant functional types (PFTs), which can simplify species diversity of vegetation, represent groups of species with similar functional traits. Among forest carbon dynamics simulation models, both, the individual-based model GUESS (General Ecosystem Simulator) [30], and the area-based dynamic global vegetation model LPJ (Lund-Potsdam-Jena) [41], can be successful in predicting the carbon flux of PFTs. Subsequently, a new vegetation dynamics model, LPJ-GUESS, was developed by combining the two other models [30].

Two model frameworks exist, the cohort and population. We employed the "cohort mode" in this study. In the "cohort mode", individual trees are distinguished, but are identical within each cohort (age class) [30]. Population processes and disturbances are modeled stochastically, and stand characteristics are averaged over 100 patches of 0.1 ha, representing "random samples" of the simulated stand. The model is driven by short-wave radiation (photosynthetically active light), temperature,

precipitation, CO_2 concentration of the air, and soil conditions. The CO_2 influences assimilation rate, and soil conditions modify plant water uptake; soil data are already provided in the model. Species information includes the physiological characteristics of PFTs, such as prescribed allometric relationships. Based on physiology, morphology, phenology, and on the response to disturbance and to bio-climatic limiting factors, the model defines ten PFTs, of which 8 are woody, and two are herbaceous [42]. We used the full set of PFTs and added a new PFT for *Picea crassifolia* to reproduce the current stage of the vegetation.

2.3. Model Forcing and Simulation Protocol

The simulation normally follows two or three phases and begins with "bare ground", which means that the modelled area is bare, with no vegetation present. The first phase of the simulation is known as the "spin-up"; in this phase, input data are normally based on the first few years of available (historical) data. During the subsequent, "historical" phase, the model uses "observed" climate and CO_2 data as input. We chose two phases, "spin-up" and "historical" to run the model for the last fifty years. Climate data for an initial 300-year "spin-up" phase were not available; such "spin-up" equilibrates the initial vegetation and carbon pools with climate at the beginning of the study period. The model was first "spun-up" for 300 years, recycling the observed time series from 1964–1993 [30,43]. The "historical" period then ran from 1964 to 2013; the simulation time interval for the LPJ-GUESS model is five years.

In a study to investigate the ability of LPJ-GUESS to reproduce features of real vegetation, the model was demonstrated to not require site-specific calibration and could be used to simulate vegetation dynamics on a regional basis or under past or future climates and atmospheric CO_2 levels for reparameterization becauase plant growth is modeled mechanistically [31]. Many of the parameters of species are decided by its PFTs, such as whether it is needle-leaved or broad-leaved; or whether it is boreal or temperate species. The species-specific parameters such as tree longevity are defined in the article. We referred to the relevant parameters for the boreal forest to define the parameters of *Picea crassifolia* [31,44]. We specified the mean length of the life of foliage at 11.8 years, as determined in a field investigation [45], and tree longevity at 250 years, as described in the literature [46]. Data used for biomass calculations for the Qilian Mountains were obtained from the literature [28,47–49] and were used to verify the accuracy of those that were calculated.

2.4. Sensitivity Analysis of Temperature, CO_2, and Extreme Whether

Sensitivity analysis is an important aspect of evaluating the resilience of ecosystems to climate change and can be combined with models to measure the effect of changing input parameters under some climate scenarios and extreme weather conditions [50,51]. Based on the simulation of LPJ-GUESS, further research was conducted to determine the relative effect of climate variables and CO_2 concentration on the carbon flux of montane boreal forests in Qilian Mountains for the period 1964–2013.

The temperature increased during the simulation period, but this trend could not be fit by a linear model. Further, the trend in precipitation was not clear. Thus, we first examined the climate effect by simulating the temperature, precipitation, and CO_2 independently of each other. Using these climate simulations as a baseline, the uncertainties of these parameters were then compared. The influence of the temperature was observed for an increase or decrease of 1 and 2 °C; precipitation was changed multiplicatively, because it is a zero-based variable, by increasing or decreasing by 10% and 20%. The influence of CO_2 was examined by removing its trend and increasing the value by 50 ppm and 100 ppm.

Because the climate variables are strongly related to each other, a comparison of the effects of climate change on carbon flux based on changing a single parameter in the data was incomplete [6,16]. Hence, to preserve the relationship of temperature, precipitation, and radiation, we represented extreme weather as follows to determine the impact of climate factors on carbon mass. Local weather

in the study area was ranked in terms of temperature or precipitation levels (annual mean temperature from April to October, and annual mean precipitation from May to September), and the top five warmest, coldest, wettest, and driest years; these were then cycled through the model repeatedly to simulate an extreme climate.

3. Results

3.1. Changes in Carbon Mass with Altitude

The monthly mean temperature and precipitation in the simulated period followed normal distribution. Warm periods were concentrated in April to October, and high precipitation was concentrated in May to September; almost all of the stations exhibited the same trends. Mean annual temperature at the twelve stations increased by 0.29–3.69 °C between 1964 and 2013, with an average increase of 0.73 °C/10a. Differences in annual precipitation among altitudes were not apparent.

Carbon stocks of the montane boreal forest were concentrated at 2700–3100 m and exhibited a single peak of 11.787 kg/m^2 at 2700–2900 m in 2013, with the average carbon mass at 2700–3100 m of 10.503 kg/m^2. The calculation of the biomass of *Picea crassifolia* was different for the different measurement methods and research areas, but the results of our simulation were within the range of other studies (Table 2). The proportion of montane boreal forest was >28% at all altitudes. Specifically, montane boreal forest accounted for 30% at 2300 to 2700 m, increasing to 93% at 2700–2900 m and 97% at 2900–3100 m, declining to 37%, and again reaching 49% at 3300–3500 m (Figure 2). The carbon stored in the ecosystem at 2300–2700 m was 7.068–7.591 kg·C/m^2, declining to about 0.242–0.645 kg·C/m^2 at 3100–3500 m.

Table 2. Carbon mass calculations for *Picea crassifolia* in the literature.

Method	Research Area	Carbon Mass	Sources
LPJ-GUESS	Qilian Mountains	10.924 (kg/m^2)	This study
Sample measured	Sunan County	28.250 (kg/m^2)	[48]
Sample measured	Qilian Mountains	20.920 (kg/m^2)	[28]
Vegetation survey and Tree-ring research	Pailugou Watershed	12.861 (kg/m^2)	[49]
Sample measured	Haxi forest farm	13.290 (kg/m^2)	
Model simulation	Qilian Mountains	16.980 (kg/m^2)	
Sample measured	north-eastern edge Qilian Mountains	8.270(kg/m^2)	[47]

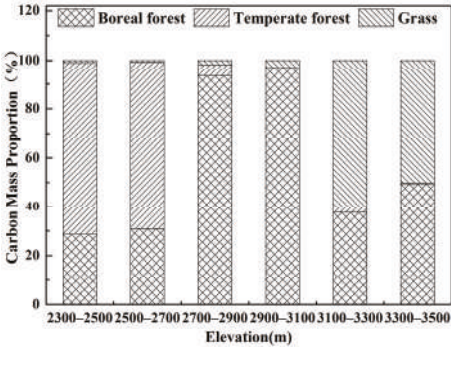

Figure 2. Carbon mass proportion at different elevations for twelve meteorological stations. Data are the means of simulated values for each range in elevation.

We investigated the NEE (Net ecosystem exchange) and carbon mass change in the mountain boreal forest ecosystem (at 2700–3100 m where the boreal forest accounted for the largest carbon mass) (Figure 3). In the model, a positive value of NEE indicated that the ecosystem was a carbon source, while a negative value indicated a carbon sink. Boreal forest was a carbon sink before the 1980s; sink strength at elevation 2700–2900 m declined, until the sink activity became a carbon source after 1980, and it became a relatively strong source in the 1990s. However, the strength of the carbon source weakened and the forest ecosystem at 2900–3100 m became a carbon sink again after the year 2000. We analysed the change in carbon mass during 1964–2013 and found the there was an upward trend for this montane boreal forest. The biomass of *Picea crassifolia* forest below 3100 m decreased in the study period, with the greatest decline of 2.595 kg/m^2 at 2700–3100 m, and least of 0.125 kg/m^2 at 2300–2500 m. The carbon mass increased by 0.035 kg/m^2 at 3100–3300 m, and by 0.256 kg/m^2 at 3300–3500 m. As the NEE indicated, the decreasing trend of carbon mass for montane boreal forest at 2700–2900 m stabilized in the 2000s and even exhibited a slight increase; carbon mass at 2900–3100 m was stable before the 1990s, and increased after that.

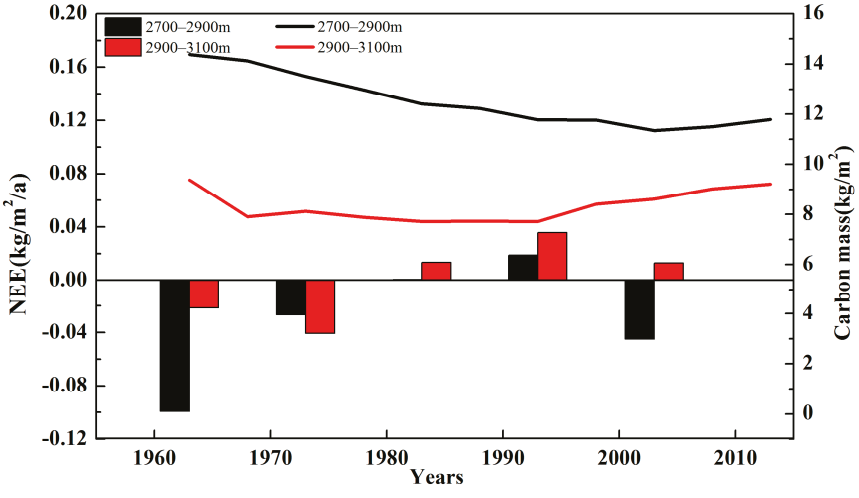

Figure 3. The carbon flows change in montane boreal forest ecosystem from 1964–2013. kg/m^2/a: kg/m^2/year.

3.2. The Sensitivity Analysis of Carbon Mass of Montane Boreal Forest to Climate Variables and CO_2

The simulation showed that the carbon carrying capacity of *Picea crassifolia* increased in the study period, given no changes to any variable. Mean carbon mass increased by 1.202 kg/m^2 from 1964–2013, and the 5-year (simulation time interval for the LPJ-GUESS model) mean NPP increased by 0.023 kg/m^2/year to between 0.997 and 1.122 kg/m^2/year in the simulation period. Subsequently, each of the climatic variables was changed one at a time.

Following a change in temperature, the trend in NPP did not change, but the NPP value was higher than before (Figure 4). The effect of lower temperature on NPP was greater than that of higher temperature. When the temperature increased by 1 °C, 5-year mean NPP increased by 0.090 kg/m^2/year; when the temperature increased by 2 °C, mean NPP increased by 0.148 kg/m^2/year per five years. When the temperature decreased by 1 °C, mean NPP decreased 0.113 kg/m^2/year per five years; when the temperature decreased by 2 °C, mean NPP decreased by 0.292 kg/m^2/year per five years. However, the change in carbon stocks was not consistent with NPP when the temperature changed; increased or decreased temperature appeared to suppress carbon stocks of the montane boreal forest. Mean carbon stock decreased between 1964–2013 by 0.768 kg/m^2 per five years; the increments decreased from 12.37% to 6.32% as the temperature increased by 1 °C. As the temperature

increased by 2 °C, mean carbon stock decreased by 0.893 kg/m^2 per five years, and carbon mass was reduced by 8.24%. With the temperature decrease of 1 °C, carbon stock increased by 0.026 kg/m^2 per five years and the increments increased to 13.28%. With the temperature decrease of 2 °C, mean carbon stock decreased by 1.307 kg/m^2 per five years, and carbon mass decreased by 10.11% during the last 50 years.

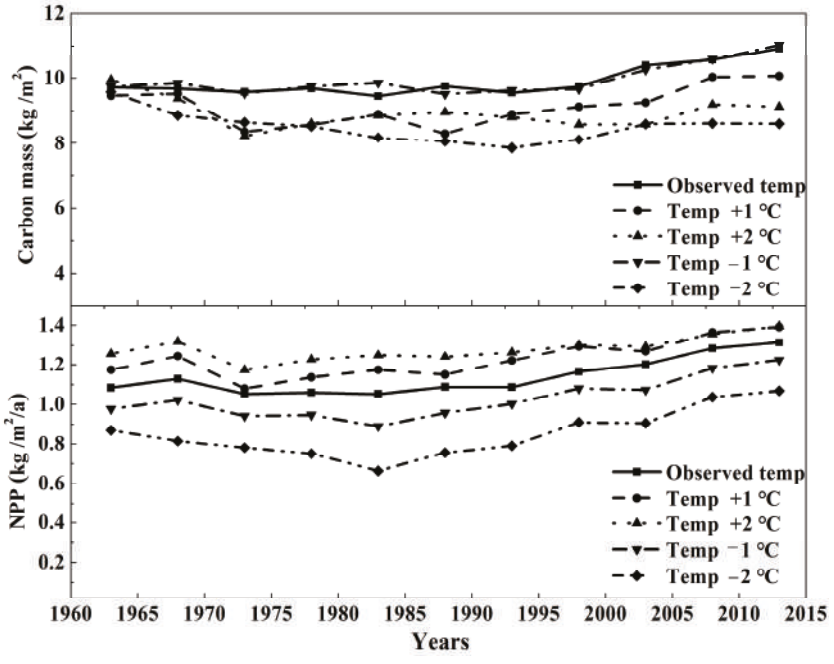

Figure 4. LPJ-GUESS output showing the effects on stored carbon (top panel) and NPP (bottom panel) of changing the temperature only. Temperature was modified by adding or subtracting 1 (or 2) °C to each daily climate value. Lines represent the means of the simulations. Temp: the abbreviation of temperature.

The trend in NPP changed over the course of simulation following changes in precipitation (Figure 5); the more precipitation, the higher the NPP, and the less precipitation, the lower the NPP. The impact of reduced precipitation was greater than that of increased precipitation. A 20% increase in precipitation resulted in a mean 5-year NPP increase of 0.024 kg/m^2/year, while a 20% decrease reduced NPP by 0.080 kg/m^2/year per five years.

The changes in carbon stock were consistent with NPP. Mean carbon stocks increased 0.242 kg/m^2 per five years as precipitation increased by 10%, and 1.165 kg/m^2 per five years as the precipitation increased by 20%. As precipitation decreased by 10 and 20%, mean carbon stocks decreased 1.517 and 2.969 kg/m^2 per five years, respectively. The increase in carbon mass resulting from increased precipitation was 24.39%, and 24.93%, respectively, (basic value 12.37%), and carbon mass decreased 19.17%, and 34.01%, respectively, if precipitation decreased.

Mean NPP decreased when the CO_2 concentration remained unchanged (de-trended) and increased when the CO_2 concentration increased (Figure 6). Carbon mass decreased when the CO_2 concentration remained unchanged, but it increased as the CO_2 concentration levels rose. Overall, the CO_2 concentration had an increasingly positive effect as atmospheric levels rose. Carbon mass decreased by 0.240 kg/m^2 for the simulation years if CO_2 concentrations did not increase

after 1964. Mean carbon storage increased by 0.746 and 0.866 kg/m^2 per five years for CO_2 concentration increases of 50 and 100 ppm. De-trended CO_2 supressed carbon mass by about 2.45%, and increased CO_2 promoted carbon storage from 12.37% to 18.98%, and to 24.74% in response to 50 and 100 ppm, respectively.

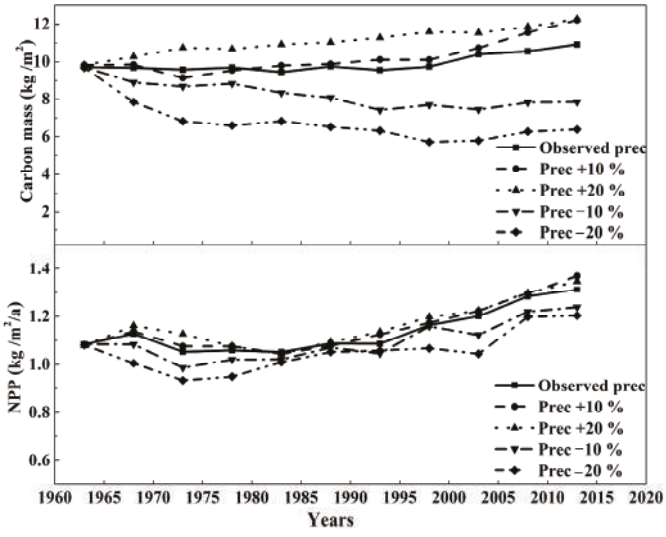

Figure 5. LPJ-GUESS output showing the effects on stored carbon (top panel) and NPP (bottom panel) of changing precipitation only. Precipitation was changed multiplicatively because it is a zero-based variable. Lines represent the means of the simulations. Prec: the abbreviation of precipitation.

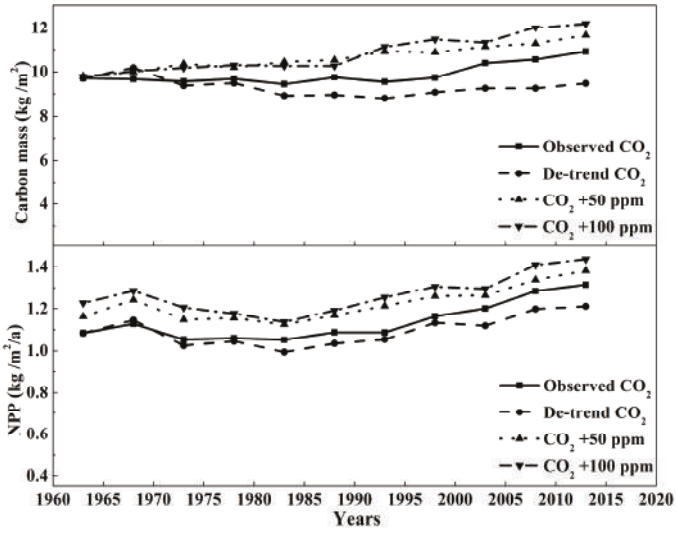

Figure 6. LPJ-GUESS output showing the effect on stored carbon (top panel) and NPP (bottom panel) of changing CO_2 concertration only. CO_2 concertration was de-trended by using 1964 levels throughout and was modified by adding values to each year value. Lines represent the means of simulations.

Indeed, in the simulation period, the NPP and carbon mass of the montane boreal forest increased. Combined with the analysis of single-factor changes, carbon stocks decreased as temperature rose but increased as CO_2 concentration increased. The actual temperature increased in the study area from 1964 to 2013, precipitation fluctuated, and CO_2 concentration increased, and the positive effect of CO_2 concentration contributed more to the carbon stocks than the negative effect of temperature.

3.3. The Sensitivity Analysis of Carbon Mass of Montane Boreal Forest to Extreme Weather

We analyzed the extremes in weather events from 1964–2013 in stations we chose by ranking the mean value of heat and water in concentration months (annual mean temperature from April to October, and annual mean precipitation from May to September) of each year.

Under warm and wet conditions, NPP increased, and under warm conditions alone, NPP increased more (Figure 7). Under cold and dry conditions, NPP decreased, and it decreased further under dry conditions alone. However, the living biomass was greatly suppressed under dry conditions alone and decreased by 42% compared to the no-change simulation; mean decrease in NPP was 1.816 kg/m^2 per five years. Under the other three conditions, biomass production performed better than under the actual climate. Biomass production increased (10% at the end of period) most notably under wet conditions, with a mean increase of 1.085 kg/m^2 per five years.

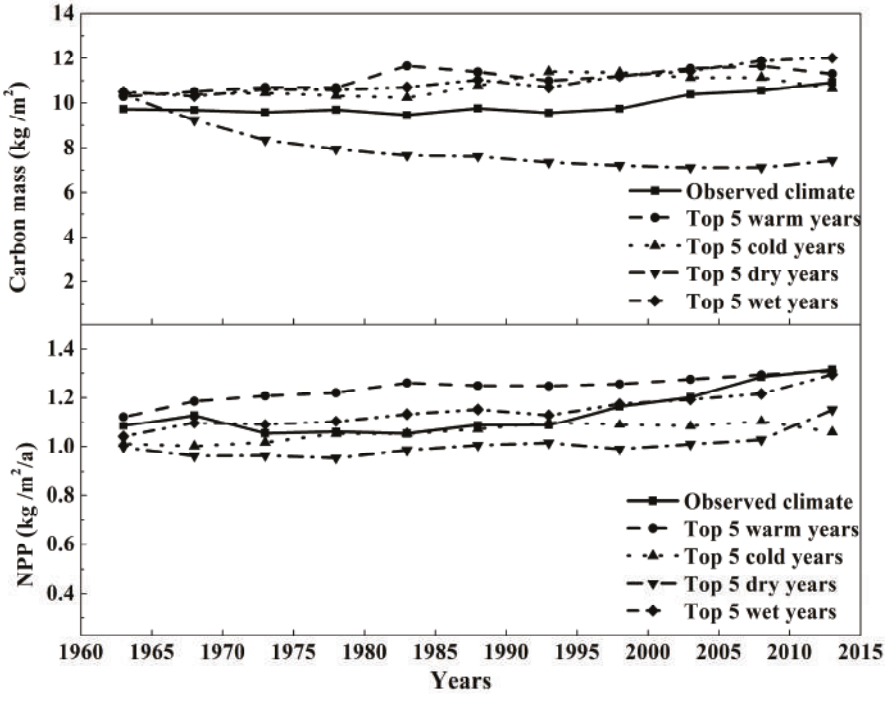

Figure 7. LPJ-GUESS output showing the effects of extreme weather conditions on stored carbon (top panel) and NPP (bottom panel). Local weather data were used to determine the most extreme high /low temperature and high/low rainfall from a 5-year period.

4. Discussion

4.1. Model Applicability and Carbon Mass at Different Altitudes

Our LPJ-GUESS model simulation showed that the main distribution of *Picea crassifolia* in the Qilian Mountains was at 2700 to 3100 m, and the average carbon storage was 10.503 kg/m^2, with a maximum of 11.787 kg/m^2. The biomass pools at elevations 2300–2700 m contained more carbon than those at 3100–3500 m for the different dominant species.

The vertical distribution pattern of *Picea crassifolia* influenced the distribution of carbon density and NPP. Altitude was a dominant factor influencing the soil organic carbon concentration and community pattern of *Picea crassifolia* [52]; further, altitude exerted a strong influence on the growth of *Picea crassifolia* by affecting the microclimate, including air temperature and humidity, and soil moisture [24]. Trees were low and forest density was often low at low altitudes, increasing gradually at mid-altitudes, and exhibiting a pattern of isolated trees or scattered patches at the upper growth limit [53]. The most suitable conditions for the growth of *Picea crassifolia* forest were observed between 2800 and 2900 m [49], with grassland between 3000 to 3700 m [54]. Density and basal area of *Picea crassifolia* were also higher between 2650 to 3100 m than at other altitudes, and beyond 3100 m, the density decreased with an increase in altitude [55].

Evergreen conifers in cold and high-altitude zones of the montane boreal forest have lower carbon biomass due to low photosynthesis and respiration rates than that in warmer habitats [56]. Carbon mass in the biomass pools examined in this study, i.e., 5.462 kg·C/m^2, was similar to the estimate for northern montane boreal forests ranging from 4.2 to 5.3 kg·C/m^2 [47]. The focus of current research in the Qilian Mountains is on the main tree species, *Picea crassifolia*, but results are not uniform. Initial surveys at the Sidalong forest farm on the Qilian Mountain showed that *Picea crassifolia* biomass was about 24.298 kg/m^2 (Chang et al., 1995). Recently, the aboveground carbon stocks of *Picea crassifolia* at the north-eastern edge of Qilian Mountains were calculated as 4.3 kg/C·m^2 [47]. The estimate of the above-ground biomass in southern Qilian Mountains was between 0.1885 and 22.065 kg/m^2 [57]. Our simulation of *Picea crassifolia* NPP was between 0.52–0.58 kg·C/m^2/year, which is in the range of 0.3–0.7 kg·C/m^2/year for boreal ecosystem productivity examined by remote sensing [58], and higher than the mean NPP (0.38 kg·C/m^2/year) of Qilian Mountains [59]. Hydrothermal conditions drove carbon density differences in boreal forests; also, carbon density first increased, and then decreased with stand age, with the highest value at age 183 years [28]. Thus, carbon density calculations were different due to vertical distribution of vegetation patterns and the age of the forest in this study.

The carbon mass and NEE change in *Picea crassifolia* forest ecosystem we calculated revealed that this mountain forest tended to becoming a carbon source from a carbon sink in the last 50 years; this trend was slow and even reversed in the 2000s. The carbon mass of *Picea crassifolia* decreased at low elevations and increased at high elevations, showing an upward trend in vegetation distribution, but the highest carbon mass proportion region for the forest did not change in the study period. Similar to other boreal forests, the mountain boreal forest also tended to become a carbon source under climate change [60–62], but this trend in the Qilian Mountains slowed in the 2000s.

The LPJ-GUESS model has been used in a large number of studies, and its performance has been evaluated several times. The model has also been used in China. Combined LPJ-GUESS and High Accuracy Surface Modeling (HASM) allowed for an economical estimation of forest biomass and the research used climate data from 735 meteorological stations in Chinese mainland from 1950–2010 and compared the results with the Seventh National Forest Resources Inventory data in China [40]. The results presented in this article indicated that the LPJ-GUESS model was suitable for these 735 meteorological stations; stations used in our study were contained in those stations. A carbon balance calculation by LPJ-GUESS of three deciduous forests in a mountainous area near Beijing showed that the model can be applied to a warm temperate forest in China [37]. Also, the forest production and carbon dynamics study of Masson Pine Forest in the Jigongshan region demonstrated that the model can simulate growth dynamics of subtropical forests [39]. Finally, the simulation

of the carbon cycle of a *Larix chinensis* forest at Taibai Mountains, China, indicated the model was suitable for analyzing vegetation characteristics in mountainous areas [38]. Similar to previous biomass calculations (Table 2), we found that the LPJ-GUESS model was suitable for simulating carbon change of the montane boreal forest in northwestern China. The carbon density calculated by the model is based only on foliage, fine roots, and sapwood and heartwood; thus, the results of the model can be expected to be lower than results of some field measurements.

4.2. The Effects of The Climate Variables on Carbon Cycling in Montane Boreal Forest

Carbon density and NPP in this montane boreal forest ecosystem were concentrated at 2700–3100 m. Mean carbon mass increased by 13.37%, with a 5-year mean of 1.202 kg/m^2 from 1964 to 2013; mean NPP increased by 0.023 kg/m^2/year per five years.

In this study, NPP clearly increased as temperature increased and under warm conditions. The effect of temperature on carbon storage was complex in this montane boreal forest. Increasing temperature limited the storage of carbon, while decreasing temperature promoted its storage. Under warm conditions, carbon storage increased, and if temperature decreased considerably, carbon mass was reduced. The temperature sensitivity of biomass allocation may be an important but not obvious regulator of the carbon cycle in the boreal forest [19,56]. With an increase in mean annual temperature, and only a modest expected increase in precipitation, a shift in boreal forest may be observed to a woodland/shrubland ecosystem type, which is more suited for such an environment [63]. Further, the overall warming trend may lead to earlier seasonal plant growth; however, incomplete development of green tissues exposed to colder environments may negatively influence tree growth and carbon storage [6]. To the contrary, some researchers concluded that increased temperature and longer growing seasons will increase the NPP and enhance carbon uptake of boreal forests; this response, however, was weak in interannual variations [64]. Boreal forests store vast amounts of carbon in soil, but the temperature effects on soils are challenging to measure. The temperature relationship with above-ground carbon density was affected by baseline temperature such that, at mean annual temperature <8 °C, the relationship was positive, and negative in regions with a mean annual temperature >10 °C for mature boreal forests [65].

Precipitation is positively related to the biomass and NPP of the montane boreal forest. Precipitation has a much greater impact on montane boreal forests than temperature; especially in reduced precipitation and in dry environments, both biomass and NPP decreased significantly and hindered productivity and biomass storage. Drought conditions likely affected the radial growth of *Picea crassifolia* forest in Qilian Mountains in the last half-century [66]. Drought was the major driver of the release of total original carbon, which reduced soil respiration and NPP in a large boreal watershed [67]. Extreme drought decreases carbon assimilation and reduces the carbon sink strength of forests [6]. Under extremely dry conditions, boreal forests may degrade to low-productivity open woodlands [63].

In this study, the effect of CO_2 concentration on the biomass and NPP of montane boreal forest was also consistent, and the parameters were positively correlated. We showed that, if the CO_2 concentration remained at the level present 50 years ago, the ability of the montane boreal forest to produce and store carbon would decrease. However, the capacity of forests to store carbon improved with increasing CO_2 concentration, and the higher the CO_2 amounts, the greater the carbon storage capacity. Although not as pronounced as that in tropical and temperate forests, the increase in CO_2 concentration led to an increase in NPP and carbon stocks in boreal forests both at local and global scales [62,68]. A physiologically-based forest model showed that the total NPP and the carbon storage in biomass improved under elevated CO_2 concentration due to an increase in net photosynthetic rates at leaf-level and smaller shifts in carbon residence time [56,67]. Using combined satellite and ground observations for 1950–2011, Denos and others (2013) demonstrated that the sequestration of atmospheric CO_2 increased due to higher net CO_2 uptake associated with spring and fall growth extensions in northern ecosystems. Increasing atmospheric CO_2 is expected to increase boreal forest carbon in western China [69]. A simulation by the BIOME-BGC

model in *Picea crassifolia* forest showed that the effect of CO_2 concentration on NPP was more significant than that of climate change for future climate [70].

5. Conclusions

The carbon mass of montane boreal forest simulated by LPJ-GUESS was comparable, though lower than that reported in other studies. Carbon storage was concentrated at the altitude of 2700–3100 m in the Qilian Mountains. Within this altitudinal range, carbon storage of *Picea crassifolia* increased by 1.202 kg/m^2 per five years, and NPP was between 0.52–0.58 $kg{\cdot}C/m^2/year$ during the last 50 years. *Picea crassifolia* exhibited a trend toward climbing higher in elevation and becoming a carbon source in the last 50 years.

The boreal forest is significantly affected by climate change and has a slow recovery process. Under steady precipitation, carbon storage increased with increasing atmospheric CO_2 concentration despite the negative effects of warming on montane boreal forest in the Qilian Mountains in the last 50 years. A lack of water is the greatest threat for carbon storage in *Picea crassifolia*. Under the changing CO_2 concentration and precipitation conditions, carbon mass and NPP were positively correlated. The relationship between climate factors, CO_2 concentration, extreme conditions, and carbon storage was largely impacted by stand age, geographical location, altitude, and the environment; therefore, further research needs to examine the drivers of interannual variability in the carbon cycle at different scales and under different conditions of climate change.

Acknowledgments: We are very grateful to Kathryn Piatek for her comments and editorial assistance. This work was supported by the National Natural Science Foundation of China (No. 41621001, 41522102 and 41601051) and the Foundation for Excellent Youth Scholars of "Northwest Institute of Eco-Environment and Resources", Chinese Academy of Sciences.

Author Contributions: Zhibin He and Shu Fang conceived and designed the experiments; Shu Fang performed the experiments, analyzed the data and wrote the paper; Jun Du, Longfei Chen, Pengfei Lin, and Minmin Zhao optimized the experiment and modified the manuscript.

Conflicts of Interest: The authors declare no conflict of interest. The founding sponsors had no role in the design of the study; in the collection, analyses, or interpretation of data; in the writing of the manuscript, and in the decision to publish the results.

References

1. Rössler, O.; Diekkrüger, B.; Löffler, J. Potential drought stress in a Swiss mountain catchment—Ensemble forecasting of high mountain soil moisture reveals a drastic decrease, despite major uncertainties. *Water Resour. Res.* **2012**, *48*. [CrossRef]
2. Hartl-Meier, C.; Dittmar, C.; Zang, C.; Rothe, A. Mountain forest growth response to climate change in the Northern Limestone Alps. *Trees* **2014**, *28*, 819–829. [CrossRef]
3. Savva, Y.; Oleksyn, J.; Reich, P.B.; Tjoelker, M.G.; Vaganov, E.A.; Modrzynski, J. Interannual growth response of Norway spruce to climate along an altitudinal gradient in the Tatra Mountains, Poland. *Trees* **2006**, *20*, 735–746. [CrossRef]
4. Affolter, P.; Büntgen, U.; Esper, J.; Rigling, A.; Weber, P.; Luterbacher, J.; Frank, D. Inner alpine conifer response to 20th century drought swings. *Eur. J. For. Res.* **2010**, *129*, 289–298. [CrossRef]
5. Orlowsky, B.; Seneviratne, S.I. Global changes in extreme events: Regional and seasonal dimension. *Clim. Chang.* **2012**, *110*, 669–696. [CrossRef]
6. Frank, D.; Reichstein, M.; Bahn, M.; Thonicke, K.; Frank, D.; Mahecha, M.D.; Smith, P.; Velde, M.; Vicca, S.; Babst, F. Effects of climate extremes on the terrestrial carbon cycle: Concepts, processes and potential future impacts. *Glob. Chang. Biol.* **2015**, *21*, 2861–2880. [CrossRef] [PubMed]
7. Thurner, M.; Beer, C.; Carvalhais, N.; Forkel, M.; Santoro, M.; Tum, M.; Schmullius, C. Large-scale variation in boreal and temperate forest carbon turnover rate related to climate. *Geophys. Res. Lett.* **2016**, *43*, 4576–4585. [CrossRef]
8. Schlesinger, W.H.; Dietze, M.C.; Jackson, R.B.; Phillips, R.P.; Rhoades, C.C.; Rustad, L.E.; Vose, J.M. Forest biogeochemistry in response to drought. *Glob. Chang. Biol.* **2016**, *22*, 2318–2328. [CrossRef] [PubMed]

9. Stocker, T. *Climate Change 2013: The Physical Science Basis: Working Group I Contribution to the Fifth Assessment Report of the Intergovernmental Panel on Climate Change*; Cambridge University Press: Cambridge, UK, 2014.
10. McCain, C.M.; Colwell, R.K. Assessing the threat to montane biodiversity from discordant shifts in temperature and precipitation in a changing climate. *Ecol. Lett.* **2011**, *14*, 1236–1245. [CrossRef] [PubMed]
11. Allen, C.D.; Macalady, A.K.; Chenchouni, H.; Bachelet, D.; McDowell, N.; Vennetier, M.; Kitzberger, T.; Rigling, A.; Breshears, D.D.; Hogg, E.T. A global overview of drought and heat-induced tree mortality reveals emerging climate change risks for forests. *For. Ecol. Manag.* **2010**, *259*, 660–684. [CrossRef]
12. Kurz, W.A.; Dymond, C.C.; Stinson, G.; Rampley, G.J.; Neilson, E.T.; Carroll, A.L.; Ebata, T.; Safranyik, L. Mountain pine beetle and forest carbon feedback to climate change. *Nature* **2008**, *452*, 987–990. [CrossRef] [PubMed]
13. Ruiz-Labourdette, D.; Nogués-Bravo, D.; Ollero, H.S.; Schmitz, M.F.; Pineda, F.D. Forest composition in mediterranean mountains is projected to shift along the entire elevational gradient under climate change. *J. Biogeogr.* **2012**, *39*, 162–176. [CrossRef]
14. Trumbore, S.; Brando, P.; Hartmann, H. Forest health and global change. *Science* **2015**, *349*, 814–818. [CrossRef] [PubMed]
15. Rocca, M.E.; Brown, P.M.; MacDonald, L.H.; Carrico, C.M. Climate change impacts on fire regimes and key ecosystem services in rocky mountain forests. *For. Ecol. Manag.* **2014**, *327*, 290–305. [CrossRef]
16. Allen, K.A.; Lehsten, V.; Hale, K.; Bradshaw, R. Past and future drivers of an unmanaged carbon sink in European temperate forest. *Ecosystems* **2016**, *19*, 545–554. [CrossRef]
17. Williams, C.A.; Collatz, G.J.; Masek, J.; Huang, C.; Goward, S.N. Impacts of disturbance history on forest carbon stocks and fluxes: Merging satellite disturbance mapping with forest inventory data in a carbon cycle model framework. *Remote Sens. Environ.* **2014**, *151*, 57–71. [CrossRef]
18. Wit, H.A.; Bryn, A.; Hofgaard, A.; Karstensen, J.; Kvalevåg, M.M.; Peters, G.P. Climate warming feedback from mountain birch forest expansion: Reduced albedo dominates carbon uptake. *Glob. Chang. Biol.* **2014**, *20*, 2344–2355. [CrossRef] [PubMed]
19. Elkin, C.; Gutiérrez, A.G.; Leuzinger, S.; Manusch, C.; Temperli, C.; Rasche, L.; Bugmann, H. A 2 °C warmer world is not safe for ecosystem services in the European alps. *Glob. Chang. Biol.* **2013**, *19*, 1827–1840. [CrossRef] [PubMed]
20. He, Z.; Zhao, W.; Liu, H.; Tang, Z. Effect of forest on annual water yield in the mountains of an arid inland river basin: A case study in the pailugou catchment on northwestern China's Qilian Mountains. *Hydrol. Process.* **2012**, *26*, 613–621. [CrossRef]
21. Du, J.; He, Z.; Yang, J.; Chen, L.; Zhu, X. Detecting the effects of climate change on canopy phenology in coniferous forests in semi-arid mountain regions of China. *Int. J. Remote Sens.* **2014**, *35*, 6490–6507. [CrossRef]
22. Baranova, A.; Schickhoff, U.; Wang, S.; Jin, M. Mountain pastures of Qilian Shan: Plant communities, grazing impact and degradation status (Gansu province, NW China). *Hacquetia* **2016**, *15*, 21–35. [CrossRef]
23. Chen, L.; He, Z.; Du, J.; Yang, J.; Zhu, X. Patterns and controls of soil organic carbon and nitrogen in alpine forests of northwestern China. *For. Sci.* **2015**, *61*, 1033–1040. [CrossRef]
24. He, Z.; Zhao, W.; Zhang, L.; Liu, H. Response of tree recruitment to climatic variability in the alpine treeline ecotone of the Qilian Mountains, northwestern China. *For. Sci.* **2013**, *59*, 118–126. [CrossRef]
25. He, Z.; Du, J.; Zhao, W.; Yang, J.; Chen, L.; Zhu, X.; Chang, X.; Liu, H. Assessing temperature sensitivity of subalpine shrub phenology in semi-arid mountain regions of China. *Agric. For. Meteorol.* **2015**, *213*, 45–52. [CrossRef]
26. Chang, X.; Zhao, W.; He, Z. Radial pattern of sap flow and response to microclimate and soil moisture in Qinghai spruce (*Picea crassifolia*) in the upper Heihe river basin of arid northwestern China. *Agric. For. Meteorol.* **2014**, *187*, 14–21. [CrossRef]
27. Tian, F.; Zhao, C.; Feng, Z.-D. Simulating evapotranspiration of Qinghai spruce (*Picea crassifolia*) forest in the Qilian Mountains, northwestern China. *J. Arid Environ.* **2011**, *75*, 648–655. [CrossRef]
28. Peng, S.; Zhao, C.; Zheng, X.; Xu, Z.; He, L. Spatial distribution characteristics of the biomass and carbon storage of Qinghai spruce (*Picea crassifolia*) forests in Qilian mountains. *Chin. J. Appl. Ecol.* **2011**, *22*, 1689–1694.
29. Thomas, S.C.; Martin, A.R. Carbon content of tree tissues: A synthesis. *Forests* **2012**, *3*, 332–352. [CrossRef]
30. Smith, B.; Prentice, I.C.; Sykes, M.T. Representation of vegetation dynamics in the modelling of terrestrial ecosystems: Comparing two contrasting approaches within European climate space. *Glob. Ecol. Biogeogr.* **2001**, *10*, 621–637. [CrossRef]

31. Hickler, T.; Smith, B.; Sykes, M.T.; Davis, M.B.; Sugita, S.; Walker, K. Using a generalized vegetation model to simulate vegetation dynamics in northeastern USA. *Ecology* **2004**, *85*, 519–530. [CrossRef]
32. Ahlström, A.; Schurgers, G.; Arneth, A.; Smith, B. Robustness and uncertainty in terrestrial ecosystem carbon response to CMIP5 climate change projections. *Environ. Res. Lett.* **2012**, *7*, 044008. [CrossRef]
33. Korth, H.; Tsyganenko, N.A.; Johnson, C.L.; Philpott, L.C.; Anderson, B.J.; Al Asad, M.M.; Solomon, S.C.; McNutt, R.L. Modular model for mercury's magnetospheric magnetic field confined within the average observed magnetopause. *J. Geophys. Res. Space Phys.* **2015**, *120*, 4503–4518. [CrossRef] [PubMed]
34. Knorr, W.; Arneth, A.; Jiang, L. Demographic controls of future global fire risk. *Nat. Clim. Chang.* **2016**, *6*, 781–785. [CrossRef]
35. De Kauwe, M.G.; Medlyn, B.E.; Zaehle, S.; Walker, A.P.; Dietze, M.C.; Hickler, T.; Jain, A.K.; Luo, Y.; Parton, W.J.; Prentice, I.C.; et al. Forest water use and water use efficiency at elevated CO_2: A model-data intercomparison at two contrasting temperate forest face sites. *Glob. Chang. Biol.* **2013**, *19*, 1759–1779. [CrossRef] [PubMed]
36. Rosenzweig, C.; Elliott, J.; Deryng, D.; Ruane, A.C.; Müller, C.; Arneth, A.; Boote, K.J.; Folberth, C.; Glotter, M.; Khabarov, N.; et al. Assessing agricultural risks of climate change in the 21st century in a global gridded crop model intercomparison. *Proc. Natl. Acad. Sci. USA* **2014**, *111*, 3268–3273. [CrossRef] [PubMed]
37. Liu, R.G.; Li, N.; Su, H.X.; Sang, W.G. Simulation and analysis on future carbon balance of three deciduous forests in Beijing mountain area, warm temperate zone of China. *Chin. J. Plant Ecol.* **2009**, *33*, 516–534.
38. Li, L.; He, X.; Hu, L.; Li, J. Simulation of the carbon cycle of *Larix chinensis* forest during 1958 and 2008 at Taibai Mountain, China. *Acta Ecol. Sin.* **2013**, *33*, 2845–2855.
39. Peng, X.; Cheng, R.; Xiao, W.; Wang, R.; Wang, X.; Liu, Z. Productivity and carbon dynamic of the masson pine stands in Jigongshan region based on lpj-guess model. *Sci. Silvae Sin.* **2013**, *49*, 7–8.
40. Zhao, M.; Yue, T.; Zhao, N.; Sun, X.; Zhang, X. Combining lpj-guess and hasm to simulate the spatial distribution of forest vegetation carbon stock in China. *J. Geogr. Sci.* **2014**, *24*, 249–268. [CrossRef]
41. Sitch, S. *The Role of Vegetation Dynamics in the Control of Atmospheric CO_2 Content*; Department of Ecology, Lund University: Lund, Sweden, 2000.
42. Sitch, S.; Smith, B.; Prentice, I.C.; Arneth, A.; Bondeau, A.; Cramer, W.; Kaplans, J.O.; Levis, S.; Lucht, W.; Sykes, M.T.; et al. Evaluation of ecosystem dynamica, olant geography and terrestrial carbon cycling in the lpj dynamic global vegetation model. *Glob. Chang. Biol.* **2003**, *9*, 161–185. [CrossRef]
43. Hickler, T.; Fronzek, S.; Araújo, M.B.; Schweiger, O.; Thuiller, W.; Sykes, M.T. An ecosystem model-based estimate of changes in water availability differs from water proxies that are commonly used in species distribution models. *Glob. Ecol. Biogeogr.* **2009**, *18*, 304–313. [CrossRef]
44. Hickler, T.; Vohland, K.; Feehan, J.; Miller, P.A.; Smith, B.; Costa, L.; Giesecke, T.; Fronzek, S.; Carter, T.R.; Cramer, W. Projecting the future distribution of European potential natural vegetation zones with a generalized, tree species-based dynamic vegetation model. *Glob. Ecol. Biogeogr.* **2012**, *21*, 50–63. [CrossRef]
45. Wu, Q.; Hu, Q.W.; Zheng, L.; Zhang, F.; Song, M.H.; Liu, X.D. Variations of leaf lifespan and leaf mass per area of *Picea crassifolia* along altitude gradient. *Acta Bot. Boreal. Occident. Sin.* **2010**, *30*, 1689–1694.
46. Chen, F.; Yuan, Y.-J.; Wei, W.-S.; Yu, S.-L.; Fan, Z.-A.; Zhang, R.-B.; Zhang, T.-W.; Li, Q.; Shang, H.-M. Temperature reconstruction from tree-ring maximum latewood density of Qinghai spruce in middle Hexi corridor, China. *Theor. Appl. Clim.* **2012**, *107*, 633–643. [CrossRef]
47. Wagner, B.; Liang, E.; Li, X.; Dulamsuren, C.; Leuschner, C.; Hauck, M. Carbon pools of semi-arid *Picea crassifolia* forests in the Qilian Mountains (north-eastern Tibetan Plateau). *For. Ecol. Manag.* **2015**, *343*, 136–143. [CrossRef]
48. Jing, W.-M.; Liu, X.-D.; Zhao, W.-J.; Ma, Y. Study on biomass and net productivity of typical forest stand in the Qilian mountains. *J. Gansu Agric. Univ.* **2011**, *6*, 017.
49. Zhang, L.; Yu, P.; Wang, Y.; Wang, S.; Liu, X. Biomass change of middle aged forest of Qinghai spruce along an altitudinal gradient on the north slope of Qilian mountains. *Sci. Silvae Sin.* **2015**, *51*, 1–7.
50. Allen, D.; Mackie, D.; Wei, M. Groundwater and climate change: A sensitivity analysis for the grand forks aquifer, southern British Columbia, Canada. *Hydrogeol. J.* **2004**, *12*, 270–290. [CrossRef]
51. Katz, R. Extreme value theory for precipitation: Sensitivity analysis for climate change. *Adv. Water Res.* **1999**, *23*, 133–139. [CrossRef]
52. Zhao, C.; Chen, L.; Ma, F.; Yao, B.; Liu, J. Altitudinal differences in the leaf fitness of juvenile and mature alpine spruce trees (*Picea crassifolia*). *Tree Phys.* **2008**, *28*, 133–141. [CrossRef]

53. Zhao, C.; Nan, Z.; Cheng, G.; Zhang, J.; Feng, Z. Gis-assisted modelling of the spatial distribution of Qinghai spruce (*Picea crassifolia*) in the Qilian mountains, northwestern china based on biophysical parameters. *Ecol. Model.* **2006**, *191*, 487–500. [CrossRef]
54. Liang, B.; Di, L.; Zhao, C.; Peng, S.; Peng, H.; Wang, C.; Wang, Y.; Liu, Y. Altitude distribution of aboveground biomass of typical shrubs in the tianlaochi watershed of Qilian mountains. *Acta Agrestia Sin.* **2013**, *21*, 664–669.
55. Zhang, L.; Liu, H. Response of *Picea crassifolia* population to climate change at the treeline ecotones in Qilian mountains. *Sci. Silvae Sin.* **2012**, *1*, 006.
56. Reich, P.B.; Rich, R.L.; Lu, X.; Wang, Y.-P.; Oleksyn, J. Biogeographic variation in evergreen conifer needle longevity and impacts on boreal forest carbon cycle projections. *Proc. Natl. Acad. Sci. USA* **2014**, *111*, 13703–13708. [CrossRef] [PubMed]
57. Tian, X.; Li, Z.; Su, Z.; Chen, E.; Tol, C.V.D.; Li, X.; Guo, Y.; Li, L.; Ling, F. Estimating montane forest above-ground biomass in the upper reaches of the Heihe river basin using landsat-tm data. *Int. J. Remote Sens.* **2014**, *35*, 7339–7362. [CrossRef]
58. Zhou, Y.; Zhu, Q.; Chen, J.M.; Wang, Y.Q.; Liu, J.; Sun, R.; Tang, S. Observation and simulation of net primary productivity in Qilian mountain, western china. *J. Environ. Manag.* **2007**, *85*, 574–584. [CrossRef] [PubMed]
59. Wang, P.; Sun, R.; Hu, J.; Zhu, Q.; Zhou, Y.; Li, L.; Chen, J.M. Measurements and simulation of forest leaf area index and net primary productivity in northern China. *J. Environ. Manag.* **2007**, *85*, 607–615. [CrossRef] [PubMed]
60. Wramneby, A.; Smith, B.; Zaehle, S.; Sykes, M.T. Parameter uncertainties in the modelling of vegetation dynamics—Effects on tree community structure and ecosystem functioning in European forest biomes. *Ecol. Model.* **2008**, *216*, 277–290. [CrossRef]
61. Smith, B.; Knorr, W.; Widlowski, J.-L.; Pinty, B.; Gobron, N. Combining remote sensing data with process modelling to monitor boreal conifer forest carbon balances. *For. Ecol. Manag.* **2008**, *255*, 3985–3994. [CrossRef]
62. Hickler, T.; Smith, B.; Prentice, I.C.; Mjöfors, K.; Miller, P.; Arneth, A.; Sykes, M.T. CO_2 fertilization in temperate face experiments not representative of boreal and tropical forests. *Glob. Chang. Biol.* **2008**, *14*, 1531–1542. [CrossRef]
63. Clemmensen, K.; Bahr, A.; Ovaskainen, O.; Dahlberg, A.; Ekblad, A.; Wallander, H.; Stenlid, J.; Finlay, R.; Wardle, D.; Lindahl, B. Roots and associated fungi drive long-term carbon sequestration in boreal forest. *Science* **2013**, *339*, 1615–1618. [CrossRef] [PubMed]
64. Piao, S.; Liu, Z.; Wang, T.; Peng, S.; Ciais, P.; Huang, M.; Ahlstrom, A.; Burkhart, J.F.; Chevallier, F.; Janssens, I.A. Weakening temperature control on the interannual variations of spring carbon uptake across northern lands. *Nat. Clim. Chang.* **2017**, *7*, 359–363. [CrossRef]
65. Liu, Y.; Yu, G.; Wang, Q.; Zhang, Y. How temperature, precipitation and stand age control the biomass carbon density of global mature forests. *Glob. Ecol. Biogeogr.* **2014**, *23*, 323–333. [CrossRef]
66. Zhang, Y.; Shao, X.; Wilmking, M. Dynamic relationships between *Picea crassifolia* growth and climate at upper treeline in the Qilian Mts., northeast Tibetan Plateau, China. *Dendrochronologia* **2011**, *29*, 185–199. [CrossRef]
67. Lepistö, A.; Futter, M.N.; Kortelainen, P. Almost 50 years of monitoring shows that climate, not forestry, controls long-term organic carbon fluxes in a large boreal watershed. *Glob. Chang. Boil.* **2014**, *20*, 1225–1237. [CrossRef] [PubMed]
68. Schimel, D.; Stephens, B.B.; Fisher, J.B. Effect of increasing CO_2 on the terrestrial carbon cycle. *Proc. Natl. Acad. Sci. USA* **2015**, *112*, 436–441. [CrossRef] [PubMed]
69. Friend, A.D.; Lucht, W.; Rademacher, T.T.; Keribin, R.; Betts, R.; Cadule, P.; Ciais, P.; Clark, D.B.; Dankers, R.; Falloon, P.D. Carbon residence time dominates uncertainty in terrestrial vegetation responses to future climate and atmospheric CO_2. *Proc. Natl. Acad. Sci. USA* **2014**, *111*, 3280–3285. [CrossRef] [PubMed]
70. Peng, S.; Zhao, C.; Chen, Y.; Xu, Z. Simulating the productivity of a subalpine forest at high elevations under representative concentration pathway (RCP) scenarios in the Qilian Mountains of northwest China. *Scand. J. For. Res.* **2016**, *32*, 1–31.

forests

MDPI

Article

Forest Floor and Mineral Soil Respiration Rates in a Northern Minnesota Red Pine Chronosequence

Matthew Powers [1,*], Randall Kolka [2], John Bradford [3], Brian Palik [2] and Martin Jurgensen [4]

1 Department of Forest Engineering Resources and Management, Oregon State University, 280 Peavy Hall, Corvallis, OR 97331, USA
2 USDA Forest Service Northern Research Station, 1831 Hwy 169 E, Grand Rapids, MN 55744, USA; rkolka@fs.fed.us (R.K.); bpalik@fs.fed.us (B.P.)
3 US Geological Survey Southwest Biological Science Center, 2255 N. Gemini Dr., Flagstaff, AZ 86001, USA; jbradford@usgs.gov
4 School of Forest Resources and Environmental Science, Michigan Technological University, 1400 Townsend Drive, Houghton, MI 49931, USA; mfjurgen@mtu.edu
* Correspondence: matthew.powers@oregonstate.edu; Tel.: +1-541-737-6550

Received: 31 October 2017; Accepted: 25 December 2017; Published: 29 December 2017

Abstract: We measured total soil CO_2 efflux (R_S) and efflux from the forest floor layers (R_{FF}) in red pine (*Pinus resinosa* Ait.) stands of different ages to examine relationships between stand age and belowground C cycling. Soil temperature and R_S were often lower in a 31-year-old stand (Y31) than in 9-year-old (Y9), 61-year-old (Y61), or 123-year-old (Y123) stands. This pattern was most apparent during warm summer months, but there were no consistent differences in R_{FF} among different-aged stands. R_{FF} represented an average of 4–13% of total soil respiration, and forest floor removal increased moisture content in the mineral soil. We found no evidence of an age effect on the temperature sensitivity of R_S, but respiration rates in Y61 and Y123 were less sensitive to low soil moisture than R_S in Y9 and Y31. Our results suggest that soil respiration's sensitivity to soil moisture may change more over the course of stand development than its sensitivity to soil temperature in red pine, and that management activities that alter landscape-scale age distributions in red pine forests could have significant impacts on rates of soil CO_2 efflux from this forest type.

Keywords: carbon cycling; *Pinus resinosa*; soil respiration; stand age

1. Introduction

Soil respiration represents about 70% of ecosystem respiration in temperate forests [1,2], and includes a combination of respiration from plant roots, mycorrhizae, and microorganisms in the leaf litter, humus, and mineral soil. Variables such as soil temperature [3,4], soil moisture [2,5–7], litter quality and quantity [4,8], and local stand structure [3,9] exert strong controls over soil respiration in forests. Soil temperature and soil moisture may also covary seasonally, or show varying relationships across sites, leading to confounded effects on soil respiration [10,11]. Changes in these variables that occur over the course of stand development could also lead to changes in soil respiration as forests age. Soil temperatures and moisture availability, for instance, may vary between young, open-canopied regenerating stands and stands with a dense, closed canopy representative of the stem exclusion phase of development. As land management agencies begin to incorporate C storage and sequestration into their management goals there is an increasing need to understand how developmental changes influence belowground C cycling.

Soil C cycling can display a large amount of within-system and among-system variability as forests age and develop. Estimates of soil respiration derived from relationships between net primary production and net ecosystem production suggest a characteristic age-related trend in which

the heterotrophic components of soil respiration (micro- and macro-fauna) in temperate forests are expected to decline with age, and the autotrophic portion of soil respiration (plant roots and associated mycorrhizae) are expected to peak in middle-aged stands as net primary production (NPP) and, therefore, substrate supplies peak [12]. Direct measurements of soil respiration in stands of different ages, however, have shown that total soil CO_2 efflux (R_S) can (1) initially increase with age, peaking in young-intermediate-aged, closed canopy stands before declining with age in mature to older stands [4,13,14]; (2) decrease with age [15]; (3) increase steadily from young to old-growth stands [6,16]; or (4) show opposing age-related trends across the geographic range of the same forest type [17]. This variability in age-related soil respiration trends among different systems underscores the need for ecosystem-specific studies.

While respiration from roots and associated mycorrhizae make up the largest proportion of soil respiration [18], estimates of respiration associated with decomposition of the forest floor layers range from 5–48% of total soil respiration in temperate forests [4,18–22]. There are no clearly established patterns of respiration from the forest floor layers (R_{FF}) across stands of different ages, but R_S generally has positive correlations with forest floor mass or thickness [3,15,23]. This suggests that R_{FF} could increase with stand age in forests that are characterized by slow litter decay rates and a resulting increase in forest floor thickness over time. Forests dominated by evergreen conifers, for instance, often accumulate forest floor mass and thickness as they age [24,25], which could lead to increased R_{FF} in older stands. The accumulation of forest floor layers during stand development can also exert a large indirect influence on mineral soil respiration by altering soil temperature and moisture or providing leachate of labile substrate into the mineral soil [26,27].

Understanding how stand age influences C cycling is particularly important because forest management activities have direct impacts on landscape-scale age distributions. Different rotation lengths, for instance, can result in dramatically different abundances of young vs. old stands. This would have significant impacts on soil C losses for systems that show a high degree of variability in soil respiration among age classes. The collection of harvest residues and residual wood as a feedstock for biofuel production can also reduce forest floor and mineral soil C and nutrient stocks [28–30], and litter removal clearly impacts both soil respiration and other soil processes [20,31].

We conducted an experiment to characterize age-related differences in total soil respiration (R_S) and respiration from the forest floor layers (R_{FF}) in red pine (*Pinus resinosa* Ait.) stands aged 9–123 years. Productivity in managed red pine systems peaks between 130 and 140 years across a range of basal areas [32], so we expected R_S to increase steadily with age across our chronosequence due to increases in autotrophic respiration linked to increasing NPP [33]. We also predicted that R_{FF} would increase with age across the chronosequence because forest floor C (and thus, forest floor mass) increases steadily with age up to at least 150 years in red pine forests [25], and forest floor mass is positively correlated with R_S [3,15,23].

2. Materials and Methods

2.1. Study Area

Our study sites included four red pine stands on the Chippewa National Forest in northern Minnesota, USA. The study sites included an open, 9-year-old stand of red pine saplings that were planted following the clearcutting of the previous red pine stand (Y9), a 31-year-old plantation in the early stages of stem exclusion (Y31), a 61-year-old plantation with a well-developed shrub layer and some tree recruitment in the understory (Y61), and a 123 year-old naturally-regenerated stand with a well-develop shrub and understory tree layer (Y123). Three of the stands were located in close proximity (within 1000 m of one another), and the fourth (Y61) was located 5 km to the west.

Forest floor and soil characteristics, live tree density, and basal area varied somewhat by stand age (Table 1). Red pine represented 94–98% of the basal area of stems $\geq$2.5 cm in diameter in Y31, Y61, and Y123, with eastern white pine (*Pinus strobus* L.), paper birch (*Betula papyrifera* Marsh.), balsam fir

(*Abies balsamea* L.), and northern red oak (*Quercus rubra* L.) each representing anywhere from 0–3.4% of the remaining basal area within these stands. Y9 had very little basal area of stems ≥2.5 cm in diameter. Hardwoods represented < 2% of basal area in any stand. Beaked hazel (*Corylus cornuta* Marsch.), balsam fir, juneberries (*Amelanchier* spp.), and blueberries (*Vaccinium* spp.) were the dominant understory shrubs and saplings, with a much more developed shrub, sapling, and herbaceous layer in the young, open-canopied Y9 than the other stands.

Study sites were selected to minimize variability in edaphic and physiographic characteristics that could contribute to differences in the soil environment or local microclimate. All stands were located on coarse-textured, excessively drained outwash sands classified as Menahga mixed, frigid Typic Udipsamments to minimize variability in physical soil characteristics that could contribute to differences in soil respiration [34]. Topographic variation across the study sites was very limited with less than 10 m variability in elevation among sites, slopes less than 10%, and plots within each site located on predominantly south or southeast facing aspects. The study area has an average annual temperature of 3.9 °C and average annual precipitation of 700 mm.

Table 1. Forest floor, soil (0–30 cm), and overstory structure characteristics of 9, 31, 61, and 123 year-old red pine stands used to study age-related changes in soil respiration, forest floor respiration, and litter decomposition.

Stand	Age in 2009 (years)	FF Thickness (cm)	FF Mass (kg/m^2)	FF %C	FF %N	FF C:N	Soil %C	Soil %N	Soil C:N	pH A	pH A-30	Overstory Density (TPH)	Basal Area ($m^2\ ha^{-1}$)
Y9	9	1.67	1.11	40.23	1.30	30.76	2.09	0.10	19.17	4.03	4.96	67	0.04
Y31	31	4.04	2.59	36.51	0.91	39.94	0.69	0.04	19.92	4.48	4.38	2167	40.06
Y61	61	4.90	2.18	49.38	1.11	44.87	0.89	0.06	15.00	4.51	4.80	633	38.18
Y123	123	4.33	2.43	49.76	1.29	38.81	0.72	0.04	19.51	4.40	4.60	650	40.63

FF = forest floor; TPH = trees ha^{-1}; pH A = soil pH from the surface to the top of the A horizon; pH A-30 = soil pH from the top of the A horizon to a depth of 30 cm; all pH values measured in a $CaCl_2$ solution. Forest floor and soil %C and %N measured on a LECO Total Elemental Analyzer. Note that %C and %N data were not ash-corrected. Forest floor mass is an estimate based on a companion study in the same stands [35] and mass from the actual collars in this study.

2.2. Field and Laboratory Methods

We selected a chronosequence of 4 red pine stands at 9, 31, 61, and 123 years of age. We placed 25 cm (inside diameter) PVC (polyvinyl chloride) collars into the soil in November of 2008 after leaf fall of deciduous trees and shrubs (approximately 6 months prior to our first sampling). Nine collars were placed at three randomly located sample plots in each stand, for a total of 27 collars per stand. The nine collars in each plot were placed in groups of three at a distance of four meters from plot center along transects centered at azimuths of 60, 180, and 300 degrees at each plot.

Since the presence of leaf litter can exert a large indirect influence on mineral soil respiration by altering soil temperature and moisture or providing leachate of labile substrate into the mineral soil [26,27], we used forest floor manipulation treatments to examine direct and indirect impacts of forest floor removal on R_S and estimates of R_{FF}. In this context, "direct" implies the additive contribution of CO_2 efflux from litter decomposition to total R_S, while "indirect" implies the effects that modification of the soil environment due to the presence of an intact litter layer could have on both autotrophic and heterotrophic contributions to R_S from the mineral soil. In April of 2010, we removed the forest floor (down to mineral soil) from one randomly selected collar at each transect (the "no litter" treatment) to evaluate how complete forest floor removal impacts soil respiration. Since complete forest floor removal could create indirect impacts on soil respiration by altering the soil environment, we also removed the forest floor from a second PVC collar at each transect, and replaced it with a removable, 20-mesh (841 micron) bag (filled with litter collected from an area near each transect of collars equal in size to the cross-sectional area of the collars themselves. In this treatment (the "removable bag" treatment) the mesh bags were removed immediately prior to taking soil respiration measurements, with the intention of maintaining mineral soil conditions similar to those under intact

litter while removing the direct contribution of CO_2 efflux from the forest floor from estimates of soil respiration. The third collar in each transect was left as an untreated control.

Total soil CO_2 efflux (R_S) was measured on a monthly basis on all 27 collars in each stand from May through October in 2009 (pre-manipulation; i.e., prior to litter removal and removable bag installation) and from April through October in 2010 (post-manipulation; i.e., after litter removal and removable bag installation) using a custom-built, closed-chamber system with an LI-820 gas analyzer (LI-Cor, Inc., Lincoln, NE, USA) connected to a datalogger programmed to record the CO_2 concentrations in the system at 2 s intervals. Equipment malfunctions prevented us from completing the August 2009 measurement.

Since our closed-chamber system calculates CO_2 flux rates by first scrubbing CO_2 out of the chamber and then measuring the rate of increase as chamber CO_2 rises back to a pre-set upper boundary, measurement times on individual collars varied based on instantaneous flux rates. R_S measurements were conducted over a 2–3 day period each month, with all collars in each stand being sampled on a single day in each month. Individual stands were sampled at alternating the times of day (0930–1200 or 1200–1500) from one month to the next in an effort to average out variability associated with taking measurements at different locations at different times of day.

Temperature readings from the top 10 cm of soil suggest soils were frozen from mid-late November until mid-April during both years of measurement, so we assume that soil respiration was minimal during the November to April period. All fresh litter inputs were removed from the no litter treatments on a bi-weekly to monthly basis throughout our 2010 measurements, and respiration measurements in the removable bag treatment were made five to ten minutes after removing the bags from the collars to allow the CO_2 environment within the collar to equilibrate after removing the bag. We measured mineral soil temperature at a depth of 10 cm next to each collar, and measured volumetric soil moisture content in the top 12 cm of the mineral soilusing a HydroSense Soil Water Measurement System consisting of a CS620 sensor attached to a CD620 display (Campbell Scientific, Inc., Logan, UT, USA). Soil moisture measurements were taken at four points around each collar during each soil respiration measurement. After litter treatment in 2010, temperature and moisture measurements for the no litter and removable bag treatments were made within similar treatment areas next to each treatment collar to capture treatment effects without disturbing the soil environment within the collars used for respiration measurements.

We estimated R_{FF} based on the differences of R_S measurements between the control and treatment collars as Equations (1) and (2):

$$R_{FF\ NO\ LITTER} = R_{S\ CONTROL} - R_{S\ NO\ LITTER} \quad (1)$$

and

$$R_{FF\ REMOVABLE\ BAG} = R_{S\ CONTROL} - R_{S\ REMOVABLE\ BAG} \quad (2)$$

where R_{FF} is respiration from the forest floor layers, $R_{S\ CONTROL}$ is the measured respiration from the control collar in a transect, $R_{S\ CONTROL}$ is the measured respiration from the "no litter" treatment collar in that transect (i.e., collars that received a complete litter removal treatment), and $R_{S\ REMOVABLE\ BAG}$ is the measured respiration from the "removable bag" collar in that same transect (i.e., collars in which the litter was removed from the collar and replaced with a mesh bag filled with litter that could be left in place between measurements and removed immediately prior to measurements).

2.3. Analytical Methods

We analyzed litter treatment and stand age effects on R_S, R_{FF}, soil temperature, and soil moisture using linear mixed models. Models included litter treatment, stand age, month of measurement, and the interactions among these three factors as fixed effects along with random effects to account for the spatial nesting of litter treatments within plots and the temporal nesting of measurements within plots. We used averages of litter treatments or litter types from the three transects at each plot as the

dependent variable in each analysis. Respiration data, temperature data, and moisture data from 2009 and 2010 were analyzed separately because the measurements spanned different months in the two years. Bonferroni-adjusted t-tests were used to evaluate significant differences between treatment levels. Model assumptions were evaluated with residual plots.

We analyzed relationships between R_S and soil temperature based on the exponential growth function (Equation (3)):

$$R_S = \beta_1 \exp(\beta_2 \times T) \quad (3)$$

where R_S is soil respiration and T is temperature. To include nested random effects (which do not have built-in support for mixed-effects nonlinear models in SAS version 9.2 (SAS Institute, Cary, NC, USA)) to account for repeated measurements on collars representing different treatments within plots, we log-transformed the exponential growth function, and analyzed the soil respiration—temperature relationship using linear mixed models of the form (Equation (4)):

$$LN(R_S) = LN(\beta_1) + (\beta_2) \times T \quad (4)$$

where LN refers to the natural logarithm, R_S is soil respiration, and T is soil temperature. To test for potential stand age and litter treatment effects on the relationship between soil respiration and temperature, we fit models that allowed β_1 and β_2 to vary both individually and in tandem across the levels of both stand age and litter treatment. We used AIC scores to choose the model with the best fit to our data, but also considered the *p*-values of individual model terms to judge the significance of age and litter treatment effects. All models relating R_S to temperature included random effects to account for the use of repeated measurements and the nesting of treatments within plots in each stand. We estimated the sensitivity of soil respiration to temperature using Q_{10} values. We calculated Q10 as Equation (5):

$$Q_{10} = (R_2/R_1)^{(10/(T_2-T_1))} \quad (5)$$

where R_1 and R_2 are modeled soil respiration rates at temperatures T_1 and T_2, respectively.

We also used linear mixed models to analyze relationships between soil respiration and soil moisture. All soil moisture models followed the general form (Equation (6)):

$$R = \beta_1 + \beta_2 \times SM \quad (6)$$

where R is either an absolute, or one of two normalized measure of soil respiration and SM is volumetric soil moisture. Thus, we ran three sets of models relating soil respiration to soil moisture including (1) one set including our direct, field-based R_S estimates as the dependent variable; (2) a second set using a normalized expression of soil respiration (we refer to this as R_{SN}) calculated as the ratio of observed R_S to the value predicted by our best-fitting temperature model based on soil temperatures at the time of field R_S sampling; and (3) a third set expressing soil respiration as the difference between our observed value from field measurements of R_S, and the value predicted by our best-fitting temperature model based on soil temperatures at the time of field R_S sampling (we refer to this variable as R_{SDIF}).

Like our respiration-temperature models, we fit respiration-moisture models that allowed β_1 and β_2 to vary by both individually and in combination across the levels of stand age and litter type, then used AIC scores to choose the best model. We used residual plots to analyze model assumptions regarding the normality and homogeneity of error variances for all of our regression models, and applied transformations when necessary. We used Bonferroni-adjusted *t*-tests for all multiple comparisons. We calculated a conditional R^2-type goodness of fit value for the respiration—temperature and respiration—moisture models as Equation (7):

$$R^2{}_C = 1 - \left[\Sigma(y_{ij} - \hat{y}_{ij})^2 / \Sigma(y_{ij} - \overline{y})^2\right] \quad (7)$$

where y_{ij} and $\hat{y}_{ij}$ are the observed and predicted respiration rates for each individual subject and $\bar{y}$ is the overall mean of the observed respiration rates [36]. All statistical analyses were performed using SAS version 9.2 (SAS Institute, Cary, NC, USA) at $\alpha = 0.05$ significance level.

3. Results

3.1. Total Soil Respiration

Litter treatment had significant impacts on R_S ($p = 0.010$ for post-manipulation measurements), and stand age ($p < 0.001$ and $p = 0.001$), month of measurement ($p < 0.001$ for both years), and the stand age *x* month of measurement interaction ($p < 0.001$ for both years) were also significant in the pre-manipulation and post-manipulation measurement years. There were no significant interactions involving litter treatment in either year of measurement. There were no significant differences in R_S among collars assigned different litter treatments prior to litter treatment ($p = 0.285$), but R_S was significantly lower for the no litter treatment than for the control treatment after litter treatment (Table 2).

Table 2. Effects of forest floor removal treatments on total soil respiration (R_S), forest floor respiration (R_{FF}) (calculated after litter treatment in 2010 only), and soil moisture (SM) before (2009) and after (2010) experimental litter removal treatment in red pine stands. Different letters indicate significant differences among treatments within a column. Respiration rates reported in μmol CO_2 m^{-2} s^{-1}.

Treatment	R_S 2009	R_S 2010	R_{FF} 2010	SM (%) 2009	SM (%) 2010
No Litter	3.23 (a)	2.93 (b)	0.35 (a)	10.36 (a)	14.02 (b)
Removable Bag	3.30 (a)	3.21 (ab)	0.06 (b)	10.62 (a)	12.67 (b)
Control	3.17 (a)	3.27 (a)	–	10.60 (a)	12.79 (a)

Averaged across months, R_S was highest in Y9 and lowest in Y31 in 2009, and generally lowest in Y31, but similar among other stands in 2010 (Table 3). However, the age effect was variable across the individual months of measurement (Figure 1). From May through September of 2009 (Figure 1e) and June through August of 2010 (Figure 1f), R_S was generally lowest in Y31. There were no differences in R_S among stands in October of 2009, or in April, May, or October of 2010, when soil temperatures were at their lowest for each year. Y61 had higher R_S than any other stand in September of 2010, but was generally similar to the Y9 and Y123 stands in other months. Monthly variability in R_S generally paralleled soil temperature trends in both years. In 2009, R_S monthly patterns of Y61 and Y123 closely followed the temperature trend, although R_S in Y9 and Y31 began declining in July while soil temperatures remained high. In 2010, R_S patterns closely followed the monthly temperature trends, showing a steady increase through August followed by a decline in September and October.

Table 3. Mean values of total soil respiration (R_S), volumetric soil moisture (SM), soil temperature (T), and forest floor respiration (R_{FF}) before experimental litter removal (2009) and after litter removal (2010) in red pine stands aged 9 (Y9), 31 (Y31), 61 (Y61), and 123 (Y123) years. Values represent annualized averages across multiple months of measurement in each year. R_{FF} was calculated only after litter removal (i.e., only in 2010). Different letters indicate significant differences among treatments within a column. Respiration rates reported in μmol CO_2 m^{-2} s^{-1}.

Stand ID	R_S 2009	R_S 2010	R_{FF} 2010	T (°C) 2009	T (°C) 2010	SM (%) 2009	SM (%) 2010
Y9	3.78 (a)	3.11 (ab)	0.08 (a)	12.51 (a)	10.02 (a)	13.36 (a)	15.72 (a)
Y31	2.32 (b)	2.46 (b)	0.42 (a)	10.05 (c)	8.98 (b)	9.39 (b)	12.71 (b)
Y61	3.54 (c)	3.76 (a)	0.05 (a)	11.26 (b)	9.99 (a)	9.71 (b)	11.14 (b)
Y123	3.30 (c)	3.20 (ab)	0.27 (a)	10.49 (c)	8.95 (b)	9.96 (b)	13.07 (b)

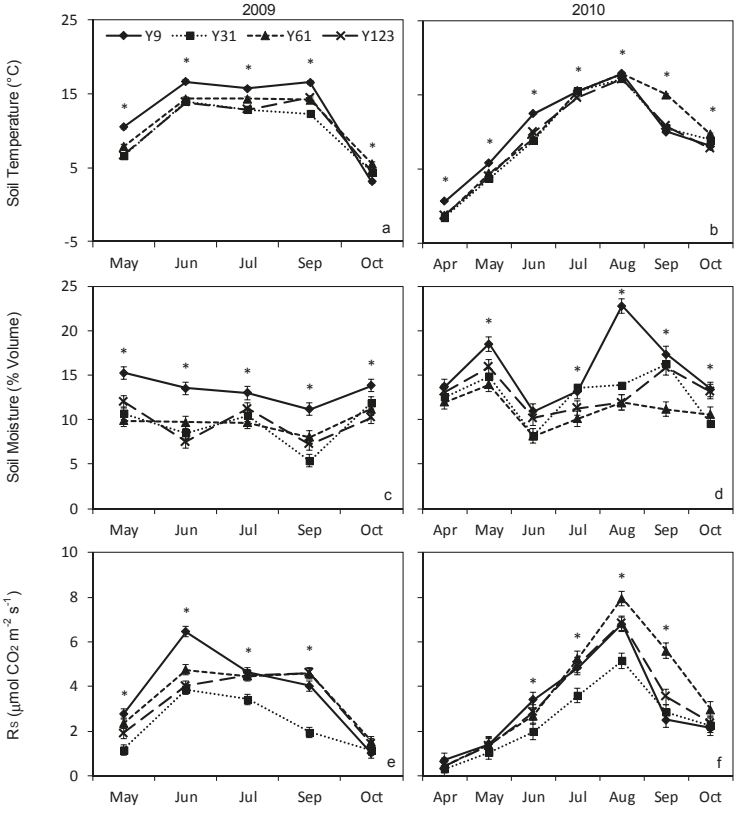

Figure 1. Soil temperatures (a, b), soil moisture (c, d), and soil respiration (R_S, e, f) from two years of measurement in 9, 31, 61, and 123 year-old red pine stands in northern Minnesota, USA. Error bars indicate standard error. An asterisk indicates a month with significant differences among stand ages.

3.2. Forest Floor Respiration

Our estimates of R_{FF} were more than five times higher for the no litter treatment than for the removable bag treatment ($p = 0.044$, Table 2). R_{FF} was not significantly affected by stand age (Table 3) or month of measurement, and there were no significant interactions between stand age, month of measurement, and litter treatment type (i.e., $R_{FF\ LITTER}$ vs. $R_{FF\ REMOVABLE\ BAG}$). R_{FF} represented 13.1% of R_S in the no litter treatment compared to 3.9% of R_S in the removable bag treatment ($p = 0.018$, Table 2). This percentage varied by month of measurement ($p < 0.001$), but the month effect was not consistent across stands of different ages ($p = 0.027$). R_{FF} generally represented the smallest percentage of R_S in April when soil temperatures were lowest across all stands, but differences among other months were highly variable across stands (Figure 2). There were no significant interactions involving litter treatment, so monthly values displayed in Figure 2 have been expressed as the mean of R_{FF} estimates calculated using the removable bag treatment and the mineral soil treatment.

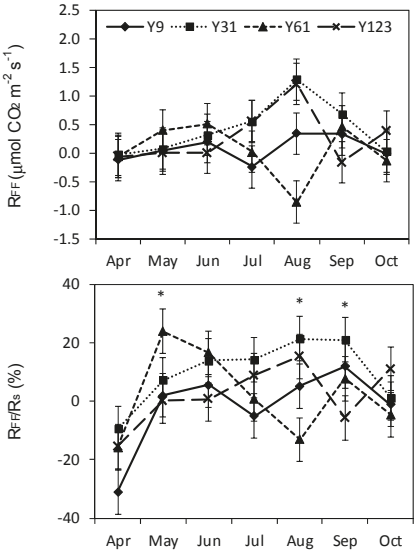

Figure 2. CO_2 efflux from forest floor layers (R_{FF}, top panel) and the percentage of total soil respiration (R_S) represented by the forest floor (bottom panel) in 9, 31, 61, and 123 year-old red pine stands in northern Minnesota, USA. Error bars indicate standard error. An asterisk indicates a month with significant differences among stand ages. R_{FF} estimates displayed here reflect the mean of values calculated from two separate treatments (complete litter removal and temporary removal of litter in a mesh bag).

3.3. Soil Temperature and Moisture

Litter treatment did not have a significant effect on soil temperature in either pre- or post-treatment measurements ($p = 0.999$ and 0.372, respectively), but stand age ($p < 0.001$ for both years) and month of measurement ($p < 0.001$ for both years) each did, and the stand age effect varied across months ($p < 0.001$ for both years). There were no significant interactions involving litter treatment in either year of measurement. Averaged across months, soil temperatures were generally highest in Y9, lowest in Y31 and Y123, and intermediate to high in Y61 (Table 3), but these patterns changed in October, when soil temperatures were lowest in Y9 and highest in Y61 (Figure 1). The temporal trends of soil temperature were somewhat different from 2009 to 2010. In 2009, soil temperatures increased from May to June, were similar in June, July, and August, and then declined rapidly (Figure 1a). In 2010, soil temperatures rose steadily from April through August then declined in September and October (Figure 1b). Soil temperatures in the spring of 2009 were somewhat higher than those during the spring of 2010 but the reverse was true during late summer and autumn.

Litter treatment had a significant impact on soil moisture in 2010 ($p < 0.001$), and stand age, month of measurement, and the stand age *x* month of measurement interaction were each significant in both the pre-manipulation and post-manipulation years of measurement ($p < 0.001$ for all). There were no significant interactions involving litter treatment in either year of measurement. Although there were no differences between collars assigned different litter treatments prior to manipulation in 2009 ($p = 0.174$), soil moisture was higher in the no litter treatment than in the removable bag and control treatments after litter treatment in 2010 (Table 2). In 2009, soil moisture was typically highest in Y9, and similar among other treatments (Table 3, Figure 1c). In 2010, soil moisture was similar among stands during April and October, highest in Y9 during May and August, and generally low in Y61 during July and September (Figure 1d).

3.4. Relationships between Soil Respiration, Temperature, and Moisture

There was a significant, exponential relationship between R_S and temperature ($p < 0.001$, $R^2_C = 0.787$), but stand age and litter treatment did not have significant effects on the R_S—temperature relationship (Figure 3). There was also a significant, logarithmic relationship between R_S and soil moisture ($p < 0.001$), but model predictions were not well correlated with field observations ($R^2_C = 0.083$). Additionally, the shape of the R_S—moisture relationship varied with stand age ($p < 0.001$ for both soil moisture and the soil moisture *x* stand age interaction). Our model predicted positive relationships between R_S and moisture in Y9 and Y31, but negative relationships between these two variables in Y61 and Y123 stands (Figure 4).

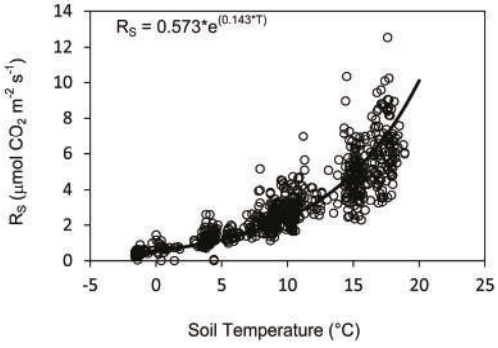

Figure 3. Relationships between soil respiration (R_S) and soil temperature in red pine stands in northern Minnesota, USA.

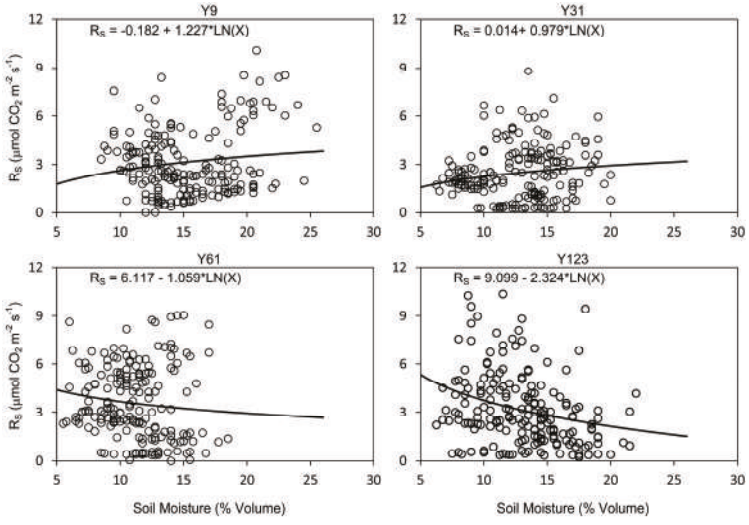

Figure 4. Relationships between soil respiration (R_S) and soil moisture in 9 (Y9), 31 (Y31), 61 (Y61), and 123 (Y123) year-old red pine stands in northern Minnesota, USA.

R_{SN} was not significantly correlated with soil moisture ($p = 0.407$), and age, litter treatment, and the interactions among these three variables did not have significant effects on R_{SN} in any of the models we tested (Figure 5). Further, no R_{SN} models including any combination of soil moisture, age,

litter treatment and their interactions performed better than the null model for R_{SN} that included only the intercept and mixed-effects terms accounting for the spatial nesting of collars within plots and the repeated measurements of individual collars and plots over time. R_{SDIF} did have a significant, negative relationship with soil moisture ($p = 0.0137$), but stand age, litter treatment, and their interactions were never significant, and no models including stand age or litter treatment as fixed effects improved on the fit of the general R_{SDIF} to soil moisture model (Figure 5). Further, the correlation between R_{SDIF} and soil moisture was extremely weak ($R^2_C = 0.009$).

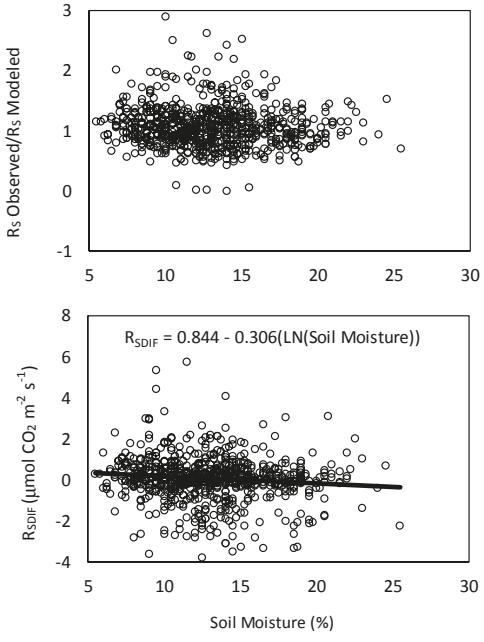

Figure 5. Relationships between two normalized estimates of soil respiration (R_S) and soil moisture in red pine stands in northern Minnesota, USA. R_S Observed (top panel) indicates direct, field-based measurements of soil CO_2 efflux, and R_S modeled (bottom panel) indicates estimates of soil CO_2 efflux derived from our best-fitting regression model relating R_S to temperature. R_{SDIF} was calculated as the differences between R_S Observed and R_S Modeled.

4. Discussion

Our results suggest that stand age may have significant impacts on soil carbon cycling in red pine ecosystems, but stand age had different effects on R_S and R_{FF}. Our young, closed-canopy stand in the early stages of stem exclusion (Y31) showed a distinct seasonal pattern of R_S compared to a young stand regenerating after a clearcut, a mature stand, and an old stand. In contrast, stand age had little impact on R_{FF} or R_{FF}'s contribution to R_S. Our results also suggest that the forest floor influences soil respiration both directly, through the contribution of CO_2 efflux associated with the decomposition of litter material, and indirectly, by altering the physical environment within the upper mineral soil.

4.1. Stand Age Effects on Soil Respiration

Our results do not support the increasing trend of R_S that was predicted based on linkages between productivity and respiration [33]. Although theory predicts a possible decline in R_S from middle-aged to older forests [12], several studies have reported positive relationships between stand

age and soil respiration rates spanning various stages of forest development [6,13,16,17]. We found no evidence of either of these patterns, but we did find that soil respiration rates were often lower in Y31 than in the other stands during the middle of the growing season, particularly in July and August when soil temperatures were highest. Y31 often had lower soil temperatures than the other stands, particularly Y9 and Y61. As other studies have indicated [10,19,37], we found that R_S increased exponentially with increasing soil temperature, so low soil temperatures are a likely cause of the low soil respiration rates in Y31. In our study system, Y31 is representative of plantations in the stem exclusion stage of development. Dense canopies that severely limit understory light availability are common characteristics of this phase [38], which could explain the low soil temperatures we observed in Y31. Although we did not directly measure either understory light availability or overstory leaf area index in these stands, we anecdotally observed that Y31 had very limited understory forb and shrub development in comparison with the other sites, which could be indicative of lower light levels on the forest floor, and thus, lower soil temperatures.

Although the R_S-temperature relationship appeared relatively stable across our stands, we did find evidence that the R_S-soil moisture relationship varied among different-aged stands. Some studies have reported that soil respiration's sensitivity to temperature can change with stand age or successional status [13,16,19], but few have reported different age-related trends in the R_S-moisture relationship. Like Irvine and Law [6], we found that soil respiration rates were generally higher in our older stands than in our younger stands during periods of low soil moisture. As soil moisture increased, however, soil respiration rates increased in Y9 and Y31 stands, but declined in Y61 and Y123. While the cause of declining R_S as soil moisture increased in Y61 and Y123 stands is unclear, the effect (i.e., decreasing differences in R_S between young and older stands as soil moisture increases) is consistent with Irvine and Law's [6] proposal that the larger trees in older stands may avoid drought impacts on metabolic processes by accessing water in deeper soil horizons. The possibility of reduced drought impacts on metabolic processes in older stands is also consistent with findings from foliar gas exchange studies that suggest larger trees in older stands show less physiological response to drought than smaller trees in younger stands [39–41]. Thus, the age-related trends we observed for the R_S-moisture relationship are likely driven by more pronounced physiological responses (including respiratory functions associated with growth and maintenance) to drought in younger stands. However, we caution that relationships between R_S and soil moisture in our dataset were extremely weak, so soil moisture availability was not likely a major driver of R_S variability in our system. Soil moisture typically exerts strong controls on R_S in forests only when soils are very dry or very wet [10,42], so it is possible that the 5–15% range of volumetric soil moisture content observed in this study simply did not produce conditions that would limit either decomposer activity or root respiration.

Although we found only limited evidence of age-related variability in the R_S-moisture relationship, seasonal patterns of R_S appeared to closely track soil temperature trends, regardless of stand age. The plateaued pattern of R_S characteristic of most stands in 2009 and the late summer peak in R_S observed in all stands in 2010 paralleled the monthly soil temperature variability for those two years, and the high R_S values observed in Y61 during September 2010 occurred during a period with higher soil temperatures in that stand than in any other stand. In contrast the seasonal dips in soil moisture observed in September of 2009 and June of 2010 did not appear to have a large influence on R_S and the correlation coefficient for our R_S-moisture relationship was an order of magnitude lower than that of our R_S-temperature relationship. Annualized averages of R_S across months of measurement in both years also closely tracked stand-level average soil temperatures, and the generally low soil temperatures in the dense-canopied Y31 appear to be a primary driver of this stand's low R_S, particularly when compared with the young, open-canopied Y9, which had considerably higher average soil temperatures.

Additionally, our two normalized estimates of R_S (i.e., R_{SN} and R_{SDIF}), which expressed observed R_S relative to predictions from our R_S-temperature model, showed little to no relationship with soil moisture. This suggests that some of the apparent soil moisture impacts on R_S across stand of different

ages that we observed were likely driven by covarying temperature trends as was observed in other studies e.g., [10,11]. Collectively, these results underscore the importance of soil temperature as a driver of R_S variability e.g., [3,4], and suggest that variations in stand structure that influence soil temperatures (such as the transition from an open-canopy during cohort establishment or stand initiation phase to a dense, closed-canopy during stem exclusion) could potentially exert significant controls on soil carbon cycling.

Although we did not directly test the relationships, variability in soil temperature paralleled differences in temperatures across the two years, while soil moisture generally tracked precipitation levels in the wetter 2010 sampling period, but not as closely in the drier summer of 2009 (Table 4). That both soil temperatures and soil respiration followed the summer plateau pattern of air temperatures in 2009 and the gradual rise in air temperatures through August of 2010, regardless of stand age, speaks to the strong controls that climate exerts on soil processes.

Table 4. Mean monthly temperature (T) and precipitation (P) data for our study area during the months of R_S measurement in 2009 and 2010 [43].

Month	T (°C) 2009	T (°C) 2010	P (mm) 2009	P (mm) 2010
April	4.3	9.1	31.5	28.4
May	10.6	12.6	41.7	59.1
June	16.0	16.9	85.6	91.1
July	17.6	21.1	58.4	120.4
August	17.7	20.8	63.7	129.7
September	17.4	11.7	46.7	141.5
October	3.6	8.8	125.2	66.5

4.2. Forest Floor Contributions to Soil Respiration

Our results indicate that forest floor removal reduced R_S by 4–13% over the course of our April through October sampling (when averaged across R_{FF} estimates from the no litter and removable bag treatment), but do not suggest the anticipated age-related effects on either R_{FF} or the forest floor's contributions to R_S. While several studies have found that respiration from organic horizons represents a larger percentage of R_S than our estimates [18–20,22,44], our results fall within the range reported by others [4,22,24], and support the general consensus across these studies that root respiration and decomposition of organic compounds within the mineral soil represent the largest contributions to R_S.

The reasons for the relatively low forest floor contributions to R_S found in our study are not clear, although substrate quality could be a factor. Like the mineral soil, respiration rates in the forest floor are negatively correlated with the C:N ratio of the substrate [4], and three of our four stands had relatively high forest floor C:N ratios. Forest floor C:N ratios ranged from 39–45 in our Y31, Y61, and Y123 stands. In contrast, forest floor C:N ratios range from 31–32 in young and old-growth Appalachian hardwood forests [4], 34–35 for Douglas-fir (*Pseudotsuga menziesii* Franco) stands in the western United States [24], 29–32 in young to middle-aged Chinese hardwood forests [45], and 21–27 for various components of the forest floor in a tropical montane cloud forest [41]. While the forest floor C:N ratio of our youngest stand was somewhat lower than the other three stands, this stand had a much smaller forest floor layer than the older stands. Forest floor thickness is positively correlated with respiration rates [3,15], so the thinner forest floor may have offset the effects of higher quality litter in Y9, which could explain why R_{FF} estimates were similar across stands despite the difference in forest floor C:N ratios.

The result that R_S in the removable bag treatment was similar to R_S for the control treatments suggests that at least some portion of the difference between control and no litter treatments was due to the influence that forest floor layers exert on the mineral soil environment [31]. Soil temperatures, however, were similar among the three litter treatments. Soil moisture was higher in the no litter treatment, but soil moisture generally has a positive relationship with R_S [5,7], and had little to no

relationship with temperature-normalized estimates of R_S in our study, so increased soil moisture is not a likely explanation for lower respiration rates in the no litter treatment. If anything, increased soil moisture in the no litter treatment may have compensated in part for reductions in R_S associated with the absence of a decomposing forest floor. If the difference in soil respiration rates between no litter and control collars was due entirely to the absence of respiration contributions from the forest floor, however, we would expect a similar difference to be apparent in the removable bag treatment. The apparent importance of indirect forest floor impacts on R_S could suggest that R_{FF} and mineral soil respiration estimates from studies that do not account for the forest floor's environmental influences may contain considerable error, at least in systems with relatively thick forest floor layers, such as the red pine forest studied here. The lack of soil temperature differences between the no litter and removable bag treatments, and limited impact of soil moisture on R_S observed at our study sites, however suggest that indirect controls of the soil respiration other than soil microclimate drove the differences in R_{FF} estimates between the no litter and removable bag treatments that we observed.

Negative estimates of R_{FF} during some individual measurement periods were an artifact of our R_{FF} estimation technique, which relied on the difference in soil CO_2 efflux measurements between control collars and adjacent collars where litter was removed. Although efforts were made to place adjacent collars in similar environments and adjacent collars generally had similar soil environments (as measured by soil temperature and moisture), differences in autotrophic contributions to soil CO_2 efflux associated with variable live root biomass beneath collars may have contributed error to our R_{FF} estimates. However estimates of the contribution of R_{FF} to total R_S in a study that used similar methods of estimating R_{FF} while also controlling for root respiration via trenching were broadly similar to our estimates [18], Additionally, litter contributions to total R_S have been shown to be very low during the pre-growth and pre-dormancy period [22], which suggests that even small differences in autotrophic respiration could have contributed to the generally negative estimates of R_{FF} for our earliest and latest measurement periods.

5. Conclusions

Our results have some important implications about C cycling in red pine ecosystems. First, soil respiration responses to changes in temperature appear to be relatively constant across stand ages in red pine. Differences in soil temperature also appear to contribute to low soil respiration rates in dense, young, closed-canopy red pine plantations when compared to open-canopied regenerating stands and older stands that have transitioned out of the stem exclusion phase of development. This suggests that changes in rotation lengths for red pine management could impact soil C dynamics by modifying the proportional representation of age classes across the landscape and consequently, shifting the relative abundance of stand structures with relatively low soil respiration rates (e.g., our young, closed canopy plantation) vs. those with higher, or more seasonally-variable soil respiration rates (e.g., our young, open-canopied stand and our more mature stands).

Acknowledgments: We would like to thank Doug Kastendick, Nate Aspelin, Eric Doty, and Ryan Kolka for their assistance in locating field sites, installing respiration collars and litter bags, collecting soil respiration data, and processing litter samples in the laboratory. Funding for this project was provided by the United States Department of Agriculture Forest Service Northern Research Station and the Agenda 2020 Program. Any use of trade, product, or firm names is for descriptive purposes only and does not imply endorsement by the United States Government.

Author Contributions: R.K., J.B., B.P. and M.J. conceived and designed the experiments; M.P. performed the experiments and analyzed the data; M.P. wrote the paper with significant feedback from R.K., J.B., B.P. and M.J.

Conflicts of Interest: The authors declare no conflict of interest.

References

1. Law, B.E.; Ryan, M.G.; Anthoni, P.M. Seasonal and annual respiration of a ponderosa pine ecosystem. *Glob. Chang. Biol.* **1999**, *5*, 169–182. [CrossRef]

2. Janssens, I.A.; Lankreijer, H.; Matteucci, G.; Kowalski, A.S.; Buchmann, N.; Epron, D.; Pilegaard, K.; Kutsch, W.; Longdoz, B.; Gruènwald, T.; et al. Productivity overshadows temperature in determining soil and ecosystem respiration across European forests. *Glob. Chang. Biol.* **2001**, *7*, 269–278. [CrossRef]
3. Saiz, G.; Green, C.; Butterback-Bahl, K.; Kiese, R.; Avitabile, V.; Farrell, E.P. Seasonal and spatial variability of soil respiration in four Sitka spruce stands. *Plant Soil* **2006**, *287*, 161–176. [CrossRef]
4. Vose, J.M.; Bolstad, P.V. Biotic and abiotic factors regulating forest floor CO_2 flux across a range of forest age classes in the southern Appalachians. *Pedobiologia* **2007**, *50*, 577–587. [CrossRef]
5. Orchard, V.A.; Cook, F.J. Relationship between soil respiration and soil moisture. *Soil Biol. Biochem.* **1983**, *15*, 447–453. [CrossRef]
6. Irvine, J.; Law, B.E. Contrasting soil respiration in young and old-growth ponderosa pine forests. *Glob. Chang. Biol.* **2002**, *8*, 1183–1194. [CrossRef]
7. Cook, F.J.; Orchard, V.A. Relationships between soil respiration and soil moisture. *Soil Biol. Biochem.* **2008**, *40*, 1013–1018. [CrossRef]
8. Raich, J.W.; Nadelhoffer, K.J. Belowground carbon allocation in forest ecosystems: Global trends. *Ecology* **1989**, *70*, 1346–1354. [CrossRef]
9. Søe, A.R.B.; Buchmann, N. Spatial and temporal variations in soil respiration in relation to stand structure and soil parameters in an unmanaged beech forest. *Tree Physiol.* **2005**, *25*, 1427–1436. [CrossRef] [PubMed]
10. Davidson, E.E.; Belk, E.; Boone, R.D. Soil water content and temperature as independent or confounded factors controlling soil respiration in a temperate mixed hardwood forest. *Glob. Chang. Biol.* **1998**, *4*, 217–227. [CrossRef]
11. Wang, B.; Zha, T.S.; Jia, X.; Wu, B.; Zhang, Y.Q.; Qin, S.G. Soil moisture modified the response of soil respiration to temperature in a desert shrub ecosystem. *Biogeosciences* **2014**, *11*, 259–268. [CrossRef]
12. Pregitzer, K.S.; Euskirchen, E.S. Carbon cycling and storage in world forests: Biome patterns related to forest age. *Glob. Chang. Biol.* **2004**, *10*, 1–26. [CrossRef]
13. Tang, J.; Bolstad, P.V.; Martin, J.G. Soil carbon fluxes and stocks in a Great Lakes forest chronosequence. *Glob. Chang. Biol.* **2009**, *15*, 145–155. [CrossRef]
14. Wang, B.; Jiang, Y.; Wei, X.; Zhao, G.; Guo, H.; Bai, X. Effects of forest type, stand age, and altitude on soil respiration in subtropical China. *Scand. J. For. Res.* **2011**, *26*, 40–47. [CrossRef]
15. Saiz, G.; Byrne, K.A.; Butterbach-Bahl, K.; Kiese, R.; Blujdea, V.; Farrell, E.P. Stand age-related effects on soil respiration in a first rotation Sitka spruce chronosequence in central Ireland. *Glob. Chang. Biol.* **2006**, *12*, 1007–1020. [CrossRef]
16. Martin, D.; Beringer, J.; Hutley, L.B.; McHugh, I. Carbon cycling in a mountain ash forest: Analysis of below ground respiration. *Agric. For. Meteorol.* **2007**, *147*, 58–70. [CrossRef]
17. Gough, C.M.; Seiler, J.R.; Wiseman, P.E.; Maier, C.A. Soil CO_2 efflux in loblolly pine (*Pinus taeda* L.) plantations on the Virginia Piedmont and South Carolina Coastal Plain over a rotation-length chronosequence. *Biogeochemistry* **2005**, *73*, 127–147. [CrossRef]
18. Bowden, R.D.; Nadelhoffer, K.J.; Boone, R.D.; Melillo, J.M.; Garrison, J.B. Contributions of aboveground litter, belowground litter, and root respiration to total soil respiration in a temperate mixed hardwood forest. *Can. J. For. Res.* **1993**, *23*, 1402–1407. [CrossRef]
19. Buchmann, N. Biotic and abiotic factors controlling soil respiration rates in *Picea abies* stands. *Soil Biol. Biochem.* **2000**, *32*, 1625–1635. [CrossRef]
20. Borken, W.; Beese, F. Soil respiration in pure and mixed stands of European beech and Norway spruce following removal of organic horizons. *Can. J. For. Res.* **2005**, *35*, 2756–2764. [CrossRef]
21. Ngao, J.; Epron, D.; Brechet, C.; Granier, A. Estimating the contribution of leaf litter decomposition to soil CO_2 efflux in a beech forest using ^{13}C-depleted litter. *Glob. Chang. Biol.* **2005**, *11*, 1168–1776. [CrossRef]
22. DeForest, J.L.; Chen, J.; McNulty, S.G. Leaf litter is an important mediator of soil respiration in an oak-dominated forest. *Int. J. Biometeorol.* **2009**, *53*, 127–134. [CrossRef] [PubMed]
23. Martin, J.G.; Bolstad, P.V. Variation of soil respiration at three spatial scales: Components within measurements, intra-site variation and patterns on the landscape. *Soil Biol. Biochem.* **2009**, *41*, 530–543. [CrossRef]
24. Giesen, T.W.; Perakis, S.S.; Cromack, K., Jr. Four centuries of soil carbon and nitrogen change after stand-replacing fire in a forest landscape in the western Cascade Range of Oregon. *Can. J. For. Res.* **2008**, *38*, 2455–2464. [CrossRef]

25. Bradford, J.B.; Kastendick, D.N. Age-related patterns of forest complexity and carbon storage in pine and aspen-birch ecosystems of northern Minnesota, USA. *Can. J. For. Res.* **2010**, *40*, 401–409. [CrossRef]
26. Borken, W.; Davidson, E.A.; Savage, K.; Gaudinxki, J.; Trumbore, S.E. Drying and wetting effects on CO_2 release from organic horizons. *Soil Sci. Soc. Am. J.* **2003**, *67*, 1888–1896. [CrossRef]
27. Sulzman, E.W.; Brant, J.B.; Bowden, R.D.; Lajtha, K. Contribution of aboveground litter, belowground litter, and rhizosphere respiration to total soil CO_2 efflux in an old growth coniferous forest. *Biogeochemistry* **2005**, *73*, 231–256. [CrossRef]
28. Mendham, D.S.; O'Connell, A.M.; Grove, T.S.; Rance, S.J. Residue management effects on soil carbon and nutrient contents and growth of second rotation eucalypts. *Forest Ecol. Manag.* **2003**, *181*, 357–372. [CrossRef]
29. Walmsley, J.D.; Godbold, D.L. Stump harvesting for bioenergy—A review of the environmental impacts. *Forestry* **2010**, *83*, 17–38. [CrossRef]
30. Peckham, S.D.; Gower, S.T. Simulated long-term effects of harvest and biomass residual removal on soil carbon and nitrogen content and productivity for two Upper Great Lakes forest ecosystems. *Glob. Chang. Biol. Bioenergy* **2011**, *3*, 135–147. [CrossRef]
31. Sayer, E.J. Using experimental manipulation to assess the roles of leaf litter in the functioning of forest ecosystems. *Biol. Rev.* **2006**, *81*, 1–31. [CrossRef] [PubMed]
32. D'Amato, A.W.; Palik, B.J.; Kern, C.C. Growth, yield, and structure of extended rotation *Pinus resinosa* stands in Minnesota, USA. *Can. J. For. Res.* **2010**, *40*, 1000–1010. [CrossRef]
33. Högberg, P.; Nordgren, A.; Buchmann, N.; Taylor, A.F.S.; Ekblad, A.; Högberg, M.N.; Nyberg, G.; Ottosson-Löfvenius, M.; Read, D.J. Large-scale forest girdling shows that current photosynthesis drives soil respiration. *Nature* **2001**, *411*, 789–792. [CrossRef] [PubMed]
34. Nyberg, P.R. *Soil survey of Itasca County, Minnesota*; USDA Soil Conservation Service Government Printing Office: Washington, DC, USA, 2008.
35. Powers, M.D.; Kolka, R.K.; Bradford, J.B.; Palik, B.J.; Fraver, S.; Jurgensen, M.F. Carbon storage across a chronosequence of thinned and unmanaged red pine stands. *Ecol. Appl.* **2012**, *22*, 1297–1307. [CrossRef] [PubMed]
36. Huang, S.; Meng, S.X.; Yang, Y. Assessing the goodness of fit of forest models estimated by nonlinear mixed-model methods. *Can. J. For. Res.* **2009**, *39*, 2418–2436. [CrossRef]
37. Boone, R.D.; Nadelhoffer, K.J.; Canary, J.D.; Kaye, J.P. Roots exert a strong influence on the temperature sensitivity of soil respiration. *Nature* **1998**, *396*, 570–572. [CrossRef]
38. Oliver, C.D.; Larson, B. *Forest Stand Dynamics*; Wiley: New York, NY, USA, 1996.
39. McDowell, N.G.; Licata, J.; Bond, B.J. Environmental sensitivity of gas exchange in different-sized trees. *Oecologia* **2005**, *145*, 9–20. [CrossRef] [PubMed]
40. Ryan, M.G.; Phillips, N.; Bond, B.J. The hydraulic limitation hypothesis revisited. *Plant Cell Environ.* **2006**, *29*, 367–381. [CrossRef] [PubMed]
41. Wharton, S.; Schroeder, M.; Bible, K.; Falk, M.; Paw U, K.T. Stand-level gas-exchange responses to seasonal drought in very young versus old Douglas-fir forests of the Pacific Northwest, USA. *Tree Physiol.* **2009**, *29*, 959–974. [CrossRef] [PubMed]
42. Borken, W.; Xu, Y.; Davidson, E.A.; Beese, F. Site and temporal variation of soil respiration in European beech, Norway spruce, and Scots pine forests. *Glob. Chang. Biol.* **2002**, *8*, 1205–1216. [CrossRef]
43. NOAA National Climatic Data Centers Climate Data Online. Available online: https://www.ncdc.noaa.gov/cdo-web/ (accessed on 5 December 2017).
44. Zimmermann, M.; Meir, P.; Bird, M.; Malhi, Y.; Cahuana, A. Litter contribution to diurnal and annual soil respiration in a tropical montane cloud forest. *Soil Biol. Biochem.* **2009**, *41*, 1338–1340. [CrossRef]
45. Yang, X.; Chen, J. Plant litter quality influences the contribution of soil fauna to litter decomposition in humid tropical forests, southwestern China. *Soil Biol. Biochem.* **2009**, *41*, 910–918. [CrossRef]

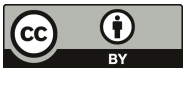

forests

MDPI

Article

Carbon Sequestration in Protected Areas: A Case Study of an *Abies religiosa* (H.B.K.) Schlecht. et Cham Forest

Pablo I. Fragoso-López [1], Rodrigo Rodríguez-Laguna [2], Elena M. Otazo-Sánchez [1], César A. González-Ramírez [1], José René Valdéz-Lazalde [3], Hermann J. Cortés-Blobaum [1] and Ramón Razo-Zárate [2,*]

1 Área Académica de Química, Instituto de Ciencias Básicas e Ingeniería, Universidad Autónoma del Estado de Hidalgo, Kilómetro 4.5 carretera Pachuca—Tulancingo, Mineral de la Reforma, Hidalgo 42090, Mexico; fr342891@uaeh.edu.mx (P.I.F.-L.); profe_4339@uaeh.edu.mx (E.M.O.-S.); cramirez@uaeh.edu.mx (C.A.G.-R.); co342890@uaeh.edu.mx (H.J.C.-B.)

2 Área Académica de Ciencias Agrícolas y Forestales, Instituto de Ciencias Agropecuarias, Universidad Autónoma del Estado de Hidalgo, Av. Universidad km. 1, Ex. Hda de Aquetzalapa, Tulancingo, Hidalgo 43600, Mexico; rlaguna@uaeh.edu.mx

3 Colegio de Postgraduados, Km 36.5 Carr. México-Texcoco, Montecillo, Texcoco 56230, Mexico; valdez@colpos.mx

* Correspondence: ramon_razo@uaeh.edu.mx; Tel.: +52-771-71-72000 (ext. 2431)

Received: 23 August 2017; Accepted: 28 October 2017; Published: 12 November 2017

Abstract: The effects of global climate change have highlighted forest ecosystems as a key element in reducing the amount of atmospheric carbon through photosynthesis. The objective of this study was to estimate the amount of carbon content and its percentage capture in a protected *Abies religiosa* forest in which the study area was zoned with satellite image analysis. Dendrometric and epidometric variables were used to determine the volume and increase of aerial biomass, and stored carbon and its capture rate using equations. The results indicate that this forest contains an average of 105.72 MgC ha^{-1}, with an estimated sequestration rate of 1.03 MgC ha^{-1} yr^{-1}. The results show that carbon capture increasing depends on the increase in volume. Therefore, in order to achieve the maximum yield in a forest, it is necessary to implement sustainable forest management that favors the sustained use of soil productivity.

Keywords: climate change; protected forest; carbon sequestration; *Abies religiosa*

1. Introduction

The negative impacts of anthropogenic emissions of greenhouse gases such as irreversible damage to ecosystems, increased pressure on water resources, alterations in food production, and damage to human health, among others, have been reported in different studies [1–10]. The need to stabilize the carbon content of the atmosphere has been manifested in a series of international and local agreements and policies, such as the Kyoto Protocol and the Treaty of Paris. The purpose of these agreements and policies is to reduce emissions of greenhouse gases (GHG), with mechanisms to optimize carbon sinks.

Currently, forests store about 800 gigatons of carbon (GtC) [11] and it is estimated that by 2050 they could sequester up to an additional 87 GtC [12,13]. It was estimated that in the period between 2000 and 2007, the carbon sequestration rate of the world's forests averaged 4.1 $GtCyr^{-1}$ [14], corresponding to approximately 30% of fossil fuel emissions in 2010 [15].

Globally, protected forests have been proposed as a potentially cost-effective strategy to counter deforestation and degradation [16–18], favoring carbon permanence in the forest. Countries with the greatest threats from their forests due to degradation and devastation have increased their percentage

of protected areas (Figure 1) in an attempt to conserve the environmental services of their forests [19,20]. Out of 3984 million hectares of forests in the world, 13.25% have a protected area status [21], and this percentage is mainly because of many of these protected sites partially fulfilling their conservation objectives [22], primarily derived from the budgetary constraints in which most of these areas operate. Financial resources managers for protected areas are increasingly emphasizing cost-effective aspects such as ecosystem services, including carbon sequestration [23].

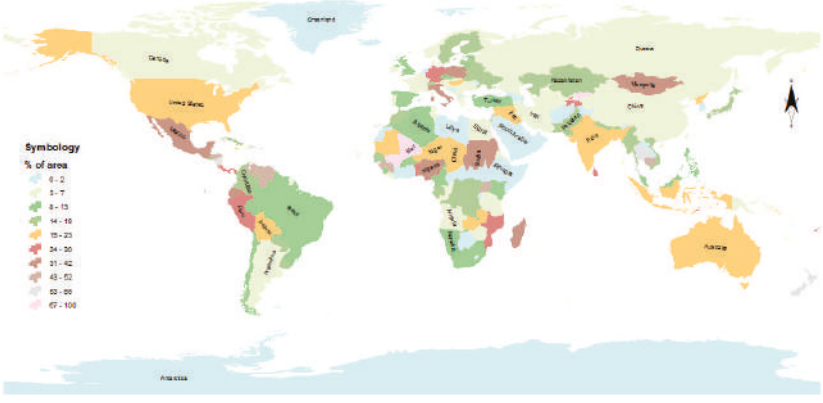

Figure 1. Percentage of protected area per country in 2015 in relation to its total forest area. Own elaboration with information of [24].

Currently, decision-makers can use a large number of methods to assess protected area management and prioritize investments, and there are over 70 methods that have been developed to provide standards for obtaining indicators, analyses, and interpretations [25,26]; however, none of these provide an estimation of carbon sequestration rates.

The present study aimed to estimate the carbon content in the above-ground biomass (baseline) of a forest of *Abies religiosa* (H.B.K.) Schlecht. et Cham., which is part of El Chico National Park, Hidalgo, Mexico. In addition, it attempted to ascertain the carbon capture rate from the annual volumetric increase of the species in the area. This information is necessary for designing the strategies that allow the environmental objectives that contribute to the reduction of the negative effects in climate change to be fulfilled.

2. Materials and Methods

2.1. Study Area

The study was carried out in the federal zone of the protected natural area called "El Chico National Park" located in the western area of the mountain range of Pachuca, in the state of Hidalgo, Mexico. Geographically, it is located between the extreme coordinates 20°11′57″ and 20°12′02″ north latitude and 98°43′08″and 98°43′06″ west longitude.

The area is owned by the Mexican nation and comprises 1,833,000 hectares [27]. The climate is C (m) (w) b (i′) gw, which is described as: a temperate-sub-humid climate with a fresh and long summer; the average annual temperature varies between 12 and 18 °C. The rainfall regime is in summer, and the percentage of winter rain in relation to the annual total is less than 5% [28].

The soil type is constituted by associations that group the following soil units: Humic cambisol-Androsol ocrico-Litosol, which has a volcanic origin association typical of mountainous zones, and humic Andosol-Humic cambisol, corresponding to forest soils associated with *Abies* and *Quercus* forests [29].

The predominant type of vegetation is *Abies religiosa* forest, which covers 67% of the park surface. The shrub stratum is dominated by the species *Archibaccharis hieracioides* Blake, *Baccharis conferta* H.B.K., *Eupatorium hidalgense* Rob., *Fuchsia thymifolia* H.B.K., *Ribes affine* H.B.K., *Salvia elegans* Vahl., *Senecio angulifolius* D.C., and *Stevia monardifolia* H.B.K. [30].

2.2. Description of the Species

The *Abies* forest is considered a component of the Leopold boreal forest [31] because of its similarity in terms flora, fauna, physiognomy, and ecological conditions to large forest masses covering northern parts of North America and Eurasia, and is also known as Taiga. This type of forest usually develops in an interval of altitude between 2400 and 3600 m, and its humidity requirement is high, registering precipitations superior to 1000 mm annually. They are dense forests, of heights that can reach up to 50 m, with canopies of a triangular contour; the high density conditions reduce the amount of light reaching the interior, which limits the development of shrubs and herbaceous species [32].

2.3. Forest Zoning

This process was performed to identify the areas where the species of interest is dominant. The stands were also identified where the species is mixed with other genera; however, these were excluded from the study. This concept is also known as stratification and consists of the division of the forest area into portions or spatial units called stands, with sections that possess similar physical and biological characteristics [33,34].

The identification of the stands was made through a RapidEye-4 satellite (provided by the Space Agency of the Mexican Government) image analysis dated 25 February 2015, with a spatial resolution of 5 m [35]. Initially, the image was corrected atmospherically and radiometrically [36]. Subsequently, it was estimated at the pixel level "Red Edge Normalized Difference Vegetation Index" ($RedEdge_{NDVI}$) [37–41].

$$RedEdge\ _{NDVI} = \frac{R710 - R705}{R710 + R705} \quad (1)$$

where R710 is the band 4 RedEdge or near red and R705 corresponds to the band 3 RedEdge. The NDVI has been used in the elaboration of the process of forest logging, and it is mentioned that it has shown acceptable results in the identification of vegetal associations.

The RedEdge NDVI results were analyzed along with altitude, latitude, and exposure values to determine the final logging through an overlay positioning process.

The obtained image analysis was validated with the records obtained through field trips. The existing vegetation types and the boundaries between them were determined by georeferenced points.

2.4. Field Information

Sampling Design and Characteristics of Sites

A random sampling design was used to define the location of 33 circular sampling sites of 1000 m^2, in which a total of 682 trees were measured. The shape and size of the sites were suitable for the purpose pursued since they have shown good results for the calculation of volumetric stocks or biomass content [42,43].

At each sampling site, the diameter information at the breast height (dap) of all trees with a diameter equal to or greater than 7.5 cm and the total height of each tree [44] was recorded. For the determination of the number of annual growth rings in 2.5 cm, known as passage time, an average tree per diameter category was selected at each sampling site by means of a 250-mm Haglöf® Presser (Haglöf, Langsele, Sweden) drill and the results were calculated as the annual volumetric increase per hectare [45], which was subsequently used for estimating carbon sequestration.

2.5. Information Processing

2.5.1. Calculation of Volumetric Stocks

With the records of each stand, we proceeded to estimate the value of the variables basal area and timber volume [36,46]. The basal area for each tree was obtained by the following equation:

$$B_A = \frac{\pi}{4} * D_{bh}^2 \quad (2)$$

where B_A is the basal area (m^2) and D_{bh} corresponds to the diameter at breast height (m), which were grouped in diametric categories of 5 cm.

The volume per hectare per stand was determined through a procedure known in the forest as the average hectare [47] by employing the following equation:

$$\overline{V}s = \sum_{i=1}^{DC} \left(B_{Ai} * \overline{H} * M_{Ci} * E_{Fi} * N_{Ti} \right) \quad (3)$$

where $\overline{V}s$ corresponds to the total volume (trunk + branches + leaves + roots) of the woodland per hectare (m^3); DC is the number of diametric categories in the stand; i is the diameter category; B_A is the basal area of the average tree by diameter category (m^2); $\overline{H}$ corresponds to the average height of the trees in the stands for each diameter category (meters); M_C is the morphic coefficient for gender Abies; E_F is the expansion factor of stem to total volume (branches, leaves, and roots) [48]; and N_{Ti} is the number of trees per hectare per diameter category.

2.5.2. Volumetric Increment

The calculation of the increment of the forest mass for each of the stands was obtained by means of the "Klepac Fast" method, which relates the number of trees per diameter category per hectare, the volume of the tree type for each diameter category, and the step time for each case [45,49]. This method considers a series of calculations between these three variables to obtain the percentage of the increase by the following equation:

$$P = \frac{1000}{Dbh} * \frac{1}{T} \quad (4)$$

where P corresponds to the percentage of increase, Dbh is the diameter at breast height, and T is the step time. It is worth mentioning that this parameter was used to obtain the carbon sequestration rate.

2.5.3. Aerial Biomass Content

This information was obtained by the equation developed by Avendaño et al. [50], for the calculation of biomass for *Abies religiosa* based on the diameter at breast height.

$$B = 0.0713\ D_{bh}^{2.5104} \quad (5)$$

where B is the total biomass of the tree (Mg) and Dbh is the diameter at breast height (m).

2.5.4. Carbon Content

The estimated carbon content for each tree was calculated using the equation developed for this species, which is based on the diameter at breast height [50].

$$A_{CC} = 0.0332\ D_{bh}^{2.5104} \quad (6)$$

where A_{CC} is the carbon content for *Abies religiosa* (Mg) and D_{bh} is the diameter at breast height (m).

The carbon content for each diameter category was obtained by the following equation:

$$Dc_{cc} = A_{cc} * N_T \quad (7)$$

where Dc_{cc} is the carbon content by diameter category (Mg), A_{cc} is the carbon content per tree (Mg), and N_T is the number of trees of the corresponding diametric category.

The carbon content per hectare was obtained by adding the carbon content from all the diametric categories.

2.5.5. Carbon Sequestration Rate

After calculating the carbon content per hectare and after having determined the volumetric increments, the carbon capture rate for each stand was determined, considering that the increment parameter refers to the volume increase per unit time. Once the amount of biomass that this forest can generate in a certain time period was obtained, the carbon stored was calculated using the following equation:

$$\overline{C}_{SR} = (\overline{C}_C / \overline{V}s) * C_{AI} \quad (8)$$

where $\overline{C}_{SR}$ is the rate of carbon sequestration per hectare per year (Mg), $\overline{C}_C$ is the carbon content (MgC ha^{-1}), $\overline{V}s$ corresponds to the volumetric stocks (m^3 ha^{-1}), and C_{AI} is the current annual increase (m^3).

3. Results

3.1. Forest Zoning and Field Information

Of the total area studied, eight stands were identified, with *Abies religiosa* covering an area of 1229.65 hectares. The rest of the area (603.35 hectares) corresponds to rock formations and other types of vegetation such as *Quercus*, *Juniperus*, and grassland. The study was addressed to *Abies religiosa* since it is the conservation species of interest in this protected area (Figure 2).

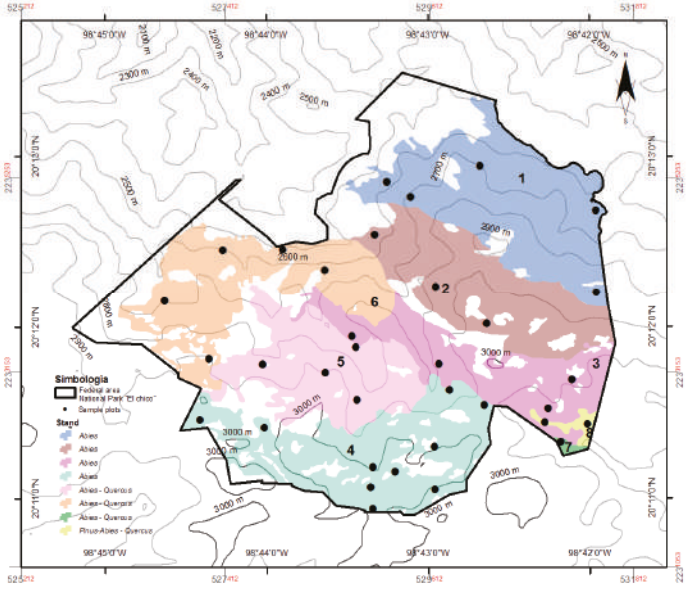

Figure 2. Forest zoning obtained through the analysis of satellite images in combination with altitude information, orientation, and slope.

The Table 1 show the values of the NDVI together with the land orientation, as well as the slope range that exists in each one of the stands, for which the criteria for the realization of the forest zoning were the values of NDVI, orientation, and species composition.

Table 1. Criteria and values used for forest zoning.

Stand	NDVI			Orientation	Slope	Species Composition
	Mean	Min	Max			
1	0.3495	0.1764	0.4350	North	10–25°	*Abies*
2	0.3709	0.2043	0.4681	North	10–25°	*Abies*
3	0.3678	0.3016	0.4806	Southeast	10–25°	*Abies*
4	0.3900	0.2004	0.4613	Northwest	10–25°	*Abies*
5	0.3849	0.2773	0.4510	Northwest	10–25°	*Abies-Quercus*
6	0.3603	0.2751	0.4360	North	10–25°	*Abies-Quercus*
7	0.3849	0.3228	0.4228	East	10–25°	*Abies-Quercus*
8	0.3441	0.2841	0.4064	Northwest	4–9°	*Abies-Pinus-Quercus*
Other *	0.2753	0.0228	0.3990	-	-	-

* Refers to other uses or plant formations, "-" refers to not obtained.

3.2. Volumetric Stocks

The total volume is 757,681.69 m^3, and the average volumetric stock per hectare is 616.18 m^3. Table 2 details the *Abies religiosa* volumes for each stand.

Table 2. Volume in m^3 per stand.

Stand	Surface (Hectares)	Number of Trees ha^{-1}	Basal Area m^2 ha^{-1}	Volumetric Stocks m^3 ha^{-1}	Volumetric Stocks m^3 $Stndl^{-1}$
1	263.43	220	47.37	771.57	203,252.50
2	194.20	210	35.18	716.46	139,139.25
3	153.63	210	32.63	672.41	103,299.63
4	223.27	282	40.44	789.37	176,238.35
5	178.26	140	22.02	462.22	82,392.82
6	203.92	70	11.86	239.33	48,805.67
7	3.29	270	36.84	727.16	2524.82
8	9.66	140	12.37	223.86	1770.21

Stands 1, 2, 3, 4, and 7 have a density of more than 200 trees per hectare, a basal area greater than 30 m^2, and a volume that exceeds 670 m^3 ha^{-1}. Stands 5, 6, and 8 have densities of less than 150 trees per hectare and volumes below 470 m^3 ha^{-1}, which is due to the presence of disturbances such as forest fires and pests that have affected the density per unit area.

3.3. Volumetric Increment

Table 3 presents the results of the calculation of volumetric increase, for which we considered the records of 165 trees. It can be observed that stands 4, 5, and 6 present smaller times of passage in relation to the rest of the stands, probably due to the age and density of the forest mass. The highest productivity is found in stands 1, 4, and 5, where the area of these stands also influences the result.

Table 3. Result of calculating volumetric increments.

Stand	Sampling Plot	Step Time Average	Drilled Trees	Current Annual Increase	
				m^3	%
1	4	19	20	6.616	3.007
2	3	22	15	4.440	2.114
3	4	24	20	4.870	2.319
4	9	17	45	7.077	2.508
5	5	16	25	5.261	3.758
6	4	15	20	2.605	3.722
7	2	23	10	4.662	1.554
8	2	26	10	1.164	0.831

3.4. Carbon Content

The estimate of the total carbon content is 130,004.02 Mg, with an average per hectare of 105.72 MgC. The results for each stand are shown in Table 4.

Table 4. Carbon content per hectare and per stand in megagrams.

Stand	Surface ha^{-1}	Content of C ha^{-1} (MgC)	Content of C Stand^{-1} (MgC)
1	263.43	164.25	43,268.71
2	194.20	110.92	21,540.97
3	153.63	100.44	15,430.38
4	223.27	129.55	28,925.22
5	178.26	70.95	12,646.44
6	203.92	36.25	7392.48
7	3.29	120.68	396.63
8	9.66	41.72	403.18

3.5. Carbon Sequestration

The result for the carbon capture rate in the *Abies religiosa* aerial biomass is 1267.66 MgC yr^{-1}, considering the studied area, with an average of 1.03 MgC yr^{-1} per hectare.

Stands 1 and 4 have higher volumetric increments. Consequently, the sequestered carbon is higher in relation to the rest of the stands (Figure 3), and this can be attributed to the north orientation of the surface where the insolation is less and more moisture is available. Stand 6 is located in a transition zone with the presence of other tree genres that were not counted but that compete with the *Abies*, decreasing its density, due to the fact that the volume and increase of biomass is reduced. Stand 8 presents a situation similar to the previous stand, only in this case the mixture of genera is due to anthropic activities (reforestation).

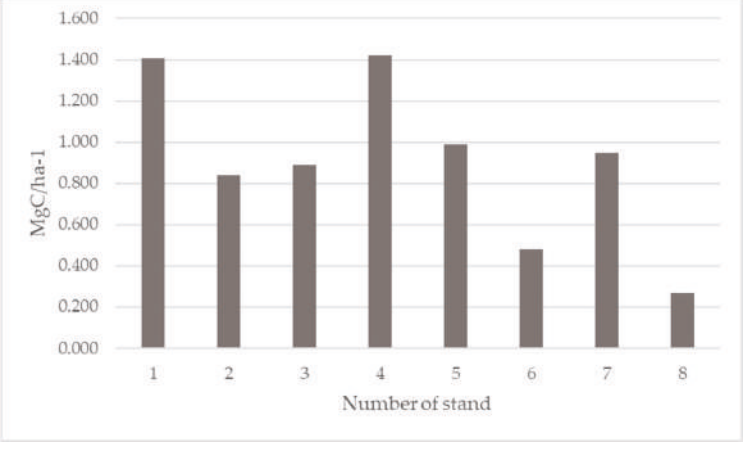

Figure 3. Annual carbon sequestration per hectare in megagrams.

Carbon sequestration in stand 1 is the one with the highest catch mainly due to the surface area and annual increment, followed by stand 4. The strata with the least carbon sequestration are the ones with the lowest surface area and the lowest density of trees (Figure 4).

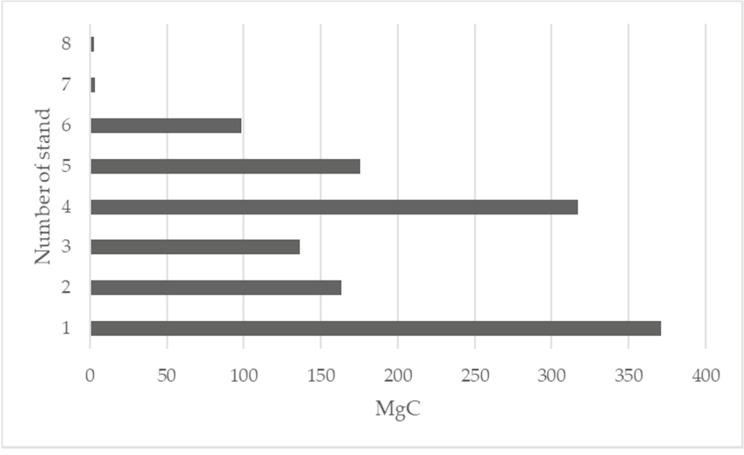

Figure 4. Annual carbon capture above-ground per stand.

4. Discussion

4.1. Carbon Content

The area of study corresponds to a protected area decreed in 1898, in which the conservation policies that prevent the modification of the forest structure have caused the longevity of this mass, placing it in the last stage of development (old fustal), and this is derived from the age and diameters present. Diameters greater than 1.10 m were recorded, while the smallest diameter registered was 7.5 cm. On average, the number of trees per hectare is 193, with a volume of 616.18 m^3. Table 5 presents comparative information of estimated carbon in protected areas with the presence of *Abies religiosa*.

Table 5. Comparison of studies in protected forests where they have calculated the carbon content in aerial biomass in *Abies religiosa*.

Author	Place of Study	Status of the Area	Species	Carbonor Estimated Mg ha^{-1}	Observations
Present study	Hidalgo, Mexico	Protected	*Abies religiosa*	105.72	Long-lived forest mass and scarce natural regeneration.
[51]	Mexico City, Mexico	Protected	*Abies religiosa*	117.00	The author makes reference to 3 associations *Abies religiosa* with shrub and/or herbaceous species. It is not mentioned the method to determine the carbon content.
[52]	Mexico City, Mexico	Protected	*Abies religiosa*	136.41	A conserved forest was studied.
[53]	Hidalgo, Mexico	Protected	*Abies religiosa*	138.62	The author details 3 carbon scenarios for this type of forest, in which include disturbed areas, the area studied was 212.95 hectares.
[54]	Veracruz, Mexico	Protected	Various conifers	146.30	It is a protected forest, the authors detail scenarios where the species of *Abies religiosa* is combined with other conifers.
[55]	Mexico State, Mexico	Protected	*Abies religiosa*	163.62	A similar methodology was used to calculate the carbon content.

There are several hypotheses about the carbon content in forest ecosystems. This storage is dependent on the amount of existing biomass, which depends on the age, diameter, and height of the trees. When woodland density is affected or altered for some cause such as: pests, diseases, forest fires, clandestination, or harvesting, the carbon content per unit area is also altered [56]. The silviculously managed forests have young stands as a result of the application of silvicultural treatments [57], where the stands with a higher density and basal area are those containing more volume of above-ground biomass, and consequently, more carbon content.

The records consulted about carbon contents in protected temperate forest are $\geq$115 MgC ha^{-1} [51–55], whereas this study estimated more than 105.72 MgC ha^{-1}. These differences can be attributed to several factors such as the quality of the site studied, and the density and age of the trees, among others. Unlike the preserved forests, disturbed forests contain less carbon, due to the affected forest mass. Aguirre et al. [57] mentions that for a managed forest of *Pinus patula* with an orientation that is contemporary, the content is 63.98 MgC ha^{-1}.

In the case of protected forests or silvically managed forests, the ecosystem service of carbon storage is fulfilled, whereas in the case of harvested forests, the carbon content is lower and mainly depends on applied silvicultural treatments. For the production of coetaneous masses, the content is variable and dependent on the age, diameter, height, and density of the trees in a given stand. The present study considers there to be 48% more carbon content in El Chico than the data provided by Aguirre et al. [57]. Masera et al. [58] mentions that managed forests with a temperate climate contain 118 MgC ha^{-1} or 10% more than the estimated data in this study. The differences between Aguirre and Masera information can be mainly attributed to the applied silvicultural system (intensive or conservative).

4.2. Carbon Sequestration

Forest ecosystems sequester carbon and are considered as an option for the mitigation of the effects of an increasing atmospheric CO_2 load [59–62]. The potential for carbon of any forest species depends on the maximum amount of biomass it can produce per unit of time. In species of accelerated growth, this parameter is relatively fast reached, whereas in species with a slow growth, the period of time required to reach the maximum biomass content is longer, and consequently, carbon sequestration is higher [63].

The volumetric increases represent the parameter which is able to determine the rate of carbon sequestration, and for the case presented in this study, the *Abies religiosa* forest captures 1.03 MgC ha^{-1} yr^{-1}, which is equivalent to 3.78 MgCO$_2$ ha^{-1} [64], with an annual average increase of 2.92%. Because it is located within a protected area, the forest mass has not been altered, which has caused the increment curve to decline. As the age of the mass increases, the increments decrease [45], and as a consequence, the potential for carbon capture is also affected.

Compared with protected forests, sustainably harvested forest areas capture more carbon [65], which is mainly due to the management of the age factor within the masses. Similarly, the use of harvested biomass for the production of long-lasting products retains carbon for long periods of time [66,67]. There are records of carbon capture in managed forests that exceed the results obtained in this study. Liu et al. [68] estimated net biomass productivity for forests in the Appalachian region where the forest harvest exists, and reported data ranging from 1.8 to 6.2 MgC ha^{-1}. Zhang et al. [69] estimated a value of 2.4 MgC ha^{-1} captured for a Massonian *Pinus* forest in China. For the specific case of *Abies religiosa* with the information of Manzanilla et al. [70], we can estimate 3.1 MgC ha^{-1}. The differences between these investigations and the estimated rate in this study can be attributed to factors such as: forest management, location of the studied area, and species, among others. Navarro et al. [65] mentioned that these results cannot be cofrontable since they correspond to different ecosystems, each with their own particularities.

Unlike carbon content, the rate of sequestration is influenced by forest management techniques; in protected forests, the amount of stored carbon is higher, but the catch rate is reduced. With sustainable forest management practices, this difference can be balanced.

Forest management should be included in protected forests, and it is desirable to consider aspects that relate the conservation of species and their habitats with the carbon storage outside forest areas. The extraction of biomass for the elaboration of long-lasting products such as furniture or infrastructure is a way to reduce the risk of leakage within this type of ecosystem, reducing the carbon content inside a warehouse, so that emissions risks are reduced and capture is encouraged by stimulating increases in forest mass in order reach the maximum biomass production potential.

5. Conclusions

The methodology used for the evaluation of a protected forest of *Abies religiosa* as aerial carbon storage and its capture capacity is adequate and reproducible in areas with similar conditions where it is not possible to use destructive methods. The use of high resolution satellite images combined with the analysis of physical aspects of the terrain allowed for detailed zoning directly related to the density of the forest mass, and its amount of biomass and carbon.

The results presented denote that the amount of carbon stored above-ground is directly related to the density and degree of disturbance. In this case, because it is a protected forest where the silvicultural activities are restricted, the productivity of the mass is lower, and consequently, the rate of carbon sequestration decreases.

The quantified carbon additionality is a parameter that depends on several factors, for which the age of the forest mass is considered one of the most important, and in the young and vigorous forests, the rate of sequestration is higher than in forests of advanced stages of development. In this study, *Abies religiosa* caught 1.03 MgC ha^{-1} yr^{-1}, with an annual average increase of 2.92%.

The implementation of silvicultural techniques governed by forest management with correct principles, foundations, and objectives greatly contributes to the reduction of atmospheric carbon. Within protected forests, the application of forest management techniques makes it possible to obtain sustainable forests and maximize the potential of forest soils to increase this important ecosystem service.

Acknowledgments: The authors thank the Mexican Government for providing the RapidEye satellite image used for stratification, as well as for the personnel who manage the El Chico National Park for the facilities granted to carry out this study.

Author Contributions: P.I.F.-L. and H.J.C.-B. drafted the document and elaborated, and designed the experiment; C.A.G.-R. contributed to the experimental design planning, data analysis, revision, and translation of the manuscript. E.M.O.-S. contributed to the revision of the document, and support and advice in the development of research. J.R.V.-L., R.R.-L., and R.R.-Z. were involved in document revision, data analysis, field phase support, and cartographic phase review.

Conflicts of Interest: The authors declare no conflict of interest.

References

1. Bassi, A.M.; Yudken, J.S.; Ruth, M. Climate policy impacts on the competitiveness of energy-intensive manufacturing sectors. *Energy Policy* **2009**, *37*, 3052–3060. [CrossRef]
2. De Vries, M.; de Boer, I. Comparing environmental impacts for livestock products: A review of life cycle assessments. *Livest. Sci.* **2010**, *128*, 1–11. [CrossRef]
3. Garnett, T. Livestock-related greenhouse gas emissions: Impacts and options for policy makers. *Environ. Sci. Policy* **2009**, *12*, 491–503. [CrossRef]
4. Getzner, M. The quantitative and qualitative impacts of clean technologies on employment. *J. Clean. Prod.* **2002**, *10*, 305–319. [CrossRef]
5. Gossling, S. *Carbon Management in Tourism: Mitigating the Impacts on Climate Change*; Routledge: Abingdon, UK, 2011.
6. Norgate, T.; Haque, N. Energy and greenhouse gas impacts of mining and mineral processing operations. *J. Clean. Prod.* **2010**, *18*, 266–274. [CrossRef]
7. Rivers, N. Impacts of climate policy on the competitiveness of Canadian industry: How big and how to mitigate? *Energy Econ.* **2010**, *32*, 1092–1104. [CrossRef]

8. Sano, F.; Akimoto, K.; Wada, K. Impacts of different diffusion scenarios for mitigation technology options and of model representations regarding renewables intermittency on evaluations of CO_2 emissions reductions. *Clim. Chang.* **2014**, *123*, 665–676. [CrossRef]
9. Valerio, F. Environmental impacts of post-consumer material managements: Recycling, biological treatments, incineration. *Waste Manag.* **2010**, *30*, 2354–2361. [CrossRef] [PubMed]
10. Bank, W. *Towards Sustainable Mineral-Intensive Growth in Orissa: Managing Environmental and Social Impacts*; World Bank: Washington, DC, USA, 2007; p. 78.
11. Brown, S. Present and Future Role of Forests in Global Climate Change. In *Ecology Today: An Anthology of Contemporary Ecological Research*; Goapl, B., Pathak, P.S., Saxena, K.G., Eds.; International Scientific Publications: New Delhi, India, 1998; pp. 59–74.
12. Metz, B.; Davidson, O.; Swart, R.; Pan, J. *Climate Change 2001: Mitigation*; Cambridge University Press: Cambridge, UK, 2001.
13. Watson, R.T.; Zinyowera, M.C.; Moss, R.H. *Climate Change 1995 Impacts, Adaptations and Mitigation of Climate Change: Scientific-Technical Analysis*; Cambridge University Press: Cambridge, UK, 1996.
14. Pan, Y.; Birdsey, R.A.; Fang, J.; Houghton, R.; Kauppi, P.E.; Kurz, W.A.; Phillips, O.L.; Shvidenko, A.; Lewis, S.L.; Canadell, J.G.; et al. A large and persistent carbon sink in the world's forests. *Science* **2011**, *333*, 988–993. [CrossRef] [PubMed]
15. Change, I.P.O.C. *Climate Change 2014–Impacts, Adaptation and Vulnerability: Regional Aspects*; Cambridge University Press: Cambridge, UK, 2014.
16. Nauclér, T.; Enkvist, P.-A. *Pathways to a Low-Carbon Economy: Version 2 of the Global Greenhouse Gas Abatement Cost Curve*; McKinsey & Company: New York, NY, USA, 2009.
17. Soares-Filho, B.; Moutinho, P.; Nepstad, D.; Anderson, A.; Rodrigues, H.; Garcia, R.; Dietasch, L.; Merry, F.; Bowman, M.; Hissa, L.; et al. Role of Brazilian Amazon protected areas in climate change mitigation. *Proc. Natl. Acad. Sci. USA* **2010**, *107*, 10821–10826. [CrossRef] [PubMed]
18. Venter, O.; Laurance, W.F.; Iwamura, T.; Wilson, K.A.; Fuller, R.A.; Possingham, H.P. Harnessing carbon payments to protect biodiversity. *Science* **2009**, *326*, 1368. [CrossRef] [PubMed]
19. Jackson, R.B.; Baker, J.S. Opportunities and constraints for forest climate mitigation. *BioScience* **2010**, *60*, 698–707. [CrossRef]
20. Lippke, B.; Perez-Garcia, J.; Manriquez, C. *Executive Summary: The Impact of Forests and Forest Management on Carbon Storage, Rural Technological Initiative, College of Forest Resources*; Box: Redwood City, CA, USA, 2003.
21. Food and Agriculture Organization of the United Nations (FAO). *Global Forest Resources Assessment 2015*; Organización de las Naciones Unidas Para la Alimentación y la Agricultura: Rome, Italy, 2015.
22. Oates, J.F. *Myth and Reality in the Rain Forest: How Conservation Strategies Are Failing in West Africa*; University of California Press: Berkeley, CA, USA, 1999.
23. Ferraro, P.J.; Pattanayak, S.K. Money for nothing? A call for empirical evaluation of biodiversity conservation investments. *PLoS Biol.* **2006**, *4*, e105. [CrossRef] [PubMed]
24. Food and Agriculture Organization of the United Nations (FAO). *Global Forest Resources Assessment 2015; How Are the World's Forests Changing?* Food and Agriculture Organization of the United Nations: Rome, Italy, 2016.
25. Leverington, F.; Hockings, M.; Costa, K.L. *Management Effectiveness Evaluation in Protected Areas—A Global Study*; Supplementary Report No. 1. Overview of Approaches and Methodologies; World Commission on Protected Areas: Brisbane, Australia, 2008.
26. Nolte, C.; Leverington, F.; Kettner, A.; Marr, M.; Nielsen, G.; Bomhard, B.; Stolton, S.; Stoll-Kleemann, S.; Hockings, M.; World Conservation Union (IUCN)-World Commission on Protected Areas (WCPA). *Protected Area Management Effectiveness Assessments in Europe*; A Review of Application, Methods and Results; BfN-Skripten: Bonn, Germany, 2010; p. 69.
27. Zabala, F. Análisis demográfico preliminar de Taxus globosa Schlecht en el Parque Nacional El Chico, Hidalgo, Mexico. I: Población de adultos y algunas características del hábitat. *CIENCIA Ergo-Sum* **2001**, *8*, 169–174.
28. Razo Zárate, R.; Martínez, A.J.G.; Laguna, R.R.; Maycotte Morales, C.C.; Acevedo Sandoval, O.A. Coeficientes de carbono para arbustos y herbáceas del bosque de oyamel del Parque Nacional El Chico. *Rev. Mex. Cienc. For.* **2016**, *6*, 10.
29. Melo Gallegos, C.; López García, J. Parque Nacional El Chico, marco geográfico-natural y propuesta de zonificación para su manejo operativo. *Investig. Geogr.* **1994**, *28*, 65–128. [CrossRef]

30. Cervantes, Á.; Reyes, E. Efectos Ecológicos de los Incendios Forestales Sobre el Bosque de Oyamel. Ph.D. Thesis, Colegio de Postgraduados Campus Montecillo, Texcoco, Mexico, 2010.
31. Leopold, A.S. Vegetation zones of Mexico. *Ecology* **1950**, *31*, 507–518. [CrossRef]
32. Rzedowski, J. *Vegetación de Mexico. 1ra*; Edición Digital; Comisión Nacional Para el Conocimiento y Uso de la Biodiversidad: Mexico City, Mexico, 2006; p. 504.
33. Castellanos Bolaños, J.F.; Gómez Cárdenas, M.; Contreras Hinojosa, J.R.; González Cubas, R. *Metodologías Para Cuantificar Biomasa y Carbono en Bosques*; Centro de Investigación Regional del Pacífico Sur: Oaxaca, Mexico, 2013.
34. Návar-Cháidez, J.D.J.; Domínguez-Calleros, P.A. Modelo de incremento y rendimietno: Ejemplos y aplicaciones para bosques templados mexicanos. *Rev. Mex. Cienc. For.* **2013**, *4*, 8–27.
35. Rafael Domingo, C.M. Monitoreo de bosques utilizando ndvi rededge de rapideye. *Instr. Gener. Para Autores* **2013**, *10*, 58–71.
36. Aguilar Arias, H.; Zamora, R.M.; Bolaños, C.V. MetodologÍa Para La Corrección Atmosférica De Imágenes Aster, Rapideye, Spot 2 Y Landsat 8 Con El MÓdulo Flaash Del Software Envi. Atmospheric Correction Methodology for Aster, Rapideye, Spot 2 and Landsat 8 Images with Envi Flaash Module Software. *Rev. Geogr. Am. Cent.* **2015**, *2*. [CrossRef]
37. Gitelson, A.; Merzlyak, M.N. Spectral Reflectance Changes Associated with Autumn Senescence of Aesculus *hippocastanum* L. and *Acer platanoides* L. Leaves. Spectral Features and Relation to Chlorophyll Estimation. *J. Plant Physiol.* **1994**, *143*, 286–292. [CrossRef]
38. Sims, D.A.; Gamon, J.A. Relationships between leaf pigment content and spectral reflectance across a wide range of species, leaf structures and developmental stages. *Remote Sens. Environ.* **2002**, *81*, 337–354. [CrossRef]
39. Tapsall, B.; Milenov, P.; Tasdemir, K. Analysis of RapidEye Imagery for Annual landcover Mapping As an Aid to European Union (EU) Common Agricultural Policy. In Proceedings of the International Archives of the Photogrammetry, Remote Sensing and Spatial Information Sciences, Vienna, Austria, 5–7 July 2010; pp. 568–573.
40. Wu, C.; Niu, Z.; Tang, Q.; Huang, W.; Rivaed, B.; Feng, J. Remote estimation of gross primary production in wheat using chlorophyll-related vegetation indices. *Agric. For. Meteorol.* **2009**, *149*, 1015–1021. [CrossRef]
41. Roslani, M.A.; Mustapha, M.A.; Lihan, T.; Wan Juliana, W.A. Applicability of Rapideye Satellite Imagery in Mapping Mangrove Vegetation Species at Matang Mangrove Forest Reserve, Perak, Malaysia. *J. Environ. Sci. Technol.* **2014**, *7*, 123.
42. Aguirre, O.; Jiménez, J.; Treviño, E.; Meraz, B. Evaluación de diversos tamaños de sitio de muestreo en inventarios forestales. *Madera Bosques* **1997**, *3*, 71–79. [CrossRef]
43. Juárez Castillo, S. *Trial to Determine Comparative Efficiency of Sampling Sites in Temperate-and Cold-Climate Forests*; Centro Interamericano de Fotointerpretación: Bogotá, Colombia, 1974.
44. Fedrigo, M.; Kasel, S.; Bennett, L.T.; Roxburgh, S.H.; Nitschke, C.R. Carbon stocks in temperate forests of south-eastern Australia reflect large tree distribution and edaphic conditions. *For. Ecol. Manag.* **2014**, *334*, 129–143. [CrossRef]
45. Klepac, D. *Crecimiento e Incremento de Árboles y Masas Forestales*; Universidad Autónoma Chapingo: Texcoco, Mexico, 1976.
46. Muñoz-Ruiz, M.Á.; Valdez-Lazalde, J.R.; de los Santos-Posadas, H.M.; Ángeles-Pérez, G.; Monterroso-Rivas, A.I. Inventario y mapeo del bosque templado de Hidalgo, Mexico mediante datos del satélite SPOT y de campo. *Agrociencia* **2014**, *48*, 847–862.
47. Hernández-Díaz, J.C.; Corral-Rivas, J.J.; Quiñones-Chávez, A.; Bacon-Sobbe, J.R.; Vargas-Larreta, B. Evaluación del manejo forestal regular e irregular en bosques de la Sierra Madre Occidental. *Madera Bosques* **2008**, *14*, 25–41. [CrossRef]
48. Razo-Zárate, R.; Gordillo-Martínez, A.J.; Rodríguez-Laguna, R.; Maycotte-Morales, C.C.; Acevedo-Sandoval, O.A. Estimación de biomasa y carbono almacenado en árboles de oyamel afectados por el fuego en el Parque nacional "El Chico", Hidalgo, Mexico. *Madera Bosques* **2013**, *19*, 73–86. [CrossRef]
49. Villa Salas, A.B.; Aguilar Ramírez, M. Rutinas de cálculo de once métodos para determinar el incremento en volumen de conífertas. *Rev. Mex. Cienc. For.* **2012**, *20*, 77.
50. Avendaño Hernandez, D.M.; Mireles, M.A.; Anzures, F.C.; Etchevers Barra, J.D. Estimación de Biomasa y Carbono en un Bosque de Abies Religiosa. *Rev. Fitotec. Mex.* **2009**, *32*, 233–238.

51. Leñero, L.A.; Nava, M.; Ramos, A.; Espinosa, M.; De Jesus Ordonez, M.; Jujnovsky, J. Servicios ecosistémicos en la cuenca del río Magdalena, Distrito Federal, Mexico. *Gaceta Ecol.* **2007**, *84–85*, 53–64.
52. Ávila-Akerberg, V. *Forest Quality in the Southwest of Mexico City: Assessment towards Ecological Restoration of Ecosystem Services*; Institut für Landespflege: Freiburg im Breisgau, Germany, 2010.
53. Razo-Zárate, R.; Gordillo-Martínez, A.; Rodríguez-Laguna, R.; Maycotte-Morales, C.; Acevedo-Sandoval, O. Escenarios de carbono para el bosque de oyamel del Parque Nacional El Chico, Hidalgo, Mexico. *Rev. Latinoam. Rec. Nat.* **2013**, *9*, 17–21.
54. Mendoza-Ponce, A.; Galicia, L. Aboveground and belowground biomass and carbon pools in highland temperate forest landscape in Central Mexico. *Forestry* **2010**, *83*, 497–506. [CrossRef]
55. Maass, S.F. *Estimación de la Captura de Carbono en Zonas Forestales: El Caso del Parque Nacional Nevado de Toluca*; Universidad Autónoma del Estado de Mexico: Toluca, Mexico, 2009.
56. Pregitzer, K.S.; Euskirchen, E.S. Carbon cycling and storage in world forests: Biome patterns related to forest age. *Glob. Chang. Biol.* **2004**, *10*, 2052–2077. [CrossRef]
57. Aguirre-Salado, C.A.; Valdez-Lazalde, J.R.; Ángeles-Pérez, G.; de los Santos-Posadas, H.M.; Haapanen, R.; Aguirre-Salado, A.I. Mapeo de carbono arbóreo aéreo en bosques manejados de pino Patula en Hidalgo, Mexico. *Agrociencia* **2009**, *43*, 209–220.
58. Masera, O.R.; Cerón, A.D.; Ordóñez, A. Forestry mitigation options for Mexico: Finding synergies between national sustainable development priorities and global concerns. *Mitig. Adapt. Strateg. Glob. Chang.* **2001**, *6*, 291–312. [CrossRef]
59. Huntington, T.G. Carbon Sequestration in an Aggrading Forest Ecosystem in the Southeastern USA. *Soil Sci. Soc. Am. J.* **1995**, *59*, 1459–1467. [CrossRef]
60. Rojo, J.M.T.; Sanginés, A.G. El potencial de Mexico para la producción de servicios ambientales: Captura de carbono y desempeño hidráulico. *Gac. Ecol.* **2002**, *63*, 40–59.
61. Bonan, G.B. Forests and Climate Change: Forcings, Feedbacks, and the Climate Benefits of Forests. *Science* **2008**, *320*, 1444–1449. [CrossRef] [PubMed]
62. Canadell, J.G.; Raupach, M.R. Managing Forests for Climate Change Mitigation. *Science* **2008**, *320*, 1456–1457. [CrossRef] [PubMed]
63. Seely, B.; Welham, C.; Kimmins, H. Carbon sequestration in a boreal forest ecosystem: Results from the ecosystem simulation model, FORECAST. *For. Ecol. Manag.* **2002**, *169*, 123–135. [CrossRef]
64. Chacón, P.; Leblanc, H.; Russo, R. Fijación de carbono en un bosque secundario de la región tropical húmeda de Costa Rica. *Tierra Trop.* **2007**, *3*, 1–11.
65. Figueroa-Navarro, C.M.; Ángeles-Pérez, G.; Velázquez-Martínez, A.; de los Santos-Posadas, H.M. Estimación de la biomasa en un bosque bajo manejo de Pinus patula Schltdl. et Cham. en Zacualtipán, Hidalgo. *Rev. Mex. Cienc. For.* **2010**, *1*, 105–112.
66. Harmon, M.E.; Harmon, J.M.; Ferrell, W.K.; Brooks, D. Modeling carbon stores in Oregon and Washington forest products: 1900–1992. *Clim. Chang.* **1996**, *33*, 521–550. [CrossRef]
67. CCMSS. *El Manejo Sostenible de los Bosques Como Estrategia de Combate al Cambio Climático en México*; Punto Verde Consultores, S.C.: Monterrey, Mexico, 2010.
68. Liu, J.; Liu, S.; Loveland, T.R. Temporal evolution of carbon budgets of the Appalachian forests in the US from 1972 to 2000. *For. Ecol. Manag.* **2006**, *222*, 191–201. [CrossRef]
69. Zhang, J.; Ge, Y.; Chang, J.; Jiang, B.; Jiang, H.; Peng, C.; Zhu, J.; Yuan, W.; Qi, L.; Yu, S. Carbon storage by ecological service forests in Zhejiang Province, subtropical China. *For. Ecol. Manag.* **2007**, *245*, 64–75. [CrossRef]
70. Manzanilla, H. *Investigaciones Epidométricas y Silvícolas en Bosques Mexicanos de Abies Religiosa*; Secretaría de Agricultura y Ganadería, Dirección General de Información y Relaciones Públicas: Mexico City, Mexico, 1974.

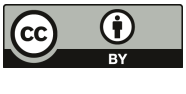

forests

MDPI

Article

Nonlinear Variations of Net Primary Productivity and Its Relationship with Climate and Vegetation Phenology, China

Jian Yang [1,2], Xin Chang Zhang [1,*], Zhao Hui Luo [2] and Xi Jun Yu [2]

[1] School of Geography and Planning, Sun Yat-sen University, Guangzhou 510275, China; yangjian@scies.org
[2] South China Institute of Environmental Sciences, Ministry of Environmental Protection, Guangzhou 510655, China; luozhaohui@scies.org (Z.H.L.); yuxijun@scies.org (X.J.Y.)
* Correspondence: eeszxc@mail.sysu.edu.cn; Tel.: +86-020-8411-5833

Received: 8 August 2017; Accepted: 19 September 2017; Published: 25 September 2017

Abstract: Net primary productivity (NPP) is an important component of the terrestrial carbon cycle. In this study, NPP was estimated based on two models and Moderate Resolution Imaging Spaectroradiometer (MODIS) data. The spatiotemporal patterns of NPP and the correlations with climate factors and vegetation phenology were then analyzed. Our results showed that NPP derived from MODIS performed well in China. Spatially, NPP decreased from the southeast toward the northwest. Temporally, NPP showed a nonlinear increasing trend at a national scale, but the magnitude became slow after 2004. At a regional scale, NPP in Northern China and the Tibetan Plateau showed a nonlinear increasing trend, while the NPP decreased in most areas of Southern China. The decreases in NPP were more than offset by the increases. At the biome level, all vegetation types displayed an increasing trend, except for shrub and evergreen broad forests (EBF). Moreover, a turning point year occurred for all vegetation types, except for EBF. Generally, climatic factors and Length of Season were all positively correlated with the NPP, while the relationships were much more diverse at a regional level. The direct effect of solar radiation on the NPP was larger (0.31) than precipitation (0.25) and temperature (0.07). Our results indicated that China could mitigate climate warming at a regional and/or global scale to some extent during the time period of 2001–2014.

Keywords: net primary production; spatiotemporal patterns; climate change; phenology; China

1. Introduction

Net primary productivity (NPP) is the net amount of carbon accumulated by plants in a given period, and has been regarded as one of the main components of the carbon cycle [1]. Due to a variety of direct and/or indirect anthropogenic activities (e.g., land clearing and conversion) and nature disturbances (e.g., fire, pests) as well as global and regional climate change, forested ecosystems have undergone substantial changes in cover and have increasingly shown declines in health over recent decades [2,3]. As a sensitive indicator of forest cover, function and health, NPP loss may affect the composition of the atmosphere, fresh water availability, biodiversity [4,5], and the ecological adjusting mechanism of energy supply and distribution [6].

Quantifying the inter-annual variability in NPP and the interactions with climate factors would help us understand the terrestrial carbon dynamics and underlying mechanisms in responses to climate change [7]. Recently, many studies have been undertaken on the spatiotemporal variation of NPP and its relationship with climate factors on global and regional scales using a range of approaches from observational [2,8,9] to a suite of remote sensing based methods [10,11]. However, the NPP results were diverse in trends and magnitudes, even in the same region among models [10,12] due to different inputs. Moderate Resolution Imaging Spaectroradiometer (MODIS) annual NPP products have been

widely used [13,14]; however, uncertainties from inputs and the algorithm resulted in biases and restrained data use regionally or globally to some extent. For instance, 70–80% accuracy of MODIS land cover products (MOD12Q1) are an assimilated meteorological dataset, not observed data with coarse spatial resolution, the cloud-contaminated MODIS FPAR/LAI (MOD15A2), and weaknesses in the MOD17 algorithm [15,16]. Therefore, it is essential to compare MODIS derived NPP to other models and/or field observed NPP, especially for China, which encompasses a wide range of ecosystems and climates. In addition, the responses of different ecosystems to different magnitudes of climate change are still far from clear, especially in China [17]. Moreover, few studies [12] have investigated the effect of solar radiation as an integrated surrogate for the effects of both day length and sunlight intensity [18] on vegetation NPP, especially when temperature and precipitation are considered simultaneously. In addition, previous studies have shown that vegetation phenology, an important factor that affects plant productivity, has changed dramatically due to climate changes and anthropogenic interference [19], but only a few studies have explored the effect of phenophase variation on NPP [20]. At present, due to the diversity of the trends and magnitudes of vegetation phenophases at different scales, its effects on NPP are still unclear, especially in China, where the vegetation phenophases are diverse at both the regional and biome levels [19]. Furthermore, a linear regression method has been applied by most studies to analyze NPP trend [10,21] despite the trend always showing a non-linear trend, or has one or more turning points within the time period [22,23]. These limitations and/or gaps have impeded our understanding of the dynamic relationship and consequently researchers may have underestimated future changes in plant productivity and/or the carbon cycle throughout China.

China encompasses a variety of ecosystems and climates. The regional climate ranging from tropical to cold-temperate, and from humid in the south to extremely dry in the northwest [24]. Land cover types are diverse, including a broad range of tropical, temperate and boreal forests, grassland, cropland and desert [25]. In recent decades, China has experienced dramatic changes in climate such as remarkably strong El Niño events [26], the freezing low temperatures in early 2008 [24], and frequent occurrences of severe droughts [27]. Meanwhile, land use and land cover changes have occurred at unprecedented rates due to quick economic development, dramatic urbanization [28], and implementation of several large scale forest plantation programs [29]. These changes have resulted in large variations in China's terrestrial ecosystem productivity and have definitely adjusted the terrestrial carbon cycle in China [30]. However, whether the temporal trend of NPP continuously increased or decreased during the study period is still unclear given the possible changes of climate derivers and anthropogenic activities. Additionally, the correlations between NPP and climate derivers as well as vegetation phenophases in recent decade still remain unclear [31].

Due to climatic variability, topographic complexity, natural ecosystem diversity, and intensive human disturbance, China is becoming one of the most critical and sensitive regions in the global carbon cycle for determining the carbon budget at regional and global scales. Furthermore, it provides a good opportunity to identify the effects of climate change on NPP to forecast the potential biosphere feedback to nature in the climate system.

Therefore, two simple models were applied to estimate NPP and the results accompanied by MODIS derived NPP were all compared with the field observed NPP. Then, the results that showed less biases with the field observed NPP were selected to analyze the vegetation NPP dynamics and its relationship with both climate and vegetation phenology in China. More specifically, the authors aim was to (1) explore which model's result was more accurate, and the quantity of uncertainty of MODIS derived NPP in China; (2) understand the spatial pattern of NPP, and investigate whether the temporal trend of NPP was continuously increasing or decreasing in China for the period 2001–2014 given climate change and anthropogenic activities; and (3) estimate the effects of climatic driving factors and vegetation phenology changes on vegetation NPP.

2. Materials and Methods

2.1. Study Area

The study focused only on Mainland China. The climate in China is extremely diverse, ranging from tropical regions in the south to subarctic in the north [11]. Therefore, the whole study area was divided into three sub-regions (Figure S1) according to the climatic regionalization of China [32]: (1) Northern China, with mean annual temperature ranges from −4 °C to 14 °C and total annual precipitation ranges from 200 mm in the northwest to 1000 mm in the southeast; (2) Southern China, where mean annual temperature ranges from 14 °C to 22 °C and total annual precipitation ranges from 1000 to 2000 mm [33]; and (3) the Tibetan Plateau, which has been called the Third Pole of the World, with an average altitude close to 4000 m above sea level, a mean annual temperature ranging from −5 °C to 12 °C and precipitation ranging from >800 mm to <200 mm [34].

2.2. Dataset and Data Processing

2.2.1. Annual Net Primary Productivity (NPP)

NPP derived from MODIS from 2001–2014 in China were used (MOD17A3, 1 km), which have been further used as an important data source for plant productivity monitoring and assessment [35]. The MODIS annual NPP algorithm relies on the summation of the daily estimation of Gross Primary Productivity (GPP) computed globally minus growth and maintenance respiration [14]. To estimate annual NPP, first, the daily estimates of maintenance respiration for leaves and fine roots are subtracted from the daily GPP values. These daily reduced GPP estimates are then summed for each year, and estimates for annual maintenance respiration of living wood tissue and annual total growth respiration are subsequently subtracted, resulting in annual NPP estimates. Full details of the algorithm in MODIS derived NPP can be found in Reference [14]. However, due to the deficiencies and uncertainty of MODIS derived NPP as above-mentioned, the Miami model and Thornthwaite Memorial model were applied in this study, as they are simple to operate with only a few parameters that were easy to obtain, and have a higher spatial and temporal resolution of climate data in China. Additionally, they have previously been applied in China [11,13]. The Miami model is calculated as follows (Equations (1)–(3)):

$$NPP_{T,P} = \min\{f_1(T),\ f_2(P)\} \tag{1}$$

$$f_1(T) = \frac{k_1}{1 + e^{k_2 - k_3 \times T}} \tag{2}$$

$$f_1(P) = k_4 \times \left(1 - e^{-k_5 \times P}\right) \tag{3}$$

where K_1, K_2 and K_3 in Equation (2) are the temperature response parameters with values of 3000, 1.315 and 0.119, respectively and T is the annual average temperature (°C); K_4 and K_5 in Equation (3) are the precipitation response parameters with values of 3000 and 0.000664, respectively, and P is the annual average precipitation (mm). The parameters of K_i (i = 1, 2, . . . , 5) were calculated using the least squares method based on the field testing of NPP, and the relative temperature and precipitation collected at 50 locations scattered across five continents [36].

The Thornthwaite Memorial model is expressed as follows (Equations (4)–(6)):

$$NPP = 3000 \times \left(1 - e^{-0.0009695 \times |v - 20|}\right) \tag{4}$$

$$v = \frac{1.05 \times R}{\sqrt{1 + (1 + 1.05\frac{R}{L})^2}} \tag{5}$$

$$L = 3000 + 25 \times T + 25T^3 \tag{6}$$

where v represents the mean annual actual evapotranspiration (mm); L represents the mean annual evapotranspiration (mm); and T and R represent the mean annual temperature and mean annual precipitation, respectively.

Due to the different inputs and parameters in the three models, all the estimated NPP results were compared with the field observed NPP (Table S1), which was calculated from flux tower data based on the eddy covariance method, a micrometeorological method with high-frequency data collection. This method provides direct measures of net carbon fluxes between vegetated canopies and the atmosphere over short and long timescales with minimal disturbance to the underlying vegetation. The observation data were collected from ChinaFLUX sites [37] directly and indirectly from the literature. High-precision CO_2 concentration measurements and surface carbon flux measures, made at eddy covariance measurement sites, can be used to improve and validate the algorithms being used by remote sensing and ecosystem models [38]. The observations almost covered the typical ecosystem types in China. Therefore, observations from carbon flux data were applied as a reference to compare the results from the three models. Sites only having one year, the corresponding yearly data for observations, and three simulated values were used directly; and for sites longer than one year, the corresponding multi-year averaged data were applied. Next, two statistical indicators, namely root mean square error (RMSE), and mean absolute error (MAE), were used to evaluate the performance of each method above-mentioned. The best estimated result was then considered in the following analysis of the NPP relationship with climatic factors and vegetation phenology. The two statistical indicators were calculated as follows (Equations (7) and (8)):

$$\mathrm{RMSE} = \sqrt{\frac{\sum_{i=1}^{n}(NPP_i - NPP^*)}{n}} \quad (7)$$

$$\mathrm{MAE} = \frac{1}{n}\sum_{i=1}^{n}|NPP_i - NPP^*| \quad (8)$$

where NPP_i is the estimated NPP, NPP^* is the field observed NPP; and n is the sample size.

2.2.2. Climate Data and Phenology Extraction

Monthly meteorological data from 2001–2014, including temperature, precipitation, and solar radiation, were acquired from the China Meteorological Data Sharing Service System (downloaded from [39]) All meteorological data used in this study were verified by China's Meteorological Information Center (located in Beijing, China) [40], thus false or missing data from some of the stations were eliminated [11]. There are 653 meteorological stations recording temperature and precipitation data (301 in Northern China, 258 in Southern China, and 94 in the Tibetan Plateau), and 99 stations recording solar radiation (50 in Northern China, 38 in Southern China, and 11 in the Tibetan Plateau; Figure S2). The Kriging method was used for the spatial interpolation of climate data across the study area [41].

Vegetation phenology metrics (Start of Season (SOS) and End of Season (EOS) for each year) were extracted using TIMESAT software (which is widely used for simulating vegetation phenology [42,43]) by applying the Savitzky–Golay (S–G) method to generate smooth time-series MODIS EVI data. We adopted an adaptation strength of 2.0, no spike filtering, seasonal parameter of 0.5, S–G window size of 2, and amplitude season start and end of 20% to calculate the phenology parameters. Length of Season (LOS) was calculated as the difference between the SOS and EOS values.

2.2.3. Land Cover Data

A 1-km spatial resolution land cover product, MOD12Q1, was applied in this study to analyze NPP and its variation across vegetation types. The MOD12Q1 land cover dataset which was extensively applied to monitor land use and land cover change [44], is mainly based on the International Geosphere–Biosphere program (IGBP) classification system that obtains a classification algorithm of

the decision tree and artificial neural network [45]. The MOD12Q1 land cover classes were further reclassified into seven major land cover classes (Figure S1) in the present study: evergreen needle-leaf forest (ENF), evergreen broadleaf forest (EBF), deciduous needle-leaf forest (DNF), deciduous broadleaf forest (DBF), farmland grassland and meadow (GM), and shrubs. However, the data only reflected the land cover classifications and could not consider changes in land cover that occurred over our study period. It was estimated that vegetation changes might be relatively stable over a short time period of approximately 10 years at a regional or global scale [42].

2.3. Data Processing

2.3.1. Trend Analysis and Turning Point Year Detection

The trends of NPP during 2001–2014 were calculated at both pixel level and regional level. Due to autocorrelation among the inter-annual time series data, a robust non-parametric Mann–Kendall (M–K) trend analysis [46] was applied. This method did not require the independence and normality of the time series data [47], which has been widely used in trend analysis [19]. Previous studies have reported that the M–K test statistic Z was approximately normally distributed when the sample size was $n \geq 8$. A positive or a negative Z value indicated an increasing or a decreasing trend respectively, which were all monotonic [46]. The formulas for the M–K method are described in detail in Reference [46]. In addition, trends of the NPP were tested at a significance level of $\alpha = 0.05$.

The Theil–Sen median slope estimator was applied to estimate the rate of change of NPP, which was more appropriate for assessing the rate of change in short or noisy time series [48]. The Theil–Sen median slope was computed as (Equation (9)):

$$\beta_i = \text{Median}\left(\frac{x_j - x_k}{j - k}\right) \text{ for } i = 1, \ldots, N \tag{9}$$

where x_j and x_k are the data values at times j and k ($j > k$), respectively.

To detect the timing and magnitude of NPP changes, a linear regression model and a piecewise linear regression model (Equation (10)) were used. This method has been widely used [41,49] as it can detect potential turning points (TPs) in a trend of time-series data. In addition, TP was limited to the years 2004 to 2010 to avoid obtaining a too-short segment before or after the TP [50]. The maximum number of TPs was specified as one given that too many TPs would make the result more complex and thus create more uncertainty in the understanding of NPP trends [23]. The models used were:

$$Y = \begin{cases} \beta_1 \times t + \beta_0 + \varepsilon & (t \leq \alpha) \\ \beta_1 \times t + \beta_2 \times (t - \alpha) + \beta_0 + \varepsilon & (t > \alpha) \end{cases} \tag{10}$$

where Y is the NPP; t is the year; α is the turning point of the NPP time series; β_0 is the intercept; β_1 is the magnitude of the NPP trend before the TP; $(\beta_1 + \beta_2)$ is the magnitude of the NPP trend after the TP; α is the year of the TP; and ε is the residual random error.

The two models were then fitted to the NPP time-series data using the least-squares method, and the Akaike Information Criterion (AIC) [51] was used to determine whether the TPs were significant as it provides a means for model selection [41,51]. The AIC values of these two models were calculated as (Equation (11)):

$$AIC = n \times \log\left(\frac{RSS}{n}\right) + 2k + \frac{2k(k+1)}{n - k - 1} \tag{11}$$

where RSS is the residual sum of squares for the estimated model; k is the number of parameters; and n is the sample size.

Finally, ΔAIC was defined as the difference of the AIC2 of the piecewise linear regression model (model 2) and the AIC1 of linear regression model (model 1); if the ΔAIC was less than −2, then model 2 was significantly preferred [8].

2.3.2. Correlations Relating Climatic Factors, LOS and NPP

Partial correlation analysis was used to explore the relationships between NPP and climatic factors (mean annual temperature, annual cumulative precipitation, and annual cumulative solar radiation from 2001–2014) as well as LOS, which excluded the effects of other variables. The significance of the correlation coefficients was tested at a significance level of 0.05.

To understand the direct and indirect effects of climatic factors, LOS on NPP variation (excluding multi-collinearity between climatic factors and LOS), a structural equation model (SEM) with standardized data was applied to examine the influences of climate and LOS change on NPP variation. The SEM was initiated by including all possible relationships. The least significant relationship was then removed stepwise until all relationships were significant and the fit of the model did not increase further [52]. SEM was conducted by the "sem" R package [53], which was then visualized by the R package "semPlot".

3. Results

3.1. Accuracy Assessment of NPP Estimation

The accuracy of three modeled NPP results (MODIS derived, the Miami model, and the Thornthwaite Memorial model) were assessed by a comparison with the in situ observations. Validation analysis indicated that the modeled NPP results were all very significantly (Figure 1; $p < 0.01$) correlated with the in situ NPP measurements. The R^2 value for the MODIS derived NPP was 0.39, which was higher than that of Miami model (R^2 = 0.27) and the Thornthwaite Memorial model (R^2 = 0.28). Furthermore, the RMSE and MAE deceased to 0.19 kg C m^{-2} a^{-1} and 0.14 kg C m^{-2} a^{-1}, respectively for the MODIS NPP data compared to 0.29 kg C m^{-2} a^{-1} and 0.23 kg C m^{-2} a^{-1} for the Miami model, as well as 0.31 kg C m^{-2} a^{-1} and 0.26 kg C m^{-2} a^{-1} for the Thornthwaite Memorial model, respectively. The results demonstrated that the NPP derived from MODIS had an improved performance of NPP simulation by increasing R^2 by 46.18% and 40.46% when compared with the Miami model and Thornthwaite Memorial models, respectively. In addition, the NPP derived from MODIS decreased the relative RMSE and MAE by 34.01% and 38.34%, respectively, when compared with the Miami model, and by 39.71% and 45.88%, respectively, when compared with the Thornthwaite Memorial model.

3.2. Spatial Pattern of NPP

The spatial pattern of mean annual NPP derived from MODIS for the period 2001–2014 is shown in Figure 2a. The spatial pattern of annual NPP was uneven, which showed gradients decreasing from the south to the north and from the east to the west. The highest value occurred in Southern China, with values generally higher than 0.6 kg C m^{-2} in most of that area. In contrast, annual NPP was usually lower than 0.2 kg C m^{-2} in the Tibetan Plateau. For the remaining regions, annual NPP ranged between 0.2 and 0.6 kg C m^{-2}. The standard deviation (Figure 2b) shows a similar spatial pattern with mean annual NPP. The highest value (more than 0.05 kg C m^{-2}) was mostly distributed in Southern China. The values in Northern China ranged from 0.02–0.05 kg C m^{-2}, with the exception of the northern and eastern parts of Northeast China, which was more than 0.05 kg C m^{-2}. The lowest standard deviation value was found in the Tibetan Plateau, with values mostly less than 0.02 kg C m^{-2}.

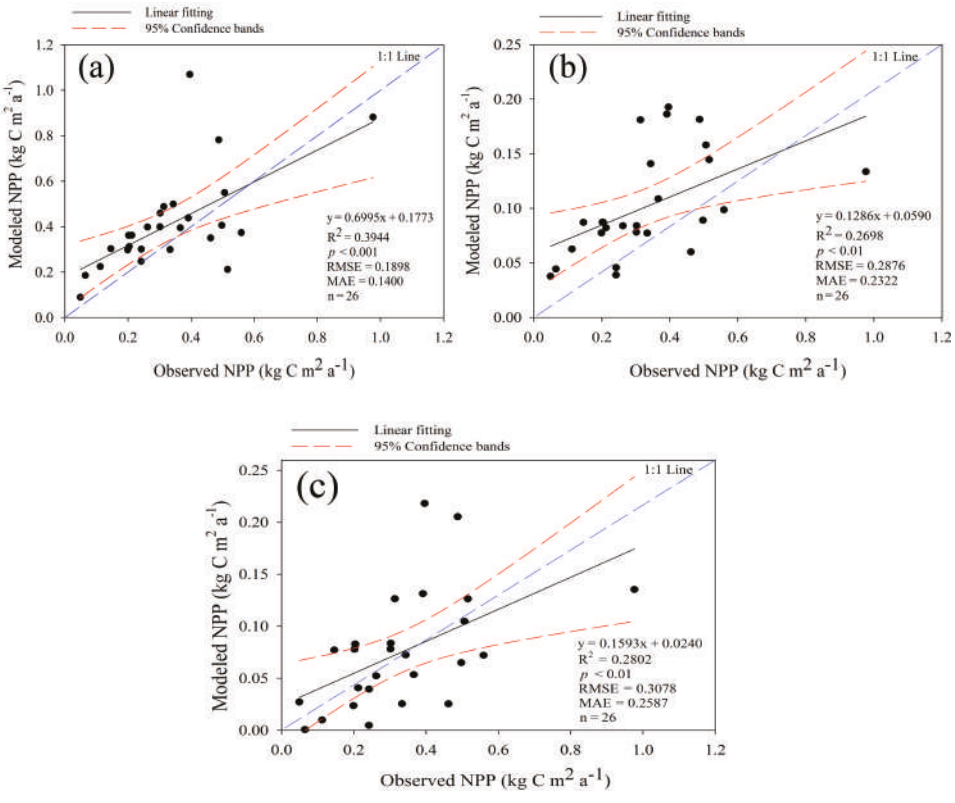

Figure 1. Comparison between the in situ Net Primary Productivity (NPP) site observations and NPP derived from MODIS (**a**); Miami model (**b**); and Thornthwaite Memorial model (**c**).

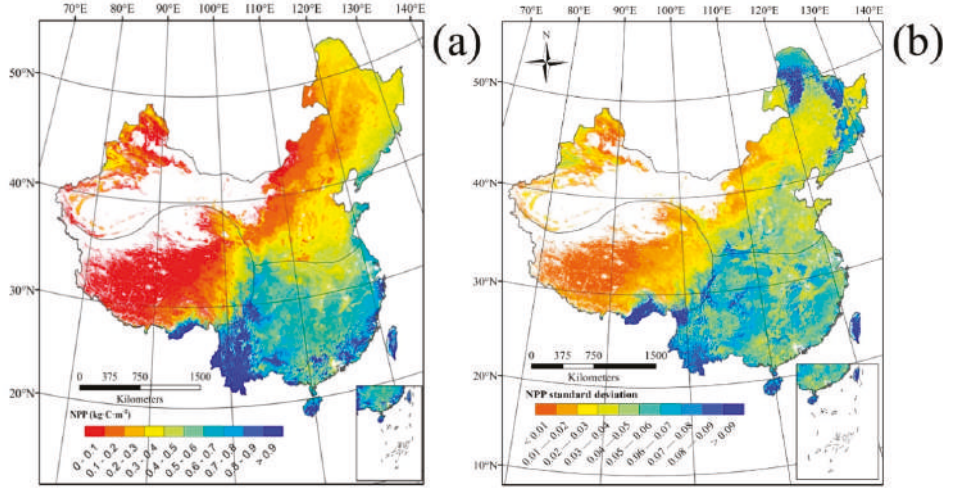

Figure 2. Spatial distribution of mean Net Primary Productivity (NPP) (**a**) and standard deviation (**b**) in China between 2001–2014.

At the biome level, NPP differs in terms of vegetation types (Figure 3). Generally, forest ecosystems have a higher annual NPP than grassland ($p < 0.001$). Among the forest ecosystems, evergreen forests show a higher NPP than deciduous forests ($p < 0.001$). The highest NPP was found in EBF, with an average annual value of 0.975 ± 0.362 kg C m^{-2}, which was almost twice that of the DBF (0.542 ± 0.301 kg C m^{-2}) and DNF (0.329 ± 0.103 kg C m^{-2}). ENF had the second largest NPP (0.605 ± 0.277 kg C m^{-2}), followed by Farmland (0.422 ± 0.159 kg C m^{-2}) and Shrub (0.317 ± 0.273 kg C m^{-2}), respectively. Grassland had the lowest annual NPP, with an average value of 0.162 ± 0.196 kg C m^{-2}.

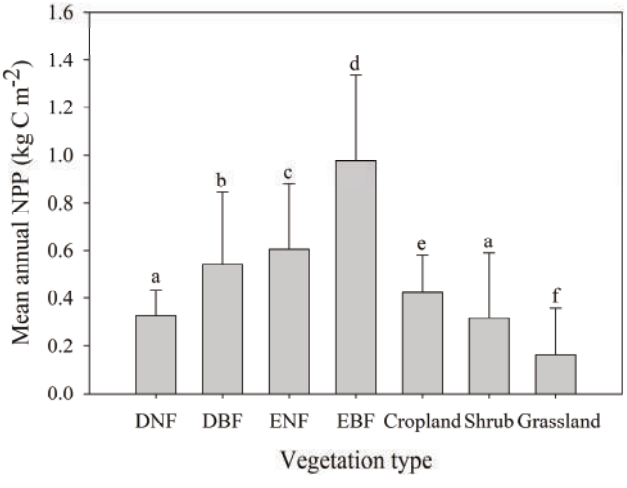

Figure 3. Mean annual Net Primary Productivity (NPP) for each vegetation type over 2001–2014. The error bar in each column indicates the standard deviation. Different lowercase letters indicate significant differences in NPP among vegetation types (one-way ANOVA and *t*-test, $p < 0.001$).

3.3. Temporal Trend of NPP

Figure 4 details the temporal trends in annual NPP across China. Over a 14-year period (2001–2014), 17.69% of total pixels displayed either significantly increased or decreased trends (Figure 4b; $p < 0.05$) in the whole study region. Pixels with a positive (i.e., increased NPP) trend in NPP accounted for 78.94% of the total pixels, and 15.18% of the total pixels exhibited a significantly positive trend (Figure 4b,c; $p < 0.05$). The increasing rate of NPP in China mainly occurred between 0 and 0.4×10^{-2} kg C m^{-2} a^{-1} (Figure 4c). At a regional scale, 79.15% of the total pixels showed a positive trend in Northern China, and the increasing rate was mostly distributed in 0–0.6×10^{-2} kg C m^{-2} a^{-1} (Figure 4d). Similarly, 88.12% of the total pixels displayed an increasing trend in the Tibetan Plateau, where an increasing magnitude mostly occurred at 0–0.4×10^{-2} kg C m^{-2} a^{-1} (Figure 4f). In contrast, negative trends occurred in 57.64% of the total pixels in Southern China, with an absolute magnitude mainly ranging from 0.2×10^{-2} kg C m^{-2} a^{-1} to 0.8×10^{-2} kg C m^{-2} a^{-1} (Figure 4e).

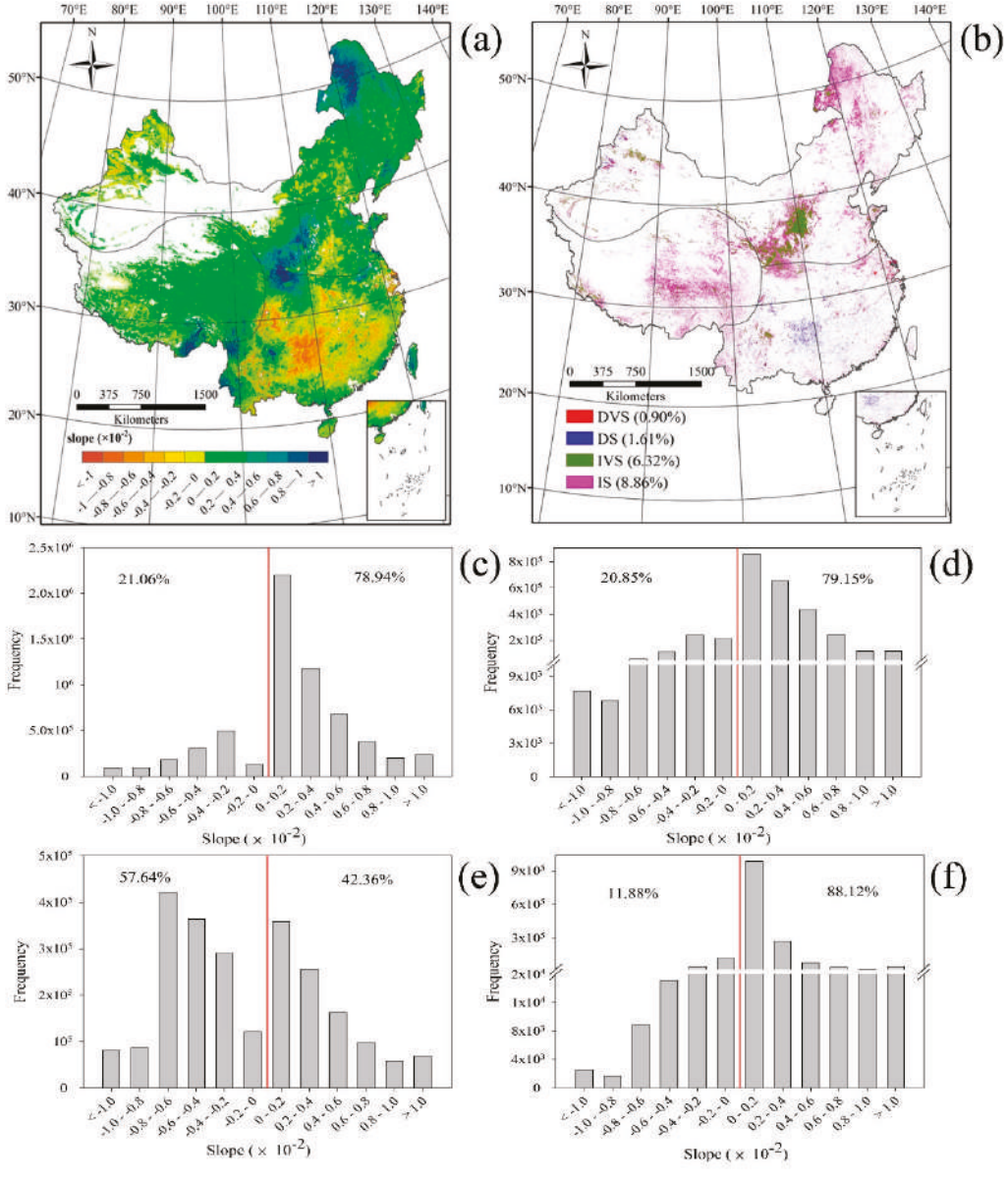

Figure 4. Trends in annual Net Primary Productivity (NPP) within China between 2001 and 2014 (**a**); and pixels with significant ($p < 0.05$) and very significant ($p < 0.01$) trends are shown in (**b**). The count distributions of NPP trends in China (**c**); Northern China (**d**); Southern China (**e**) and the Tibetan Plateau (**f**) are also shown. A positive trend indicated an increase in NPP and vice versa; DS and DVS represent decreased significantly and very significantly, respectively; and IS and IVS represent increased significantly and very significantly, respectively. The red lines in figures (**c**), (**d**), (**e**) and (**f**) represent boundary for negative slop and positive slop.

3.4. Turning Point Year of NPP

3.4.1. Turning Point Year of NPP at National and Regional Scale

To clarify the characteristics of the NPP trends, the averaged trends of the NPP and the turning point year at national and regional levels were calculated over the study period (Figure 5). At the pixel scale, 87.26% of the total pixels showed abrupt changes in inter-annual NPP variation ($\Delta AIC < -2$; Figure S3b), most of which appeared at year 2004 or year 2010 (which may also have been caused by criterion we set up in the calculation), accounting for 29.36% and 31.78%, respectively (Figure S3a). At a national scale, the linear regression model suggested an increasing trend of 0.0007 kg C m^{-2} a^{-1} ($p = 0.3118$) from 2001 to 2014 (Figure 5a). However, two distinct periods were clearly identified by the piecewise linear regression model: a trend change from a marginal significant increasing trend of 0.0104 kg C m^{-2} a^{-1} ($p = 0.0746$) before 2004 to a non-significant increasing trend of 0.0012 kg C m^{-2} a^{-1} ($p = 0.2775$) after 2004 (Figure 5a). The information criterion of the piecewise regression model was less than that of the linear regression model ($\Delta AIC = -3.1797$). At a regional scale, a marginal significant increasing trend of 0.0025 kg C m^{-2} a^{-1} ($p = 0.0509$) in Northern China was found, and the turning point year occurred in 2010 ($\Delta AIC < -2$). However, the increasing trends were all non-significant before and after 2010, with a rate of 0.0006 and 0.0068 kg C m^{-2} a^{-1}, respectively (Figure 5b). In Southern China, a rate of −0.0007 kg C m^{-2} a^{-1} ($p = 0.6559$) was found for annual NPP variation, and a turning point year occurred in 2010 ($\Delta AIC < -2$). However, the variation trend was opposite (Figure 5c). Although a significant increasing trend of 0.0016 kg C m^{-2} a^{-1} ($p < 0.01$) was found in the Tibetan Plateau over the past 14 years (Figure 5d), the increasing trend slowed down after 2006 ($\Delta AIC < -2$).

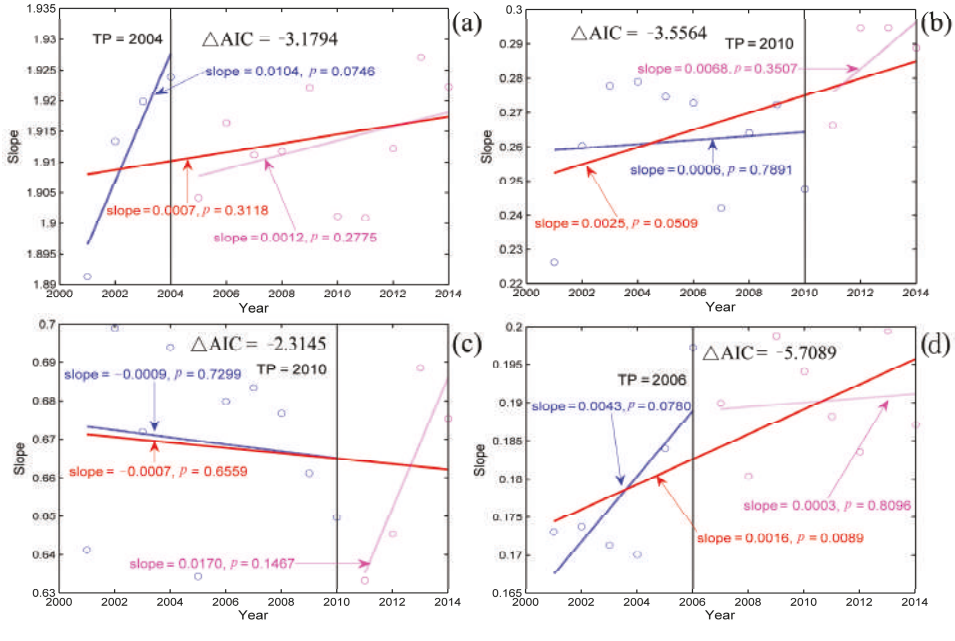

Figure 5. Inter-annual variations of Net Primary Productivity (NPP) in China at national level (**a**) and regional level (Northern China (**b**); Southern China (**c**); and the Tibetan Plateau (**d**)). Trends estimated by the least-squares linear regression are shown. The blue and pink lines indicate the linear fit before and after the turning year, respectively. The red line indicates linear fit during the period 2001–2014. TP represents the turning point year.

3.4.2. Turning Point Year of NPP at Biome Scale

At the biome level, the variation of NPP was diverse (Figure 6). All vegetation types had two clearly distinct periods over the study period ($\Delta AIC < -2$), with the exception of the EBF ($\Delta AIC = -1.9314$) which only showed a non-significant decreasing trend of -0.0001 kg C m^{-2} a^{-1} ($p = 0.9314$) during 2001–2014. Farmland and grassland all increased, with a rate of 0.0011 kg C m^{-2} a^{-1} ($p = 0.3734$) and 0.0016 kg C m^{-2} a^{-1} ($p < 0.01$), respectively. In addition, the increasing trend before 2004 was larger than that after 2004 for both farmland and grassland. An increasing trend of NPP was found for DNF, ENF, and DBF, but the opposite trend was found for shrub, despite a turning point year occurring in 2010 (all $\Delta AIC < -2$ and may also have been caused by the criterion we set up in the calculation) for all above vegetation types. In addition, a decreasing NPP occurred for ENF, DBF and shrub during 2001–2010, while an increasing NPP occurred for DNF during the same time period. After 2010, the trend of these four vegetation types was all positive, despite the existence of different magnitudes.

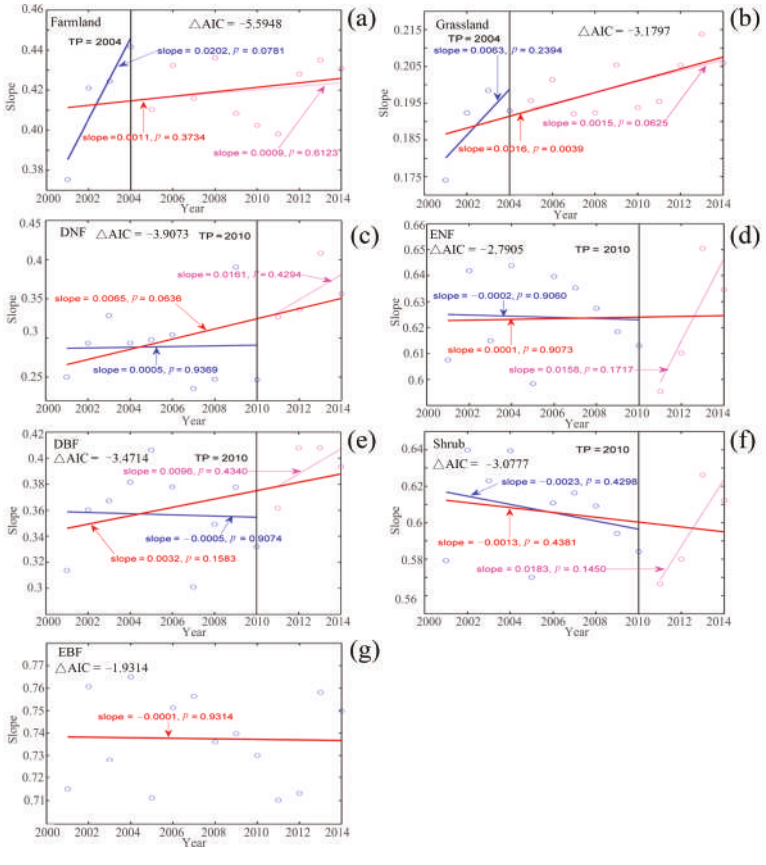

Figure 6. Inter-annual variations of Net Primary Productivity (NPP) in China at the biome level (Farmland (**a**), Grassland (**b**), Deciduous needle-leaf forest (**c**), Evergreen needle-leaf forest (**d**), Deciduous broadleaf forest (**e**), Shrub (**f**), and Evergreen broadleaf forest (**g**)). Trends estimated by the least-squares linear regression are shown. The blue and pink lines indicate the linear fit before and after the turning year, respectively. The red line indicates linear fit during the period 2001–2014. TP represents the turning point year.

3.5. Relationship Relating Climatic Factors, LOS and NPP

3.5.1. Correlation Analysis

Climatic factors were generally positively correlated with NPP on a national scale (Figure 7). Positive partial correlations were observed for 62.66%, 70.79% and 57.60% of the total pixels with temperature, precipitation, and solar radiation, respectively. The positive correlation coefficients for the climatic variables ranged from 0.1–0.7. About 56.23% of the total pixels showed positive partial correlations between NPP and LOS, and the positive partial correlation coefficient was mostly distributed between 0.1 and 0.5.

At a regional level, 62.97% of the total pixels in Northern China displayed a negative relationship between NPP and temperature, while precipitation, solar radiation and LOS all generally showed a positive relationship with the NPP (Table 1). Over 57% of the total pixels in Southern China indicated a positive relationship between the NPP and climatic factors as well as LOS. However, the relationship in the Tibetan Plateau was diverse. Specifically, over 83% of the total pixels for temperature and about 58% of the total pixels for precipitation displayed a positive relationship with the NPP, while in general, an opposite relationship occurred between the NPP and solar radiation. In addition, the relationship between the NPP and LOS in the Tibetan Plateau was ambiguous.

Table 1. Partial correlation between the Net Primary Productivity (NPP) and climatic factors as well as Length of Season (LOS).

Variable	Relationship	Northern China	Southern China	The Tibetan Plateau
Temperature	+	37.03%	67.56%	83.14%
	−	62.97%	32.44%	16.86%
Precipitation	+	84.55%	62.04%	57.83%
	−	15.55%	37.96%	42.17%
Solar radiation	+	66.93%	61.06%	34.75%
	−	33.07%	38.94%	65.25%
LOS	+	57.83%	57.56%	50.73%
	−	42.17%	42.14%	49.27%

+ Represent positive relationship; − Represent negative relationship.

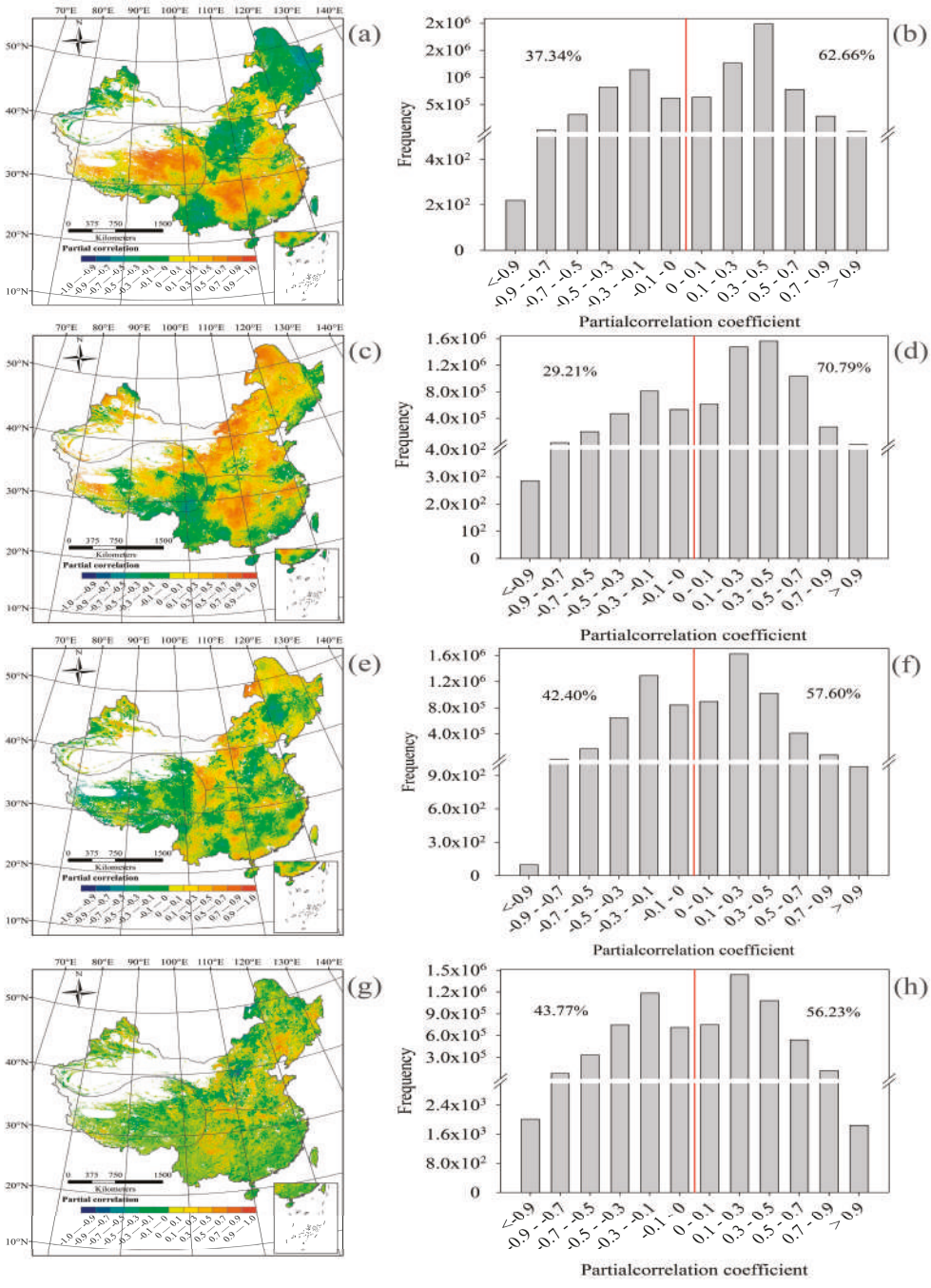

Figure 7. The partial correlation coefficients and corresponding frequency distribution between the NPP and temperature (**a**,**b**), precipitation (**c**,**d**), solar radiation (**e**,**f**) and LOS (**g**,**h**) in China from 2001 to 2014. The red lines in figures (b), (d), (f) and (h) represent boundary for negative relationship and positive relationship.

3.5.2. Structural Equation Models

Our structural equation model (SEM) did not detect a relationship between temperature, precipitation and solar radiation, which indicates that there was a strong relationship among the climatic factors, LOS and NPP. In the SEM (χ^2 = 1.0138, d.f. = 5, p = 0.9614, AIC = 21.0138, BIC = −1815), climatic factors explained a total of 23% of the variation in LOS, and temperature and solar radiation had a positive effect on LOS, while precipitation had the opposite effect (Figure 8). Moreover, the effect of climatic factors and LOS on NPP was 0.63, and explained a total of 56% of the variation in NPP. Among the climatic factors, the direct effect of solar radiation on NPP was the largest (0.31), followed by precipitation (0.25), and temperature (0.07).

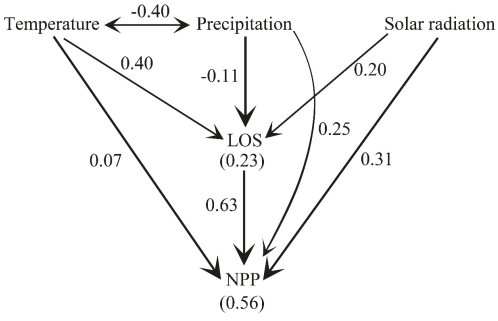

Figure 8. Structural equation model relating climatic factors, Length of Season (LOS) and Net Primary Productivity (NPP) in China. Single headed arrows indicate directional relationships, while double headed arrows indicate covariances. Numbers in brackets are R^2 values.

4. Discussion

4.1. Uncertainties in NPP Estimates

Net primary productivity (NPP), an indicator of the accumulation of atmospheric CO_2 in terrestrial ecosystems, plays a crucial role in global change [54]. The accurate estimation of NPP is a crucial step for reliably quantifying carbon fluxes between the atmosphere and terrestrial ecosystems [31], especially for regions with different topography and climatic conditions. Although deficiency and biases exist in the MODIS derived NPP, the validation illustrated that the model applied by MODIS was superior to the Miami model and Thornthwaite Memorial model, with an increased R^2 value and a decreased RMSE and MAE. The RMSE and MAE between the MODIS derived NPP and observations were only 0.19 kg C m^{-2} and 0.14 kg C m^{-2}, respectively. This indicated that the MODIS derived NPP may be suitable for analysis with relatively low regional biases in China for the period of 2001–2014 to some extent despite coarse global climate data applied in MOD17. Additionally, it illustrated that the parameters input and algorithms may affect the results. For instance, the Miami model is one of the first global empirical models that only utilizes temperature or precipitation in the model [55], while the Thornthwaite Memorial model determines NPP for a particular location as the actual evapotranspiration functions [36]. The interactions among climatic factors and other influential factors such as vegetation types are not included in these two models [11]. Furthermore, there is no mechanism to account for changing vegetation density in the two models [56]. However, the model applied by MODIS incorporates biogeochemical principles in a mechanistic modeling environment and the vegetation feedback to climate conditions through changes in Leaf Area Index and absorbed radiation, and has the advantage of providing spatially continuous estimates with a consistent methodology, which is important for any large-scale studies [35]. It should be noted that NPP is not easy to measure and only 26 field sites were included in this study, which may cause biases due to the larger study area. In addition, heterogeneity, stand density, and pixel resolution may also

affect validation results. Therefore, increased observation sites and an extended observation period has become essential for NPP estimation. Additionally, forest inventory data is the only data source that provides large-scale consistent productivity assessments [57]. Therefore, the application of forest inventory data rather than numerous field observed data in this study would be more preferable to validate the suitability of MODIS NPP in China, and more efforts should be made in the future. What is more, temporal analysis of match between models and observations based on a long time period were also a good choice for NPP estimates and comparison.

4.2. Spatiotemporal Variation of NPP

In general, all three NPP estimates showed similar spatial patterns, with mean annual NPP higher in the southeast and gradually decreasing towards the northwest (Figure 3 and Figure S2). This finding was consistent with previous studies [10–12,58]. This may have been due to the climatic gradient (e.g., temperature and precipitation) from the southeast to the northwest in China, which is more favorable for vegetation growth in southern China [11,59]. The lowest NPP value in northwest China and the Tibetan Plateau, which was consistent with References [10,11], may have resulted from low temperature and the absence of precipitation. In addition, vegetation type was also a key factor that affected NPP spatial distribution. In Southern China, the dominant vegetation type are evergreen forests (Figure S1) which have a higher productivity than that of the grassland and desert vegetation (Figure 4) distributed mostly in Northern China and the Tibetan Plateau. Productivity in the southeast Tibetan Plateau was higher than that of other areas in the Tibetan Plateau as demonstrated by our conclusion above.

The total amount of NPP increased at a rate of 0.009 Pg C a^{-1} in China from 2001–2014, which was similar with Reference [10], who found a rate of 0.008 Pg C a^{-1} in China from 1999–2010. The decreases in NPP over Southern China were more than offset by increases in NPP over Northern China and the Tibetan Plateau. The overall increased NPP could help to mitigate climate warming at regional scale and/or global scale to some extent. In terms of trend variation, a continually increasing trend of NPP in China from 2001–2014 was found, despite the occurrence of a turning point year which was similar with the previous finding in Reference [10]. This may be due to the fact that over the past three decades, the central government of China has decided to combat severe environmental degradation, including declining vegetation cover and expanding desertification [29]. To realize this goal, the Three North Shelter Forest System project, the Beijing-Tianjin Sand Source Control Program, and the Grain for Green Project [29] were implemented. Alternatively, as the turning point is related to ENSO events/cycles, it is necessary to validate this conclusion in the future.

At a regional scale, NPP trends in China showed a prominent geographical heterogeneity. The trends before and after the turning point year in Northern China and the Tibetan Plateau were all positive. In contrast, the trend in Southern China was the opposite, which may have been due to ecorestoration, forest/grassland protection, and reforestation in Northern China and the Tibetan Plateau after 2000 [29]. However, in Southern China, freezing low temperatures in early 2008, the severe drought in 2009 [31], and decreased solar radiation [12] may have all contributed to the decreasing NPP. Due to the physiological and/or local environmental conditions, the trend and turning point year among vegetation types were diverse.

4.3. Diverse NPP Correlations with Climate Drivers and LOS

Vegetation NPP is influenced by a variety of factors, and the primary one is climate-related. Temperature, precipitation, and solar radiation are the main climate drivers for vegetation growth [59], but the relationships vary with spatial scale. Nevertheless, limited efforts have been made to investigate the relative roles of different climate variables in the NPP [10]. Generally, temperature has been found to be positively correlated with the NPP at a national level, which is consistent with previous studies [10,60]. This response may in part be related to the increased activity of photosynthetic enzymes [61] and improved capacity for photosynthesis and growth [62]. However, the relationship

between temperature and NPP in Northern China was negative. This may have resulted from higher temperatures leading to increased water scarcity caused by accelerated evaporation, which would work against vegetation growth, especially for arid and semi-arid areas in Northern China [49]. Additionally, the positive relationship between precipitation and NPP in Northern China illustrated this conclusion. Precipitation showed a positive correlation with NPP at both the national scale and regional scale, which may have occurred as more precipitation increases soil moisture, satisfying the water requirements for vegetation growth and productivity increase, especially in late spring and summer, which usually have higher temperatures and more evapotranspiration [63].

Little is known about the light-related physiological mechanisms that regulate NPP due to the difficulty in distinguishing the effects of day length (i.e., photoperiod) and light intensity [18], especially when studies are extended to consider their correlations with temperature and precipitation. Therefore, in this study, solar radiation was considered as an integrated surrogate for both day length and sunlight intensity [18] to investigate the effects of solar radiation on the NPP. A positive correlation was observed between the NPP and solar radiation at both the national and regional scales, except for a negative relationship which occurred in the Tibetan Plateau. Generally, increased solar radiation provides sufficient materials and energy for vegetation photosynthesis and solar radiation is typically accompanied by warmer temperatures and sufficient sunlight intensity, both of which can enhance photosynthetic capacity and promote vegetation NPP. The negative correlations between solar radiation and NPP in the Tibetan Plateau may be partly related to larger areas of melting seasonal snow and permafrost soils caused by abundant solar radiation, leading to higher soil moisture content and creating an anaerobic soil environment within the plant root zone, thus limiting vegetation growth [64]. Alternatively, increased solar radiation may enhance surface soil evaporation and limit water availability for herbaceous plants that have shallow root systems.

Vegetation phenology has long been regarded as an important factor that affects vegetation productivity. Consistent with previous studies in References [20,65], our results also indicated a positive relationship between the NPP and LOS at both national and regional levels. This suggests that an extension of LOS is one of the most important factors that affect plant productivity [66].

4.4. Shortcomings and Uncertainties

In this study, we used data from only 99 solar radiation stations, as meteorological stations in the Tibetan Plateau are scarce. The sparse distribution of climate data limited the detail and accuracy of the relationship between climatic factors and plant productivity. Therefore, the results are likely to be subject to some ambiguity.

Vegetation NPP is influenced by a variety of factors. In this study, only three climatic factors and LOS were considered. Although these factors have explained a total of 56% of the variation of NPP (Figure 8), other climate-related factors, such as sunshine duration, soil temperature, precipitation characteristics (e.g., effective precipitation, precipitation intensity), CO_2 concentrations, N enrichment and deposition (e.g., policy and planning changes), should be considered in future studies [67]. Moreover, other phonological metrics (e.g., Start of Season, End of Season), species competition, and disturbances such as anthropogenic activities (irrigation, fertilization [68,69], harvest, land use/land cover change), wildfires, plant diseases, pests, floods, and droughts as well as the time-lag effect of the above–mentioned variables can vary by region [50], and should also be considered in future studies.

The results presented here indicate the complexity of vegetation NPP dynamics and the response or reaction strategy of vegetation to climate change during the study period. However, the trend for NPP before and after turning points were mostly non-significant despite all turning points being significant (except evergreen broadleaf forest) based on ΔAIC. This may be caused by a short time period, or a non-linear variation on NPP during the study period. Therefore, the conclusions mentioned above should be made with more caution, and more effort should be made to explore the NPP trends (e.g., non-linear trend) in the future to clarify the direction of dynamic NPP trends [70]. In addition, it is difficult to estimate future NPP dynamics using mathematical models (e.g., linear regression analysis)

due to the nonlinear characteristics of NPP dynamics in a long time series, the uncertainty about future climate change, and the time-lag effect of NPP responses to climate change. To date, the Hurst exponent, which has been widely used in hydrology, climatology, economics, geology, and geochemistry, could be considered to predict the NPP variation. The results presented here (Figure S4) indicate that NPP in China will continue to increase based on the Hurst exponent. Unfortunately, this exponent characterizes trends based only on past and present environmental conditions, without considering future environmental change, especially in developing areas, or giving a time period for dynamic NPP trends. These limitations restrict our ability to predict and anticipate future NPP variation, the carbon cycle and its relationship with and response to climate change and human activity, and hence more effort must be made to predict future NPP variation.

5. Conclusions

In this study, the spatiotemporal patterns of NPP and its correlation with climatic factors as well as vegetation phenology during 2001–2014 in China were investigated, and the main conclusions can be summarized as follows:

1. Validation results showed that NPP derived from MODIS performed well in China's ecosystem compared with the other two models, with an increased R^2 value and a decreased RMSE and MAE. However, this conclusion should be made with caution due to few observed sites.
2. During the entire study period, annual NPP showed an increasing trend at the national scale. However, the increasing trends in NPP were not linear, with a slower rate after 2004. At a regional level, annual NPP displayed an increasing trend, despite the occurrence of a turning point year in Northern China and the Tibetan Plateau. However, the NPP in Southern China decreased during the whole study period, which can mainly be explained by climate change as well as fierce anthropogenic activities.
3. Generally, climatic factors and LOS were positively correlated with NPP, and the direct effect of solar radiation on NPP was the largest compared with temperature and precipitation. Due to local climate conditions, the relationship between NPP and climatic factors were diverse at a regional scale.

Supplementary Materials: The following are available online at www.mdpi.com/1999-4907/8/10/361/s1, Table S1: Sites information of the field Net primary productivity (NPP) data used in this study; Figure S1: Vegetation types (DNF, deciduous needle-leaf forest; ENF, evergreen needle-leaf forest; EBF, evergreen broadleaf forest; DBF, deciduous broadleaf forest; and GM, grassland and meadow) as well as three sub-region divisions (**a**), and provinces distribution (**b**) in China; Figure S2: Distribution of meteorological stations across China, red points represent stations for temperature and precipitation, and black triangles represent stations for solar radiation; Figure S3: Spatial distribution of Turing Point (TP) years (**a**) and corresponding ΔAIC values (**b**) of the NPP in China for the period 2001–2014; Figure S4: Spatial distribution of the Hurst exponent in China from 2001 to 2014.

Acknowledgments: This study is supported by the National Natural Science Foundation of China (Grant No. 41431178), the Natural Science Foundation of Guangdong Province, China (Grant No. 2016A030311016), the Innovation Project of Guangdong Province Water Resources Department (Grant No. 2015-02) and the Central Fund Supporting Nonprofit Scientific Institutes for Basic Research and Development (PM-zx021-201407-007).

Author Contributions: Xinchang Zhang and Xijun Yu outlined the research topic, assisted with manuscript writing, and coordinated the revision activities. Jian Yang and Zhaohui Luo performed data collection, data analysis, the interpretation of results, manuscript writing, and coordinated the revision activities.

Conflicts of Interest: The authors declare no conflict of interest.

References

1. Haberl, H.; Erb, K.H.; Krausmann, F.; Gaube, V.; Bondeau, A.; Plutzar, C.; Gingrich, S.; Lucht, W.; Fischer-Kowalski, M. Quantifying and mapping the human appropriation of net primary production in earth's terrestrial ecosystems. *Proc. Natl. Acad. Sci. USA* **2007**, *104*, 12942–12947. [CrossRef] [PubMed]

2. Allen, C.D.; Macalady, A.K.; Chenchouni, H.; Bachelet, D.; McDowell, N.; Vennetier, M.; Kitzberger, T.; Rigling, A.; Breshears, D.D.; Hogg, E.H.; et al. A global overview of drought and heat-induced tree mortality reveals emerging climate change risks for forests. *For. Ecol. Manag.* **2010**, *259*, 660–684. [CrossRef]
3. Luo, Z.; Tian, D.; Ning, C.; Yan, W.; Xiang, W.; Peng, C. Roles of koelreuteria bipinnata as a suitable accumulator tree species in remediating Mn, Zn, Pb, and Cd pollution on Mn mining wastelands in southern china. *Environ. Earth Sci.* **2015**, *74*, 4549–4559. [CrossRef]
4. Pimm, S.L.; Raven, P. Biodiversity. Extinction by numbers. *Nature* **2000**, *403*, 843–845. [CrossRef] [PubMed]
5. Sala, O.E.; Chapin, F.S.; Armesto, J.J.; Berlow, E.; Bloomfield, J.; Dirzo, R.; Huber-Sanwald, E.; Huenneke, L.F.; Jackson, R.B.; Kinzig, A. Global biodiversity scenarios for the year 2100. *Science* **2000**, *287*, 1770–1774. [CrossRef] [PubMed]
6. Houghton, R.A.; Hackler, J.L.; Lawrence, K.T. The U.S. Carbon budget: Contributions from land-use change. *Science* **1999**, *285*, 574–578. [CrossRef] [PubMed]
7. Twine, T.E.; Kucharik, C.J. Climate impacts on net primary productivity trends in natural and managed ecosystems of the central and eastern united states. *Agric. For. Meteorol.* **2009**, *149*, 2143–2161. [CrossRef]
8. Burnham, K.P.; Anderson, D.R. *Model Selection and Multimodel Inference: A Practical Information-Theoretic Approach*; Springer Science & Business Media: Berlin, Germany, 2003.
9. Sisay, K.; Thurnher, C.; Belay, B.; Lindner, G.; Hasenauer, H. Volume and carbon estimates for the forest area of the amhara region in northwestern ethiopia. *Forests* **2017**, *8*, 122. [CrossRef]
10. Liang, W.; Yang, Y.; Fan, D.; Guan, H.; Zhang, T.; Long, D.; Zhou, Y.; Bai, D. Analysis of spatial and temporal patterns of net primary production and their climate controls in china from 1982 to 2010. *Agric. For. Meteorol.* **2015**, *204*, 22–36. [CrossRef]
11. Zhang, M.; Lal, R.; Zhao, Y.; Jiang, W.; Chen, Q. Estimating net primary production of natural grassland and its spatio-temporal distribution in china. *Sci. Total Environ.* **2016**, *553*, 184–195. [CrossRef] [PubMed]
12. Wang, J.; Dong, J.; Yi, Y.; Lu, G.; Oyler, J.; Smith, W.; Zhao, M.; Liu, J.; Running, S. Decreasing net primary production due to drought and slight decreases in solar radiation in China from 2000 to 2012. *J. Geophys. Res. Biogeosci.* **2017**, *122*, 261–278. [CrossRef]
13. Pan, Y.; Wu, J.; Xu, Z. Analysis of the tradeoffs between provisioning and regulating services from the perspective of varied share of net primary production in an alpine grassland ecosystem. *Ecol. Complex.* **2014**, *17*, 79–86. [CrossRef]
14. Brouwers, N.C.; Coops, N.C. Decreasing net primary production in forest and shrub vegetation across southwest australia. *Ecol. Indic.* **2016**, *66*, 10–19. [CrossRef]
15. Zhao, M.; Heinsch, F.A.; Nemani, R.R.; Running, S.W. Improvements of the modis terrestrial gross and net primary production global data set. *Remote Sens. Environ.* **2005**, *95*, 164–176. [CrossRef]
16. The Modis Land Cover and Land Cover Dynamics Products. Available online: https://xue.glgoo.net/scholar?cluster=16597624334725163726&hl=zh-CN&as_sdt=2005&sciodt=0,5 (accessed on 22 June 2017).
17. Gu, F.; Zhang, Y.; Huang, M.; Tao, B.; Guo, R.; Yan, C. Effects of climate warming on net primary productivity in China during 1961–2010. *Ecol. Evol.* **2017**. [CrossRef] [PubMed]
18. Calle, Z.; Schlumpberger, B.O.; Piedrahita, L.; Leftin, A.; Hammer, S.A.; Tye, A.; Borchert, R. Seasonal variation in daily insolation induces synchronous bud break and flowering in the tropics. *Trees* **2010**, *24*, 865–877. [CrossRef]
19. Luo, Z.; Yu, S. Spatiotemporal variability of land surface phenology in china from 2001–2014. *Remote Sens.* **2017**, *9*, 65. [CrossRef]
20. Wu, C.; Hou, X.; Peng, D.; Gonsamo, A.; Xu, S. Land surface phenology of china's temperate ecosystems over 1999–2013: Spatial-temporal patterns, interaction effects, covariation with climate and implications for productivity. *Agric. For. Meteorol.* **2016**, *216*, 177–187. [CrossRef]
21. Peng, J.; Liu, Z.; Liu, Y.; Wu, J.; Han, Y. Trend analysis of vegetation dynamics in qinghai–tibet plateau using hurst exponent. *Ecol. Indic.* **2012**, *14*, 28–39. [CrossRef]
22. Zhang, Y.; Gao, J.; Liu, L.; Wang, Z.; Ding, M.; Yang, X. Ndvi-based vegetation changes and their responses to climate change from 1982 to 2011: A case study in the koshi river basin in the middle himalayas. *Glob. Planet. Chang.* **2013**, *108*, 139–148. [CrossRef]
23. Wen, Z.; Wu, S.; Chen, J.; Lü, M. Ndvi indicated long-term interannual changes in vegetation activities and their responses to climatic and anthropogenic factors in the three gorges reservoir region, China. *Sci. Total Environ.* **2017**, *574*, 947–959. [CrossRef] [PubMed]

24. Piao, S.; Ciais, P.; Lomas, M.; Beer, C.; Liu, H.; Fang, J.; Friedlingstein, P.; Huang, Y.; Muraoka, H.; Son, Y. Contribution of climate change and rising CO_2 to terrestrial carbon balance in east asia: A multi-model analysis. *Glob. Planet. Chang.* **2011**, *75*, 133–142. [CrossRef]
25. Mu, Q.; Zhao, M.; Running, S.W.; Liu, M.; Tian, H. Contribution of increasing CO_2 and climate change to the carbon cycle in China's ecosystems. *J. Geophys. Res. Biogeosci.* **2008**. [CrossRef]
26. Xu, W.C.; Wang, W.; Ma, J.S.; Yang, X. The characteristics, causes of formation and climatic impact of the 1997–1998 El Niño event. *Donghai Mar. Sci.* **2004**, *22*, 1–8.
27. Lu, E.; Luo, Y.; Zhang, R.; Wu, Q.; Liu, L. Regional atmospheric anomalies responsible for the 2009–2010 severe drought in china. *J. Geophys. Res. Atmos.* **2011**. [CrossRef]
28. Liu, J.; Zhang, Q.; Hu, Y. Regional differences of China's urban expansion from late 20th to early 21st century based on remote sensing information. *Chin. Geogr. Sci.* **2012**, *22*, 1–14. [CrossRef]
29. Duan, H.; Yan, C.; Tsunekawa, A.; Song, X.; Li, S.; Xie, J. Assessing vegetation dynamics in the three-north shelter forest region of china using avhrr ndvi data. *Environ. Earth Sci.* **2011**, *64*, 1011–1020. [CrossRef]
30. Sasai, T.; Saigusa, N.; Nasahara, K.N.; Ito, A.; Hashimoto, H.; Nemani, R.; Hirata, R.; Ichii, K.; Takagi, K.; Saitoh, T.M. Satellite-driven estimation of terrestrial carbon flux over far east asia with 1-km grid resolution. *Remote Sens. Environ.* **2011**, *115*, 1758–1771. [CrossRef]
31. Liu, Y.; Ju, W.; He, H.; Wang, S.; Sun, R.; Zhang, Y. Changes of net primary productivity in china during recent 11 years detected using an ecological model driven by modis data. *Front. Earth Sci.* **2013**, *7*, 112–127. [CrossRef]
32. Liu, F.H.; Chen, X.; Chen, X.W.; Song, S. Relationship between temperature change and in climate boundary and summer precipitation over the huaihe river basin. *Clim. Environ. Res.* **2010**, *15*, 169–178.
33. Wang, H.; Dai, J.; Zheng, J.; Ge, Q. Temperature sensitivity of plant phenology in temperate and subtropical regions of china from 1850 to 2009. *Int. J. Climatol.* **2015**, *35*, 913–922. [CrossRef]
34. Shen, M.; Tang, Y.; Chen, J.; Zhu, X.; Zheng, Y. Influences of temperature and precipitation before the growing season on spring phenology in grasslands of the central and eastern qinghai-tibetan plateau. *Agric. For. Meteorol.* **2011**, *151*, 1711–1722. [CrossRef]
35. Zhao, M.; Running, S.W. Drought-induced reduction in global terrestrial net primary production from 2000 through 2009. *Science* **2010**, *329*, 940–943. [CrossRef] [PubMed]
36. Lieth, H. Modeling the primary productivity of the world. In *Primary Productivity of the Biosphere*; Lieth, H., Whittaker, R.H., Eds.; Springer: Berlin/Heidelberg, Germany, 1975; pp. 237–263.
37. ChinaFLUX Sites. Available online: http://www.chinaflux.org/ (accessed on 10 September 2017).
38. Baldocchi, D.; Falge, E.; Gu, L.; Olson, R.; Hollinger, D.; Running, S.; Anthoni, P.; Bernhofer, C.; Davis, K.; Evans, R.; et al. Fluxnet: A new tool to study the temporal and spatial variability of ecosystem–scale carbon dioxide, water vapor, and energy flux densities. *Bull. Am. Meteorol. Soc.* **2001**, *82*, 2415–2434. [CrossRef]
39. China Meteorological Data Sharing Service System. Available online: http://cdc.cma.gov.cn/ (accessed on 6 June 2016).
40. Xu, L.; Chen, X. Regional unified model-based leaf unfolding prediction from 1960 to 2009 across northern china. *Glob. Chang. Biol.* **2013**, *19*, 1275–1284. [CrossRef] [PubMed]
41. Peng, S.; Chen, A.; Xu, L.; Cao, C.; Fang, J.; Myneni, R.B.; Pinzon, J.E.; Tucker, C.J.; Piao, S. Recent change of vegetation growth trend in China. *Environ. Res. Lett.* **2011**. [CrossRef]
42. Zhu, W.; Tian, H.; Xu, X.; Pan, Y.; Chen, G.; Lin, W. Extension of the growing season due to delayed autumn over mid and high latitudes in north america during 1982–2006. *Glob. Ecol. Biogeogr.* **2012**, *21*, 260–271. [CrossRef]
43. Jönsson, P.; Eklundh, L. *Timesat 3.0 Software Manual*; Department of Earth and Ecosystem Sciences, Lund University and Center for Technology Studies, Malmö University: Malmö, Sweden, 2010.
44. Sun, L.; Wei, J.; Duan, D.H.; Guo, Y.M.; Yang, D.X.; Jia, C.; Mi, X.T. Impact of land-use and land-cover change on urban air quality in representative cities of china. *J. Atmos. Sol.-Terr. Phys.* **2016**, *142*, 43–54. [CrossRef]
45. Wei, Y.-X.; Wang, L.-W. Progress in research on land cover products of modis. *Spectrosc. Spectr. Anal.* **2010**, *30*, 1848–1852.
46. Neeti, N.; Eastman, J.R. A contextual mann-kendall approach for the assessment of trend significance in image time series. *Trans. GIS* **2011**, *15*, 599–611. [CrossRef]

47. Wang, C.; Guo, H.; Zhang, L.; Liu, S.; Qiu, Y.; Sun, Z. Assessing phenological change and climatic control of alpine grasslands in the tibetan plateau with modis time series. *Int. J. Biometeorol.* **2015**, *59*, 11–23. [CrossRef] [PubMed]
48. Zhou, J.; Cai, W.; Qin, Y.; Lai, L.; Guan, T.; Zhang, X.; Jiang, L.; Du, H.; Yang, D.; Cong, Z. Alpine vegetation phenology dynamic over 16 years and its covariation with climate in a semi-arid region of china. *Sci. Total Environ.* **2016**, *572*, 119–128. [CrossRef] [PubMed]
49. Xu, H.-J.; Wang, X.-P.; Yang, T.-B. Trend shifts in satellite-derived vegetation growth in central eurasia, 1982–2013. *Sci. Total Environ.* **2017**, *579*, 1658–1674. [CrossRef] [PubMed]
50. Xu, G.; Zhang, H.; Chen, B.; Zhang, H.; Innes, J.L.; Wang, G.; Yan, J.; Zheng, Y.; Zhu, Z.; Myneni, R.B. Changes in vegetation growth dynamics and relations with climate over China's landmass from 1982 to 2011. *Remote Sens.* **2014**, *6*, 3263–3283. [CrossRef]
51. Akaike, H. A new look at the statistical model identification. *IEEE Trans. Autom. Control* **1974**, *19*, 716–723. [CrossRef]
52. Shen, Y.; Yu, S.; Lian, J.; Shen, H.; Cao, H.; Lu, H.; Ye, W. Tree aboveground carbon storage correlates with environmental gradients and functional diversity in a tropical forest. *Sci. Rep.* **2016**, *6*, 25304. [CrossRef] [PubMed]
53. Fox, J. Teacher's corner: Structural equation modeling with the sem package in R. *Struct. Equ. Model. Multidiscip. J.* **2006**, *13*, 465–486. [CrossRef]
54. Roxburgh, S.H.; Berry, S.L.; Buckley, T.N.; Barnes, B.; Roderick, M.L. What is NPP? Inconsistent accounting of respiratory fluxes in the definition of net primary production. *Funct. Ecol.* **2005**, *19*, 378–382. [CrossRef]
55. Zaks, D.P.M.; Ramankutty, N.; Barford, C.C.; Foley, J.A. From miami to madison: Investigating the relationship between climate and terrestrial net primary production. *Glob. Biogeochem. Cycles* **2007**. [CrossRef]
56. Adams, B.; White, A.; Lenton, T.M. An analysis of some diverse approaches to modelling terrestrial net primary productivity. *Ecol. Model.* **2004**, *177*, 353–391. [CrossRef]
57. Tomppo, E.; Gschwantner, T.; Lawrence, M.; McRoberts, R. *National Forest Inventories: Pathways for Common Reporting*; Springer: Berlin, Germany, 2010.
58. Piao, S.; Fang, J.; Zhou, L.; Zhu, B.; Tan, K.; Tao, S. Changes in vegetation net primary productivity from 1982 to 1999 in china. *Glob. Biogeochem. Cycles* **2005**, *19*, 1–16. [CrossRef]
59. Richardson, A.D.; Keenan, T.F.; Migliavacca, M.; Ryu, Y.; Sonnentag, O.; Toomey, M. Climate change, phenology, and phenological control of vegetation feedbacks to the climate system. *Agric. For. Meteorol.* **2013**, *169*, 156–173. [CrossRef]
60. Yu, G.-R.; Zhu, X.-J.; Fu, Y.-L.; He, H.-L.; Wang, Q.-F.; Wen, X.-F.; Li, X.-R.; Zhang, L.-M.; Zhang, L.; Su, W.; et al. Spatial patterns and climate drivers of carbon fluxes in terrestrial ecosystems of China. *Glob. Chang. Biol.* **2013**, *19*, 798–810. [CrossRef] [PubMed]
61. Shi, C.; Sun, G.; Zhang, H.; Xiao, B.; Ze, B.; Zhang, N.; Wu, N. Effects of warming on chlorophyll degradation and carbohydrate accumulation of alpine herbaceous species during plant senescence on the tibetan plateau. *PLoS ONE* **2014**, *9*, e107874. [CrossRef] [PubMed]
62. Liu, Q.; Fu, Y.H.; Zhu, Z.; Liu, Y.; Liu, Z.; Huang, M.; Janssens, I.A.; Piao, S. Delayed autumn phenology in the northern hemisphere is related to change in both climate and spring phenology. *Glob. Chang. Biol.* **2016**, *22*, 3702–3711. [CrossRef] [PubMed]
63. Ibrahim, Y.; Balzter, H.; Kaduk, J.; Tucker, C. Land degradation assessment using residual trend analysis of gimms ndvi3g, soil moisture and rainfall in sub-saharan west africa from 1982 to 2012. *Remote Sens.* **2015**, *7*, 5471–5494. [CrossRef]
64. Yang, Y.; Guan, H.; Shen, M.; Liang, W.; Jiang, L. Changes in autumn vegetation dormancy onset date and the climate controls across temperate ecosystems in china from 1982 to 2010. *Glob. Chang. Biol.* **2015**, *21*, 652–665. [CrossRef] [PubMed]
65. Dragoni, D.; Schmid, H.P.; Wayson, C.A.; Potter, H.; Grimmond, C.S.B.; Randolph, J.C. Evidence of increased net ecosystem productivity associated with a longer vegetated season in a deciduous forest in south-central indiana, USA. *Glob. Chang. Biol.* **2011**, *17*, 886–897. [CrossRef]
66. Piao, S.; Friedlingstein, P.; Ciais, P.; Viovy, N.; Demarty, J. Growing season extension and its impact on terrestrial carbon cycle in the northern hemisphere over the past 2 decades. *Glob. Biogeochem. Cycles* **2007**. [CrossRef]

67. Suepa, T.; Qi, J.; Lawawirojwong, S.; Messina, J.P. Understanding spatio-temporal variation of vegetation phenology and rainfall seasonality in the monsoon southeast asia. *Environ. Res.* **2016**, *147*, 621–629. [CrossRef] [PubMed]
68. He, L.; Chen, J.M.; Liu, J.; Bélair, S.; Luo, X. Assessment of smap soil moisture for global simulation of gross primary production. *J. Geophys. Res. Biogeosci.* **2017**, *122*, 1549–1563. [CrossRef]
69. Liu, X.; Zhang, Y.; Han, W.; Tang, A.; Shen, J.; Cui, Z.; Vitousek, P.; Erisman, J.W.; Goulding, K.; Christie, P.; et al. Enhanced nitrogen deposition over china. *Nature* **2013**, *494*, 459–462. [CrossRef] [PubMed]
70. Li, S.C.; Zhao, Z.Q.; Gao, Y.; Wang, Y.L. Determining the predictability and the spatial pattern of urban vegetation using recurrence quantification analysis: A case study of shenzhen city. *Geogr. Res.* **2008**, *27*, 1243–1252.